

2014

USING TERRESTRIAL LIDAR TO MODEL SHRUBS FOR FIRE BEHAVIOR SIMULATION

Theodore Adams
The University of Montana

Follow this and additional works at: <http://scholarworks.umt.edu/etd>

Recommended Citation

Adams, Theodore, "USING TERRESTRIAL LIDAR TO MODEL SHRUBS FOR FIRE BEHAVIOR SIMULATION" (2014).
Theses, Dissertations, Professional Papers. Paper 4173.

This Thesis is brought to you for free and open access by ScholarWorks. It has been accepted for inclusion in Theses, Dissertations, Professional Papers by an authorized administrator of ScholarWorks. For more information, please contact scholarworks@mail.lib.umt.edu.

USING TERRESTRIAL LIDAR TO MODEL SHRUBS FOR FIRE BEHAVIOR
SIMULATION

By

THEODORE JORDAN ADAMS

B. S. Environmental Science, University of Idaho, Moscow, Idaho, 2010
U.A.C. Fire Ecology and Management, University of Idaho, Moscow, Idaho, 2010

Thesis

presented in partial fulfillment of the requirements
for the degree of

Master of Science
in Forestry

The University of Montana
Missoula, MT

May 2014

Approved by:

Sandy Ross, Dean of The Graduate School
Graduate School

Dr. Carl Seielstad, Chair
College of Forestry and Conservation

Dr. Lloyd Queen
College of Forestry and Conservation

Dr. Ragan Callaway
Division of Biological Sciences

© COPYRIGHT

by

Theodore Jordan Adams

2014

All Rights Reserved

Using Terrestrial LiDAR to Model Shrubs for Fire Behavior Simulation

Chairperson: Dr. Carl Seielstad

The purpose of this study was to spatially represent shrub fuel matrices accurately and at fine resolution for use in physics-based fire behavior simulations. Terrestrial Light Detection and Ranging (T-LiDAR) was used to measure shrub fuel beds in laboratory settings before and after fire burned through them. The primary goals of this research were to produce highly descriptive data-sets that correctly identified the locations of biomass within 3-D space without destructive sampling, and to derive attributes for fuel elements within the shrubs. This research was completed in two phases. First, a series of experiments was conducted to test the capacity of a commercially available LiDAR instrument for making detailed measurements of diffuse shrubs. Second, model shrub fuel beds were produced and evaluated for accuracy. The research tested the T-LiDAR's ability to characterize physical traits of shrubs within volumes, identified issues associated with misrepresenting the true geometry of scanned samples, developed sampling protocols for scanning shrubs prior to and following combustion experimentation, and built descriptive models of actual shrubs. The findings of this study show that T-LiDAR can be used effectively to estimate volume, structure, and biomass for individual shrubs. T-LiDAR derived models were shown to accurately predict mass of scanned shrubs (Adj. R²: 0.598, P-Value: 0.0012). The models produced show vast improvements from past estimations of physiological characteristics in fuels and fire behavior.

ACKNOWLEDGEMENTS

First and foremost, I would like to thank my advisor Dr. Carl Seielstad for his guidance, support, patience, insight, and for always challenging me to do better. Without him and his flexibility I would not have been able to pursue post-secondary education. I would like to thank Dr. Lloyd Queen and Dr. Ragan Callaway for being willing to serve as committee members. Their patience and support has been immensely helpful in achieving this goal without undue stress and heartache.

I would like to thank the partners on this project who helped with the data collection process. The staff of the Pacific Southwest Research Station-Riverside: Dr. David Weiss, Gloria Burke, and Joey Chong. I am grateful to Dr. Thomas Fletcher and his cohort at the Brigham Young University Advanced Combustion Engineering Research Center including: Dallan Prince, Jonathan Gallacher, and Marianne Fletcher.

I would like to thank the staff of the National Center for Landscape Fire Analysis, in particular: Jami Sindelar for help negotiating the rank and file of the Ivory Towers, Dr. Casey Teske for being a friend and counselor, Eric Rowell for being a code and data guru, Valentijn Hoff for being a stoic and steady positive influence, and the men and women of CHCB 442- Tara Umphries, Tyson Atkinson, Larry Lee, and Jena Ferraresse- for always providing a sounding board and frequent entertainment.

Finally, I would like to thank my family and all the friends who have encouraged me throughout this endeavor. They have put up with my rants and kept me in check with proper doses of support, sarcasm, and sedation, always reminding me that I was suffering from ‘first world problems.’

This research was made possible by funding from the Joint Fire Sciences Program.

TABLE OF CONTENTS

TABLE OF CONTENTS	v
TABLE OF FIGURES	vii
TABLE OF TABLES.....	viii
I. INTRODUCTION	9
A. Motivation	9
B. Background.....	9
1. Fire Behavior.....	9
2. Fuels Measurements.....	11
3. LiDAR	13
C. Project Goal and Objectives	14
D. Thesis Structure.....	15
I. PHASE I: DEVELOPING A METHODOLOGY FOR THE APPLICATION OF T-LiDAR FOR SHRUB FUEL MAPPING AND MODELING.....	17
A. E1. (Experiment 1): Assessing TLS Point Cloud Error and Characterizing its Causes	20
B. E2. (Experiment 2): Quantifying the Range Effect on Laser Intensity at Short Scan Distances.....	23
C. E3. (Experiment 3): Relating Discrete Samples (Fuel Elements) to Laser Response	1
D. E4. (Experiment 4): Testing the Effects of Rotational Geometry on Laser Intensity and Density	6
E. Phase I Discussion.....	8
II. Phase II. Modeling Shrubs Using T-LiDAR.....	10
A. Building a Shrub Model from TLS.....	11
1. Data Collection	11
2. Data Manipulation and Scrubbing.....	15
3. Determining Optimal Point Per Voxel Density.....	16

B.	Evaluate Constructed Model for Descriptive Capabilities.....	18
1.	Ocular Evaluation of Shrub Models	18
2.	Assessment of Shrub Interiors	22
C.	Evaluating Model Potential for Tracking Fuel Bed Change	26
1.	Combustion Mass Loss.....	26
2.	Simulated Mass Loss.....	30
D.	Attributing Fuel Elements with Bulk Densities	35
E.	Shrub Model Discussion	39
III.	Project Discussion.....	41
IV.	Conclusions.....	44
	REFERENCES.....	46
	APPENDICES	51
	DATA PROCESSING WORKFLOW	51
	DESCRIPTIVE STATISTIC SPREADSHEETS	57
	<i>PHASE I-EXPERIMENT 1</i>	57
	<i>PHASE I-EXPERIMENT 2</i>	57
	<i>PHASE I-EXPERIMENT 3</i>	60
	<i>PHASE I-EXPERIMENT 4</i>	63
	<i>PHASE II-COMBUSTION MASS LOSS</i>	65
	<i>PHASE II-SIMULATED MASS LOSS</i>	66
	<i>PHASE II-INTERIOR VOLUME REPRESENTATION</i>	67
	<i>PHASE II-VOXEL BULK DENSITY</i>	71
	DATA PROCESSING CODE AND OUTPUT.....	74
	<i>PHASE I-EXPERIMENT 1</i>	74
	<i>PHASE I-EXPERIMENT 2</i>	75
	<i>PHASE I-EXPERIMENT 3</i>	76
	<i>PHASE I-EXPERIMENT 4</i>	78

<i>PHASE II-COMBUSTION MASS LOSS</i>	78
<i>PHASE II-SIMULATED MASS LOSS</i>	79
<i>PHASE II-INTERIOR VOLUME REPRESENTATION</i>	80
<i>PHASE II-VOXEL DENSITY DISTRIBUTION</i>	82
<i>MASS PREDICTION</i>	84

TABLE OF FIGURES

FIGURE I-A. CHAMISE SAMPLE USED IN EXPERIMENTATION.....	19
FIGURE I-B. COMPARISON OF PICTURE TO TLS DATA RETURNS.....	20
FIGURE I-C. ARRANGEMENT OF CHAMISE, U.S. QUARTER, AND ACE OF SPADES.....	21
FIGURE I-D. PROFILE VIEW OF CHAMISE STRUCTURE.....	22
FIGURE I-E. SCATTERPLOT OF GHOST POINTS.....	23
FIGURE I-F. SAMPLES 4-6 HELD	24
FIGURE I-G. SCATTERPLOT OF AVERAGE INTENSITY FOR EACH 2 CM	27
FIGURE I-H. POINT CLOUD FOR SAMPLES 4-6.	2
FIGURE I-I. LASER METRICS PLOTTED AGAINST BIOPHYSICAL TRAITS.	4
FIGURE I-J. SCATTERPLOT OF INTENSITY	7
FIGURE II-A. CHAMISE IN EARLY JUNE.....	12
FIGURE II-B. CHAMISE BURNING IN THE RIVERSIDE BURN FACILITY.....	13
FIGURE II-C. SAGEBRUSH SAMPLE 11 DURING COMBUSTION	14
FIGURE II-D. VOXEL MODELS OF SAGEBRUSH SAMPLE 10.....	20
FIGURE II-E. SAGEBRUSH SAMPLE 10.....	21
FIGURE II-F. CHAMISE SAMPLE 9.....	23
FIGURE II-G. HISTOGRAM OF THE NUMBER OF VOXELS.....	24
FIGURE II-H. HISTOGRAM OF PROPORTION OF TOTAL NOT REPRESENTED	25
FIGURE II-I. MASS LOSS AND ADJUSTED VOLUME LOSS.....	28

FIGURE II-J. SAGEBRUSH SAMPLE 1.....	30
FIGURE II-K. SCATTERPLOT OF MASS AND VOLUME.....	32
FIGURE II-L. VOXEL MODELS OF BRANCH THAT UNDERWENT A DIAMETER REMOVAL....	34
FIGURE II-M. PICTURES OF BRANCH THAT UNDERWENT A DIAMETER REMOVAL.....	35
FIGURE II-N. HISTOGRAM OF VOXEL DENSITIES.....	37
FIGURE II-O. TLS VOLUME PREDICTED MASS PLOTTED AGAINST MEASURED MASS.....	38
FIGURE IV-A. INSTRUMENT COLLECTING SCAN INFORMATION.....	52
FIGURE IV-B. ILRIS PARSER 5.0.2.7 SOFTWARE WITH SETTINGS DIALOGUE BOX.	53
FIGURE IV-C. POLYWORKS IMALIGN SOFTWARE ALIGNING TWO POINT CLOUDS.....	54
FIGURE IV-D. POLYWORKS IMSURVEY SOFTWARE SELECTING A BOUNDING BOX.	55
FIGURE IV-E. ARCMAP 10 PROJECTING POINT CLOUD ON THE X-Z	56

TABLE OF TABLES

Table I-1. Descriptive Statistics and Linear Regression Models Created From Comparing TLS Data Metrics to Biophysical Traits.....	3
Table II-1. Descriptive Statistics for Linear Regression models Created at Differing Point Density Thresholds.....	18
Table II-2. Branch Descriptions for Simulated Mass Loss Samples.	31
Table VI-1. Descriptive Statistics for the Number of Ghost Points.....	57
Table VI-2. Descriptive Statistics for Range-Intensity Relationship Within 3.5-6 m.....	57
Table VI-3. Descriptive Statistics for 2 cm Chamise Samples.....	61
Table VI-4. Descriptive Statistics for Rotational Geometry Experiment	63
Table VI-5. Descriptive Statistics for Combustion Mass and Volume Loss.....	65
Table VI-6. Descriptive Statistics for Simulated Mass Loss Experiment.....	66
Table VI-7. Descriptive Statistics for Hull Depth	67
Table VI-8. Descriptive Statistics for Missing Volume Distribution.....	68
Table VI-9. Descriptive Statistics for Chamise Voxel Density Distribution.	71

I. INTRODUCTION

A. MOTIVATION

The motivation for this research stems from the need to improve characterization of fuel bed models for physics-based fire behavior simulations and to develop shrub fire models that consider spatial heterogeneity of fuel elements. Precise 3-D models of fuels form the basis for accurate, replicable inputs to a variety of models, yet the state of science for fuel models remains semi-statistical distributions of fuel elements within simple volumes such as cubes and spheres. Terrestrial Light Detection and Ranging (T-LiDAR) provides a new source of data for spatially representing fuel structures more accurately, yet application of the technology to this problem is limited. Confounding the issue of limited application, the absence of discrete fuel elements presents additional complications for fire and fuel modelers. Shrub species such as chamise and sagebrush present a highly diffuse fuel bed structure that has proven difficult to characterize for fire behavior simulations.

This thesis is part of a larger project involving fuels researchers and fire behavior modelers. The intent of the larger project is to produce and validate a leaf-scale fire behavior model in chamise and sagebrush. That project is five-fold: 1) to make many leaf-scale measurements of fire behavior; 2) to map 'leaves' (fuel elements) in 3-D using T-LiDAR; 3) to simulate fire behavior in T-LiDAR-derived shrubs; 4) to combust T-LiDAR imaged fuel beds in a wind-tunnel under controlled conditions; and 5) to compare and refine fire behavior simulations with actual measurements of fire from the laboratory combustion experiments. The research in this thesis is confined to elements 2 and 4, above.

B. BACKGROUND

1. FIRE BEHAVIOR

Two shrub species have been identified as the primary subjects of study for this research. Chamise (*Adenostoma fasciculatum*) and sagebrush (*Artemisia tridentata*) are both prevalent species in areas where wildfires commonly occur. Current fire behavior models infer that during critical fire weather conditions, both shrub types can produce flame

lengths of greater than 20 feet, thereby placing fire activity above the threshold of standard suppression efforts (NWCG, 2006; Missoula Fire Sciences Laboratory, 2011). The widespread occurrence of shrub fuels in populated areas such as southern California, where chamise is common, and the Great Basin, where sagebrush is dominant, make important to the fire modeling community.

Fire behavior models have been developed for ease of use and rapid application and are used operationally across the western US (Agee, 1993). A semi-empirical model providing the base equation for surface fire spread was originally developed to evaluate fire behavior quantitatively in the field, based on measurements taken from the field (Rothermel, 1972). Subsequently, suites of models based on the equations produced by Rothermel have been applied to a variety of problems (Finney, 2004; Heinsch & Andrews, 2010). While the intended use for these models was field application of fire prediction during fire events, they have proven useful in research applications as well (Hoffman, et al., 2012).

In addition to semi-empirical fire behavior models, several newer models have also been developed without empiricism. Researchers have applied the fundamental laws of heat transfer to create fire progression models (Albini, 1985; Weber, 1991; Mell, et al., 2007). These physics-based models incorporate physical and heat transfer properties in lieu of experimentally derived rates of spread. In fire environments that include interacting fire lines and combustion above the surface fire (e.g., crown fire), it is important to understand heat transfer and how it affects or is influenced by wind flow not accounted for in steady-state models.

Physics-based computer modeling has begun to prove useful in studying ignition of vegetation or structures in critically important environments, such as the wildland-urban interface and bark beetle attacked timber stands (Mell, et al., 2009; Hoffman, et al., 2012). The characteristics of these models that make them different from previous models is their spatial complexity on a landscape and their ability to predict combustion dynamics in three dimensions. In other models, the spatial heterogeneity of fuels within a single plant can strongly influence fire behavior in computational fluid dynamics models (Parsons, et al., 2011), and lack of knowledge about fuels variability is now limiting advancement of the models. Further, the inherent limitation of a fully physical model is the vast amount of computational time and power needed to model a fire environment, making it useful in research or pre-planning, but rarely beneficial for timely, on-the-ground model projections

(Mell, 2013). Consequently, fire modelers are attempting to validate the models on smaller domains (sub-grids) such as individual shrubs with the goal of developing computational short-cuts intended to speed up modeling on larger grids.

Considerable time and effort has been spent identifying combustion characteristics of individual fuel elements that make up a plant structure (Fletcher, et al., 2007; Pickett, et al., 2009). By collecting empirical measurements from individual fuel elements, researchers have been able to develop hybrid empirical and physics based models that combine and transfer flaming combustion from one fuel element to another at leaf scale (Pickett, et al., 2010). To date, these modelers have described the spatial characteristics of fuel elements by randomly distributing leaves within volumetric arrays (voxels) roughly the size of an individual plant (Andersen, et al., In Progress). This method of describing an entire plant from statistical distributions of leaves requires each fuel element to have combustion characteristics derived from an empirical collection of data from individual fuel element combustion experiments (Andersen, et al., In Progress). While current multi-leaf combustion models are beneficial for understanding combustion interaction and heat transfer, the generation of whole shrubs in a model environment currently lacks a basis in the actual geometry of real shrubs.

2. *FUELS MEASUREMENTS*

Whether physical or empirical, the ability to accurately model fire behavior has been dependent upon fuels inputs that are related to fire characteristics. The location, amount, and arrangement of fuels have been recognized as important factors in modeling on the scale of an individual plant and subsequently on a landscape. Efforts have been made to translate a three-dimensional description of fuel particles into one-dimensional indicators of fire behavior (Anderson, 1982; Ottmar, et al., 2007). Descriptions of fuel characteristics in operational fire behavior models have been limited to estimations such as: tons per acre, surface area to volume ratio, bulk density, height, depth, and heat content (Rothermel, 1983). Fuel models designed for use in Rothermel's mathematical spread equation are described as steady-state, homogenous fuel beds with quantitative values specific to each fuel model (Albini, 1976). The fuel models designed for this use have been expanded to incorporate more variability from site to site; however, they still operate with the same assumption of uniform distribution of fuels within a particular fuel bed (Scott & Burgan, 2005; Ottmar, et al., 2007).

Earlier work describes the physical characteristics of chamise and sagebrush as a fuel in wildland fire, and characteristic inputs for fire behavior modeling are based on destructively sampled and measured vegetation (Frandsen, 1983). Fire behavior in chamise was found to be highly dependent upon the loose arrangement of material and a comparatively high fuel surface area (Countryman & Philpot, 1970). The experimentally derived measurements from both of these studies were tiered towards the creation of inputs for fire behavior modeling using Rothermel's surface fire spread equation.

Describing the location of biomass and branching structure within individual shrubs has not been widely discussed in the literature, particularly in chamise. The amount of biomass within a sagebrush plant has been shown to be related to the external dimensions of the shrub, which is easily measureable (Murray & Jacobson, 1982), and allometric relationships have been developed to produce reliable estimates of biomass on a landscape (Vora, 1988; Cleary, et al., 2008). However, little work has been conducted to understand the location of biomass, or burnable fuel elements within an individual shrub structure. It is the loose arrangement and high surface area to volume ratio that makes both chamise and sagebrush shrubs particularly susceptible to rapid release of energy during combustion (Countryman & Philpot, 1970; Frandsen, 1983).

Understanding the structural changes that occur in chamise plants is of particular importance as the above-ground biomass is highly influential on the characteristic inputs for fire behavior modeling (Rundel & Parsons, 1979). In addition to year-to-year changes in structure, chamise plants exhibit structural changes and leaf turnover rates seasonally (Jow, et al., 1980). On a landscape scale, there has been limited research describing the factors that contribute to the distribution chamise and chaparral in a Mediterranean environment (Odion & Davis, 2000). Like sagebrush, general biomass estimations can be made for chamise at plot-to-landscape scale using height and width measurements, but no work has been published examining the location and distribution of biomass within the shrub structure.

The branching structure and distribution of material in sagebrush and chamise is highly variable and difficult to measure or replicate. Recreating the branching structure for trees developed in a modeled environment has been approached through the use of fractal modeling (van Noordwijk & Mulia, 2002; Boudon, et al., 2006). Fractals have the potential to create a highly diffuse, highly variable structure for the purposes of fire behavior modeling, but again, have not been applied to shrub species for that specific purpose.

3. *LiDAR*

In the last three decades, light detection and ranging (LiDAR) has been increasingly applied to wide scale sampling of vegetation distribution in the natural environment (Akay, et al., 2009). Airborne LiDAR data have been used in a variety of environmental applications including, but not limited to, measuring forest height, structure and biomass, estimating fuel characteristics, and providing wildlife habitat assessments (Means, et al., 1999; Andersen, et al., 2005; Martinuzzi, et al., 2009). LiDAR is an active remote sensing technique in which ranges from an instrument to a target are determined precisely by measuring the round-trip propagation time of laser pulses. Similar to radar, LiDAR uses recorded energy from many pulses to determine range to and shape of objects. The spatial fidelity of a laser, coupled with time-of-flight referencing allows LiDAR instruments to produce highly descriptive maps of targets in three dimensions. The resulting data from a LiDAR scan are typically described in a Cartesian coordinate system (x, y, and z) that allows the information to be applied in a digital environment where it can be manipulated and examined in a variety of computer modeling systems. In addition to the three-dimensional description, many LiDAR instruments also produce a reflectance value called intensity. The intensity measured by a LiDAR instrument is a scaled measurement of the amount of energy returned to the instrument detector from an emitted and reflected laser pulse (Optech Inc. , 2009).

The ability to scan and describe a structure in 3-D makes LiDAR particularly intriguing for the purposes of plant structure modeling. This is because creating accurate descriptions of plant elements in 3-D space using manual measurements has proven to be impractical and difficult to replicate. Terrestrial laser scanners (TLS) that employ LiDAR technology have shown an ability to provide more precise descriptions of plant structures in a 3-D space (Loudermilk, et al., 2009; Côté, et al., 2009; van Leeuwen & Niewenhuis, 2010). Applications of terrestrial LiDAR (T-LiDAR) in the field of forestry have proven to be diverse, robust, and useful (Dassot, et al., 2011).

T-LiDAR is a useful alternative to time-consuming manual sampling methods (Dassot, et al., 2011). Within a timber stand, T-LiDAR has been used to provide several mensuration metrics such as: stem location, tree height, stem diameter, stem density, and timber volume (Hopkinson, et al., 2004). Even in laboratory settings, T-LiDAR has shown potential to derive robust structural information associated with canopy characteristics and allows for the derivation of attributes such as leaf area index and clumping indices, making radiative transfer modeling possible (Moorthy, et al., 2008). In addition to mensuration and

canopy metrics, the data sets produced from scanning forest canopies have been used to model realistic architectures of individual trees and to describe the location and distribution of wood and foliage (Côté, et al., 2009). State-of-the-art T-LiDAR scanners are increasingly being applied in a variety of ways to measure characteristics of forests and rangelands in lieu of using more traditional estimation methods. The amount of detail that a T-LiDAR point cloud can provide is not only highly descriptive, but it also allows for non-destructive, repeatable sampling.

While the measurements returned from a T-LiDAR unit can be highly precise, they are subject to many problems due to the nature of the instrument, as well as the set up and direction of the scan (Van der Zande, et al., 2006). One of the most obvious issues in using laser scanning to describe any natural object is that in three dimensions, the scanner often only 'sees' the first object that the laser hits and returns. Because of this, geometry behind the first object encountered is not generally captured by the TLS. This problem has been addressed to some extent by scanning objects from multiple perspectives and through the application of a probabilistic estimation of shadowed material (Watt & Donoghue, 2005; Van der Zande, et al., 2006). While scanning an object from multiple angles can increase the time taken to sample, it is the most accurate method to describe the complete geometry of an object.

The application of LiDAR in sampling natural fuel beds returns a highly descriptive data set that can describe the location of plant elements relative to each other (Hiers, et al., 2009). Unfortunately, the low stature and low density of shrubs within an ecosystem can cause inaccuracies in describing the fuel bed from an aerial platform (Streutker & Glenn, 2006). However, T-LiDAR can be used to map leaf area distributions in three-dimensions across a forest ecosystem, using the returned information to create a highly descriptive representation of the location and type of biomass material in a tree canopy (Béland, et al., 2014). The ability to scan at sub-cm scales lends T-LiDAR to the application of providing a fine-scale, accurate description of the location of plant material (Seielstad, et al., 2010). T-LiDAR is a promising tool for describing diffuse-form shrub geometry in three dimensions.

C. PROJECT GOAL AND OBJECTIVES

This project is intended to advance fuel characterization and modeling for two diffuse form shrubs: chamise and sagebrush. These species are primary carriers of fire in fuel types that are actively managed by public agencies in the United States. Both species can burn at very high intensities and their diffuse form contributes to sporadic fire behavior

that can be difficult to predict. Improving characterization of these fuel types will increase understanding of both fuel structure and fire spread. By using T-LiDAR to image diffuse shrubs, the spatial distribution of fuel elements can be accurately mapped in three dimensions for input into sub-grid fire models. By assessing the distribution of fuel elements in a number of plant structures, a realistic description of the geometry and interrelation of fuel elements within a plant could be produced for more accurate modeling. Our intent is to replace uniform or random distributions of burnable elements in a fuel bed description with an accurate, depictive model without the need to destroy the sample in the process. We accomplished this goal through two different phases of research that helped us to better understand how the TLS instrument operates in short ranges and how to best use the data produced when scanning a shrub fuel bed.

The first phase of research; “Developing a Methodology for the Application of T-LiDAR for Shrub Fuel Mapping and Modeling”, was completed to identify limitations of the TLS instrument in short range environments and to correct for those limitations in a methodology. Four objectives made up the first phase of research:

- Experiment 1: Assessing the occurrence of positional error in TLS point clouds and describe its causes
- Experiment 2: Quantifying the range effect on laser intensity at short scan distances
- Experiment 3: Relating discrete samples (fuel elements) to laser response
- Experiment 4: Testing the effects of rotational geometry on laser intensity and density

Phase II, Modeling Shrubs Using T-LiDAR, consisted of four objectives associated with the data produced from scanning shrub fuel beds:

- Build a shrub model from TLS
- Evaluate constructed model for descriptive capabilities
- Evaluate model capability for tracking change in fuel bed
- Attribute fuel elements with characteristic bulk densities

D. THESIS STRUCTURE

The research done for this project was completed in two phases and as a result, this thesis is structured to represent the two separate portions of study. Phase I is presented as

four independent experiments that each incorporate specific methodologies, results, and discussion. Each experiment was done to analyze the error structure inherent in using the ILRIS 3-D instrument in a laboratory setting and the phase concludes with a discussion of the findings and how they influence the methodology of Phase II. Phase II is presented in a more linear, traditional fashion that is founded in the overarching goal of the research. The four objectives in this phase represent independent analyses that inform the discussion of methodology and findings of applying T-LiDAR in shrub fuel beds. The final portions of this thesis are sections of discussion and concluding remarks that analyze what was learned, implications for TLS use in broader context, and future research and application in the field of fuels modeling. The attached appendices include a work flow for model construction, descriptive statistic spreadsheets for each analysis, and associated statistical code with output.

I. PHASE I: DEVELOPING A METHODOLOGY FOR THE APPLICATION OF T-LIDAR FOR SHRUB FUEL MAPPING AND MODELING

The four experiments that follow attempt to improve understanding of the data collected by the ILRIS 3-D instrument when scanning diffuse targets in areas where the range to target is limited due to available space in laboratory environments. The fine-grain nature of the sampling process necessitated a series of experiments to develop corrective actions and produce reliable methodologies for the collection of TLS data. Each individual experiment shows a strength, limitation, or need for correction regarding the data collected for diffuse-form shrubs at fine grain. Collectively, they inform the methodology and analysis of whole-shrub models which are developed and described in Phase II.

Experiment 1 was completed to determine the accuracy of point cloud locations when scanning diffuse shrub structures. This research involved scanning diffuse shrub samples containing material substantially smaller than the instrument's laser spot size. When scanning materials smaller than the spot size, discrepancies in data location can occur. Experiment 1 attempts to discern the causes of these discrepancies and to identify solutions to ensure accurate representation when scanning chamise and sagebrush plants.

Experiment 2 was conducted to quantify the relationship between T-LiDAR intensity data and the range. The relationship between range and intensity is well understood beyond 15 meters, but is not the same within 15 meters. Experiment 2 was performed to determine how range affects intensity data and to develop a correction to be applied to point clouds created while scanning in confined spaces.

Experiment 3 was used to determine how physical characteristics of chamise samples are interpreted by the instrument. This experiment was done for the purposes of attributing fuel elements with biophysical estimates. In order to assign descriptive values to shrub models information was gathered on how the TLS data depicts biophysical differences of chamise samples. The data from this experiment were used to create a statistical distribution of fuel densities associated with chamise branches.

Experiment 4 was performed to identify sample orientation bias. Shrub samples were scanned at multiple angles to identify discrepancies associated with sample orientation.

Together, these four experiments were completed to arrive at a reliable and repeatable methodology for scanning diffuse shrub structures in controlled environments prior to and after burning in a wind tunnel. Each experiment shared a common set of methods in regards to sample collection, the instrument and user specifications for each scan, and data parsing and processing for analysis. There were also experimental methods specific to each experiment. The common methods are described below and the experimentally specific methods are discussed within each experiment.

Common Methodologies

Samples of chamise were collected near the Pacific Southwest Research Station in Riverside, California and shipped to Missoula, Montana for study. Samples collected were typical of the plants with small leaves, 4-10 mm long by 1 mm wide, clustered along thin, woody branches (FIGURE I-A). Chamise plants are evergreen shrubs that grow to about 4 m in height and are found in Mediterranean climates in Southern California. The collection site was located on the San Bernardino National Forest at 33.84° N by 116.88° W, elevation ranging from 3600-3900 feet ASL. Neighboring species found on the collection site were typical of a chaparral fuel type, with manzanita (*Arctostaphylos manzanita*), scrub oak (*Quercus berberidifolia*) and wedgeleaf ceanothus (*Ceanothus cuneatus*) making up the over story with California poppy (*Eschscholzia californica*) and annual grasses the primary components of the ground species. Samples were collected throughout the year and subject to a typical Mediterranean climate pattern of cool, wet winters with hot and dry summers. Upon arrival in Missoula, Montana samples were placed in water and kept at room temperature until sampling occurred. Approximately two weeks after harvest, samples became difficult to use due to increasing fragility and brittleness. Each experiment occurred within one week of samples arriving in Missoula.



FIGURE I-A. CHAMISE SAMPLE USED IN EXPERIMENTATION.

The instrument used was an Optech Intelligent Laser Ranging and Imaging System (ILRIS™) 3⁶D-HD Terrestrial Laser Scanner (TLS). This scanner uses a class I laser (1535 nm wavelength) and has a range of 3 to 1500 m with 0.17-mrad divergence (17.6 mm spot spacing at 100 m). This instrument allows the user to specify the spot spacing and focus distance for each scan. For each scan throughout this research, spot spacing was held at 1.0mm with a focus distance specified as the range from the instrument head to the target of the scan. Data collected from the scanner is saved on an external USB drive that is placed in the instrument. The data can also be saved on the hard drive of any PC being used to control the TLS.

Raw data from the instrument is output in a binary format with notes and a .jpeg image of the scan region of interest attached. The binary files were parsed into different formats using Optech ILRIS Parser™ version 5.0.2.7. The data for this research were parsed into two different formats, both serving a unique purpose. The format used for visualization and rotation was a .pif file. Each .pif file output from the processing software describes a point cloud, with an intensity value relative to the data collected in the scan. The second format, used to a greater extent for analysis and manipulation, was a .xyz (ASCII text) file. These files describe each point within a point cloud in a Cartesian coordinate system (easting, northing, elevation; or, x, y, z). Attached to each point is an intensity value measured in 16-bit format.

A. E1. (EXPERIMENT 1): ASSESSING TLS POINT CLOUD ERROR AND CHARACTERIZING ITS CAUSES

The laser scanner produces two effects that influence geometric characterization of materials. The first, termed 'halo' effect, occurs when the laser footprint partially intersects the edge of an object. The result is the filling in of gaps smaller than the diameter of the laser footprint and the creation of halos around objects (FIGURE I-B). Although the laser scanner correctly identifies the occurrence of matter within its footprints, it translates that occurrence to the center of each footprint and thus represents objects as slightly larger than they actually are. The halo phenomenon is very consistent, occurring in every scan. It can be mitigated by removing low intensity values from the data sets, but at the cost of also removing returns from small branches.

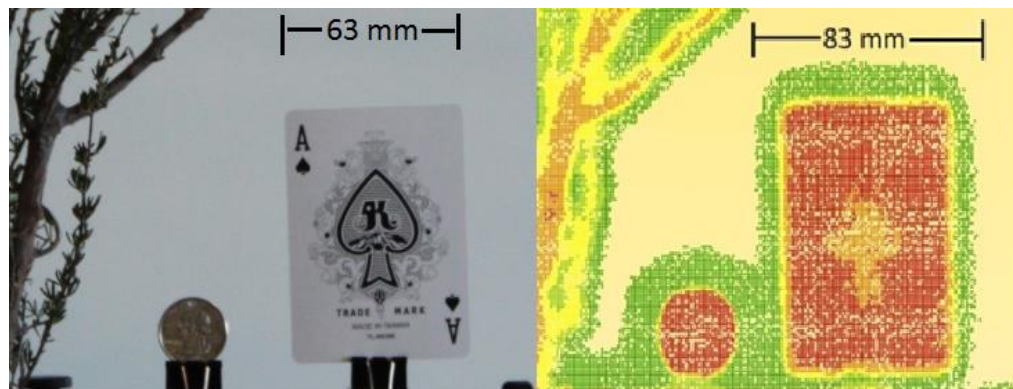


FIGURE I-B. COMPARISON OF PICTURE TO TLS DATA RETURNS AND ASSOCIATED MEASUREMENTS.

The second issue is 'ghosting.' When reflective material occurs at different depths within a footprint, the laser scanner can produce a range error in which target location is erroneously placed in the space between the reflective materials. In a sense, the instrument appears to occasionally 'average' the range and intensity of the two reflective surfaces. Given uncertainties regarding when and how ghosting occurs, an experiment was performed to quantify the relationship between the occurrence of ghosting and the proximity of diffuse targets to discrete backgrounds.

a) E1. Methods

An arrangement of chamise branches was mounted and held immobile on a stand. (Figure I-C). A common U.S. quarter dollar and a playing card were placed next to the chamise samples to provide easily recognizable discrete targets. White poster-board was used for a bright, discrete background behind the targets. The poster-board was mounted,

perpendicular to the scanning direction and moved backward step-wise from the target between each laser scan. The distance from target to background was increased from 0.3 m to 1 m by 0.1 m increments and from 1 m to 5 m by 0.5m increments. The closest the background was to the target in any scan was 0.3 meters due to the chamise branches extending towards the background. A scan was taken each time the background was moved, in addition to a control scan with no background. The arrangement of target with the background at 0.3 m is pictured in Figure I-C.



FIGURE I-C. ARRANGEMENT OF CHAMISE, U.S. QUARTER, AND ACE OF SPACES AS TARGET FOR SCAN.

The range from laser head to the chamise/coin/card structure was 5 meters and held constant throughout the experiment to maintain constant geometry between the target and laser. Spot spacing for each scan was held constant at 1 millimeter and focus distance was 5 m, in accordance with the range to the target.

Each scan was projected in the y and z plane, so as to view the data in profile. The control scan with no background was used to create a shapefile to represent the extent of the target's geometry in the y, z plane. This shapefile was overlain on each scan along with a shapefile of the background poster-board, and manually clipped from the data set. The result was an array of points located between the target and the background (ghost points) for each scan (FIGURE I-D). Ghost point counts were recorded for each scan and a statistical analysis was conducted relating ghosting to distance between target and background (n=9). Statistical analysis performed on the count of ghost points was a logarithmic regression of ghost point counts. The numbers of ghost points were reported as log base 10 values and a linear regression applied using the R statistical package. The logistic regression was chosen

to illustrate a simple relationship between the independent variable, distance between background and target, to the dependent variable, number of ghost points in the point cloud.

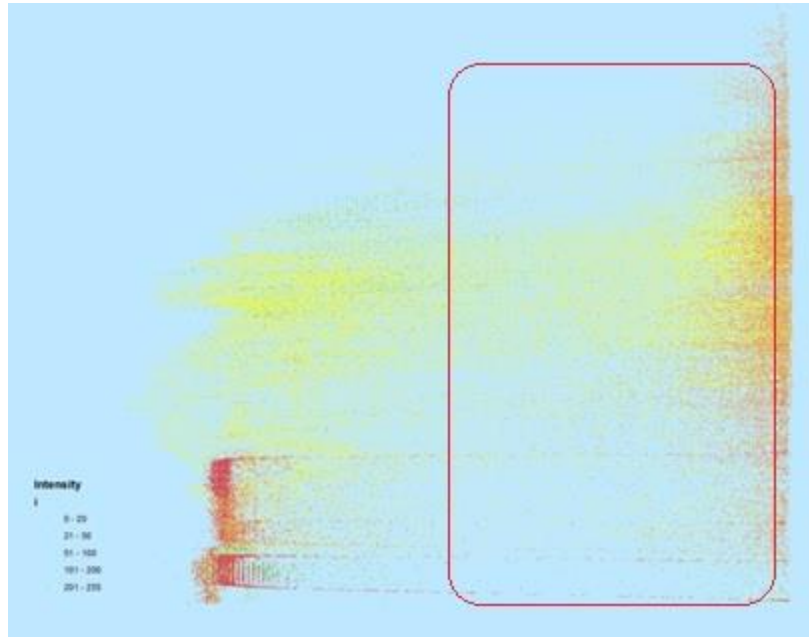


FIGURE I-D. PROFILE VIEW OF CHAMISE STRUCTURE WITH THE POSTERBOARD BACKGROUND 60 CM AWAY. RED OUTLINE INDICATES AREA IN WHICH GHOST POINTS OCCURRED.

b) E1. Results

Ghost points comprise a large proportion of total returns when a discrete background is positioned close to the target. Beyond a distance of 2.5 meters between the target and the background, the number of ghost points becomes negligible. A logarithmic regression applied to the number of ghost points in each scan was significantly related to the range of background to the target (F-statistic: 93.2 on 1 and 7 DF; p-value: <0.001) (FIGURE I-E). The model produced showed a decreasing number of ghost points with increasing range from target to background:

$$GPC = -0.01942(BGR) + 5.63885.$$

Where GPC is the Log of ghost point counts and BGR is the range in centimeters between the target and the background. The goodness of fit measurement showed strong correlation (Adj. R²: 0.92).

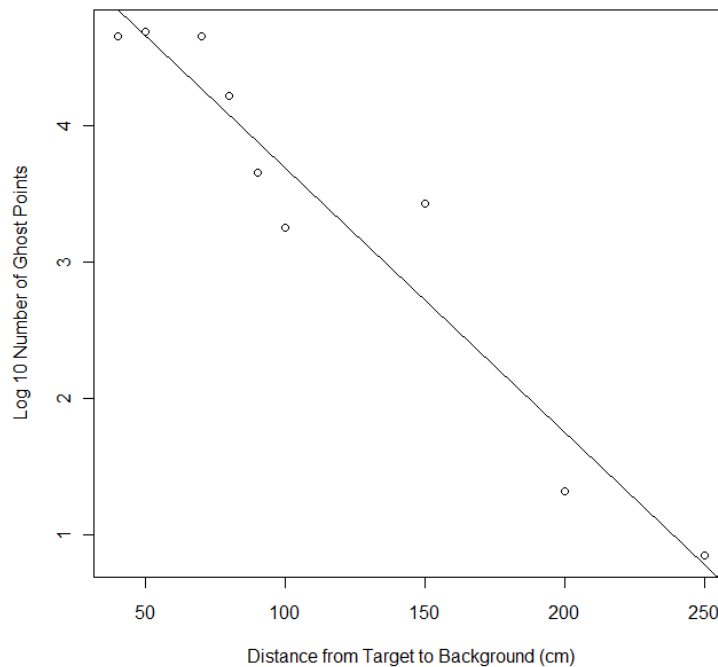


FIGURE I-E. GHOST POINTS AND RANGE FROM TARGET TO BACKGROUND.

c) E1. Discussion

If there is a background near the target, points are trans-located behind the target producing inaccurate geometry that misrepresents the target of interest. As the distance to a background increases, the number of erroneous points decreases. Understanding this phenomenon is important for developing a methodology of scanning shrubs in confined areas. In order to accurately represent the geometry of a diffuse target, scans must be taken from perspectives that eliminate backgrounds within 2.5 meters of the target. This means that for scanning whole shrubs in Phase II, our methodology needs to ensure that there is no background coincident with the target within 2.5 meters.

B. E2. (EXPERIMENT 2): QUANTIFYING THE RANGE EFFECT ON LASER INTENSITY AT SHORT SCAN DISTANCES

At ranges beyond 15 meters, return intensity decays predictably. Range correction of intensity is achieved using $1/\text{distance}^2$ (Seielstad, et al., 2010). The relationship between range and intensity changes inside 15 m due to the inability of the receiver to collect full returns. In short, the geometry of the laser, target, and receiver result in incomplete

reflections at close range. Inside 15 m, intensity actually increases with distance although it is unknown whether it does so consistently. The intent of Experiment 2 was to derive a range correction for close-range targets because the shrub fuels would be scanned at 3-6 m range. An experiment was designed and conducted to determine if changing the distance between the scan head and a diffuse shrub target produced a predictable change in intensity.

a) E2. Methods

In creating a full-shrub model (Phase II), fuel elements are represented by 2 cm voxels. The size of individual fuel elements was determined by fire modelers through extensive combustion experiments in BYU's flat-flame burner facility. Consequently, for this experiment chamise samples were cut to 2 cm lengths across a range of foliar and branch wood combinations and stem diameters. Ten samples were harvested from a single branch in order to ensure no repetition of branch location and to represent a continuum from branch stem to terminus. The largest sample (12 mm diameter) came from the bottom of the shrub and the smallest sample (1 mm diameter with no needles) came from the top. Samples were suspended using monofilament 6-pound test nylon fishing line. Each sample was hung in a strand of fishing line using single or double wraps in order to prevent the detection of knots on the sample. Strands of line were weighted on the bottom using 5 g fishing sinker weights. Each strand was mounted 5 cm away from the next, on a meter ruler, to prevent any overlap of samples in the scan (FIGURE I-F).



FIGURE I-F. SAMPLES 4-6 HELD IMMOBILE USING FISHING LINE.

The samples were scanned at the same height as the scan head. Progression of the scans started at 3 meters distance and ended at 7 m distance in increments of 0.5 m. The scan head was moved between each scan; the samples remained in constant position. The focal distance of each scan corresponded to the distance to the samples, and the spot

spacing was 1.0 mm for all. This process was repeated on the reverse side of the samples, scanning once from the North and once from the South, giving two opposing reflection angles for the array of samples. Each sample was scanned from nine different ranges and two different angles to produce 180 observations.

Processing of the TLS point cloud from each scan was completed using ArcMap10. Each scan was projected in the x, z plane. In order to remove the returns associated with the fishing line, all points with intensity of less than 15 were removed from the data set. After the fishing line was removed, each sample was manually selected from the point cloud of each scan and statistics reported on a per-sample, per-scan basis.

A mixed effect, linear regression model was applied to the data for analysis. The mixed effect was applied to account for the difference in data returns associated with the variability of each sample and direction. The dependent variable was mean intensity of each point within the area of the sample and the independent variable was range from the instrument to the sample. Mixed effects variables were sample number and direction. The model was produced using the Linear mixed-effect models using Eigen and S4 (lme4) package in R statistical package.

b) E2. Results

Statistical results for the mixed effect, linear regression showed that average intensity was correlated with range, when held independent of sample and direction (slope t-value: 11.9, p-value: <0.001; intercept t-value: 20.1, p-value: <0.001). The model produced in R was:

$$I = 7.73(r) + 117.8$$

Where I is mean intensity and r is range from instrument to sample in meters. This model was constructed with 100 observations within 20 groups. Standard errors for the value of slope were 0.651 and 5.856 for the intercept. The values for each sample are shown in figure I-G.

c) E2. Discussion

The mixed effect, linear model took into account variation between samples and tested the relationship between range and intensity. The correlation between range and intensity is statistically significant (p-value: <0.001) (FIGURE I-G). The relationship between intensity and range was consistent for all sample types, shapes, and sizes. The majority of variability in the model came from the intercept, which is anticipated due to the nature of a mixed effects model. The intercept of the equation is a mean of all samples; however, the

variable of interest, slope, is what is interesting and useful. A mixed effect model combines all samples into a common mean, allowing for the creation of a single regression line representing the pattern of change along the independent variable. Using the mean slope for each sample, a linear correction can be applied to the average intensity for samples ranging from 3.5 and 5.5 meters.

Predictably, the smallest, most-diffuse samples exhibit the lowest intensities while the larger branches produce brighter reflections. The direction of correlation between range and intensity within 5.5 meters is consistent and different from the relationship between range and intensity beyond 15 meters. Beyond 15 meters, average intensity decreases predictably with increasing range. However, the relationship predicted in this experiment shows increasing intensity with increasing range between 3.5 and 5.5 meters (Slope: 7.7). While it is counter to the long-range relationship, understanding how intensity behaves within a short range allows for more accurate interpretation of LiDAR scans taken in situations where space is limited and scan ranges greater than 15 meters are not feasible.

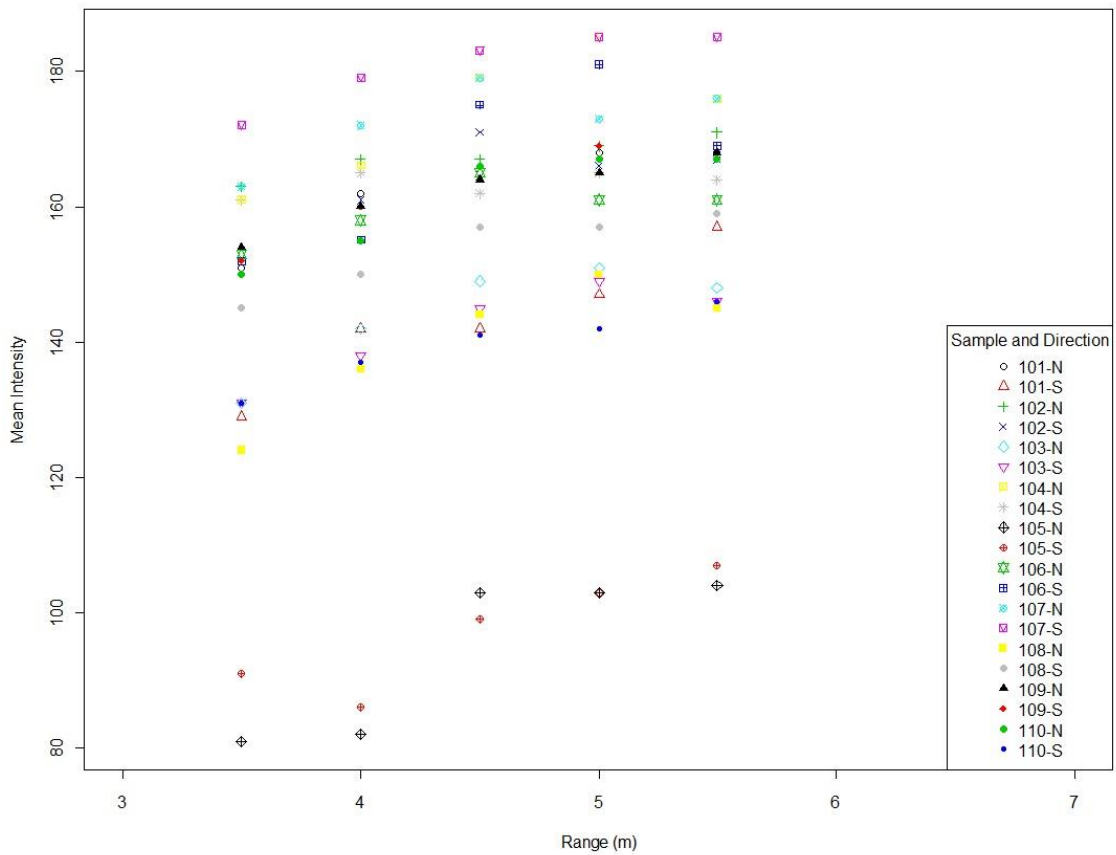


FIGURE I-G. SCATTERPLOT OF AVERAGE INTENSITY FOR EACH 2 CM SAMPLE BY RANGE. SYMBOLS INDICATE DIFFERENT SAMPLES AND WHICH DIRECTION THE SCAN WAS TAKEN FROM.

When processing .xyz files for intensity, the 16-bit intensity data format of the instrument produces a non-linear scale of output. Intensity output is written across a range of 16-bits (range from 0-65,355), but is split across two gain settings. Dim targets are scaled across the first eight bits (0-255), and brighter targets are binned from 256-65,355. However, in the latter case, brightness values are binned at steps of 100 (e.g., 256, 300, 400, 500, etc.) rather than steps of one. In order to account for this, intensity values were converted to 9-bit data using an algorithm written in Interactive Data Language (IDL). The result replaces a disjointed scale that ranges from 0-255 by one and from 256-65,355 by 100 with a linear intensity scale that ranges from 0-512.

C. E3. (EXPERIMENT 3): RELATING DISCRETE SAMPLES (FUEL ELEMENTS) TO LASER RESPONSE

The goal of this experiment was to identify and test relationships between TLS measurements and biophysical data for discrete samples of chamise with the intent of producing models to predict fuel attributes from TLS data. The scale of analysis was 8 cm³ (2x2x2cm), as in previous experiments (Experiment 2). This scale allows for fine-scale description of fuel element locations, while projecting the data in voxel format allows for a continuous description of fuel elements in three dimensions.

a) E3. Methods

Samples of chamise were clipped from the branches to span the observed range of variability. Samples were selected systematically from the bottom to the top of the branch, including larger branches (bottom), forks (middle), and terminal ends (top). Each sample was cut to a length of 2 cm so that TLS point clouds would be contained within 2 cm voxels after data collection. On each sample the following measurements were taken: main stem diameter, categorical location on branch (branch-wood, terminal, or fork), wet weight, and oven-dried weight. Samples were dried at a temperature of 75° C (167° F) for a period of 24 hours. All drying and weighing was completed after scan information had been collected.

Scanning was done at a range of 4 meters with 1.0mm spot spacing and a focus distance equal to the range. Samples were held stationary using monofilament, 6 pound-test, nylon-fishing line (**Error! Reference source not found.**). Each sample was held from a single strand and placed 5 cm from the next strand in order to prevent sample overlap. Each strand was weighted below the sample to hold the line straight and provide stability during the scans. 10 samples were scanned at a time and scans were replicated 10 times, providing information on 100 samples. During the scan process, information was lost for one replication, and one sample was omitted due to its size being inconsistent with sample protocol. For statistical analysis, n=89.

The proximity of background and the resultant ghost points made it necessary to use a constructed background for this study. An aluminum foil background was placed 1 m behind the samples and angled at 45 degrees from perpendicular to the scan direction. Preliminary experimentation showed that the presence of a highly reflective, angled background eliminates ghost points when it is not possible to scan with >2.5 m of empty space behind the targets in question. Aluminum proved to be effective in reflecting the laser

pulse away from the laser and target, ensuring that ghost points were not an issue (Experiment 1).

Scan data were collected and parsed into an x, y, z, i format and converted to a .csv file. Intensity correction was applied per the results from Experiment 2, above. The files were projected using ArcMap 10 for visualization in the x, z plane. Removing the background involved applying a query that omitted any points with a y-value greater than 4.3 m. Additionally, the holding mechanism of tripods, ruler, and fishing line weights were removed by applying similar constraints on x and z values. All range gates for x and z values were selected manually for each scan. Following the removal of the background and surrounding surfaces, the fishing line was removed from the data set by removing any point with an intensity value of less than 15. The threshold of 15 was arrived at by incrementally removing points based on intensity until the fishing line was omitted completely enough to make manual selection of samples possible. Following the manual selection of point clouds for each sample, descriptive statistics of point count, average intensity, and sum of intensity values were reported for each sample.

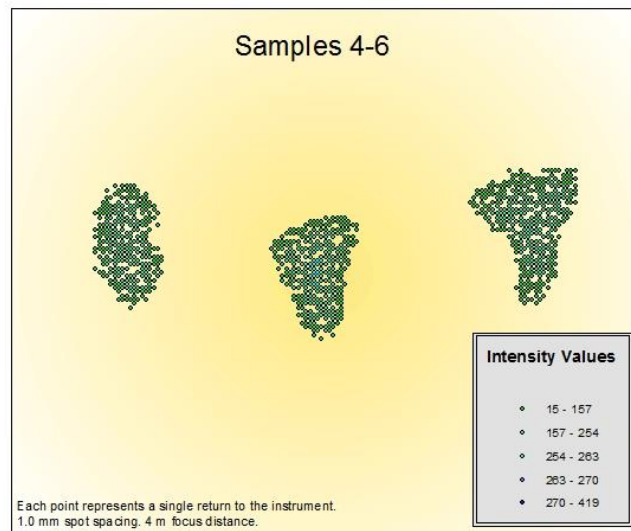


FIGURE I-H. POINT CLOUD FOR SAMPLES 4-6 PROJECTED ON X-Z PLANE IN ARCMAP 10.

Statistical analysis performed on the data was the creation of a number of linear regression models to analyze the ability of laser metrics to predict a biophysical trait of the scanned samples. Independent variables were the laser-derived metrics (point count, average intensity, and sum of intensities). Dependent variables were physical traits of the scanned samples thought to be best interpreted by the laser metrics based on surface area

exposed to the laser energy. Those variables were dry weight, diameter of the sample, and diameter factored by branch type.

b) E3. Results

The results from the multiple linear regression models show that the laser metrics are all statistically capable of discerning change in the biophysical traits (P-Values: <2.2 e-16 to 2.63 e-08). The predictive capability of each model varied greatly (Adj. R²: 0.29 to 0.67), but all showed a general positive association between the selected laser metric and associated biophysical trait (Slope: 2.20 e-05 to 0.238). The best relationship identified was between average intensity and the natural log of the dry weight (P-value: <2.2 e-16, Adj. R²: 0.6716) (TABLE I-1, FIGURE I-1).

TABLE I-1. DESCRIPTIVE STATISTICS AND LINEAR REGRESSION MODELS CREATED FROM COMPARING TLS DATA METRICS TO BIOPHYSICAL TRAITS.

Dependent Variable	Independent Variable	Intercept	Slope	RSE	Adj. R ²	P-value
Natural Log of Dry Weight	Point Count	-4.05 ± 0.240	4.17 e-03 ± 4.261 e-04	0.872	0.5189	1.07 e-15
Natural Log of Dry Weight	Average Intensity	-9.86 ± 0.598	0.0498 ± 3.70 e-03	0.720	0.6716	<2.2 e-16
Natural Log of Dry Weight	Sum of Intensities	-3.79 ± 1.90 e-06	2.20 e-05 ± 1.96 e-06	0.807	0.588	<2.2 e-16
Diameter	Point Count	0.0447 ± 0.615	6.67 e-03 ± 1.09 e-03	2.23	0.2928	2.63 e-08
Diameter	Average Intensity	-8.70 ± 1.78	0.076 ± 0.011	2.14	0.3483	6.929 e-10
Diameter	Sum of Intensities	0.446 ± 0.508	3.55 e-05 ± 5.24 e-06	2.16	0.3378	1.412 e-09
Diameter, Factored by Type	Point Count	-3.51 ± 1.51	0.0236 ± 2.69 e-03	5.51	0.4627	1.374 e-13
Diameter, Factored by Type	Average Intensity	-29.4 ± 4.74	0.238 ± 0.293	5.70	0.4243	2.882 e-12
Diameter, Factored by Type	Sum of Intensities	-1.86 ± 1.24	1.23 e-04 ± 1.28 e-05	5.26	0.5104	2.314 e-15

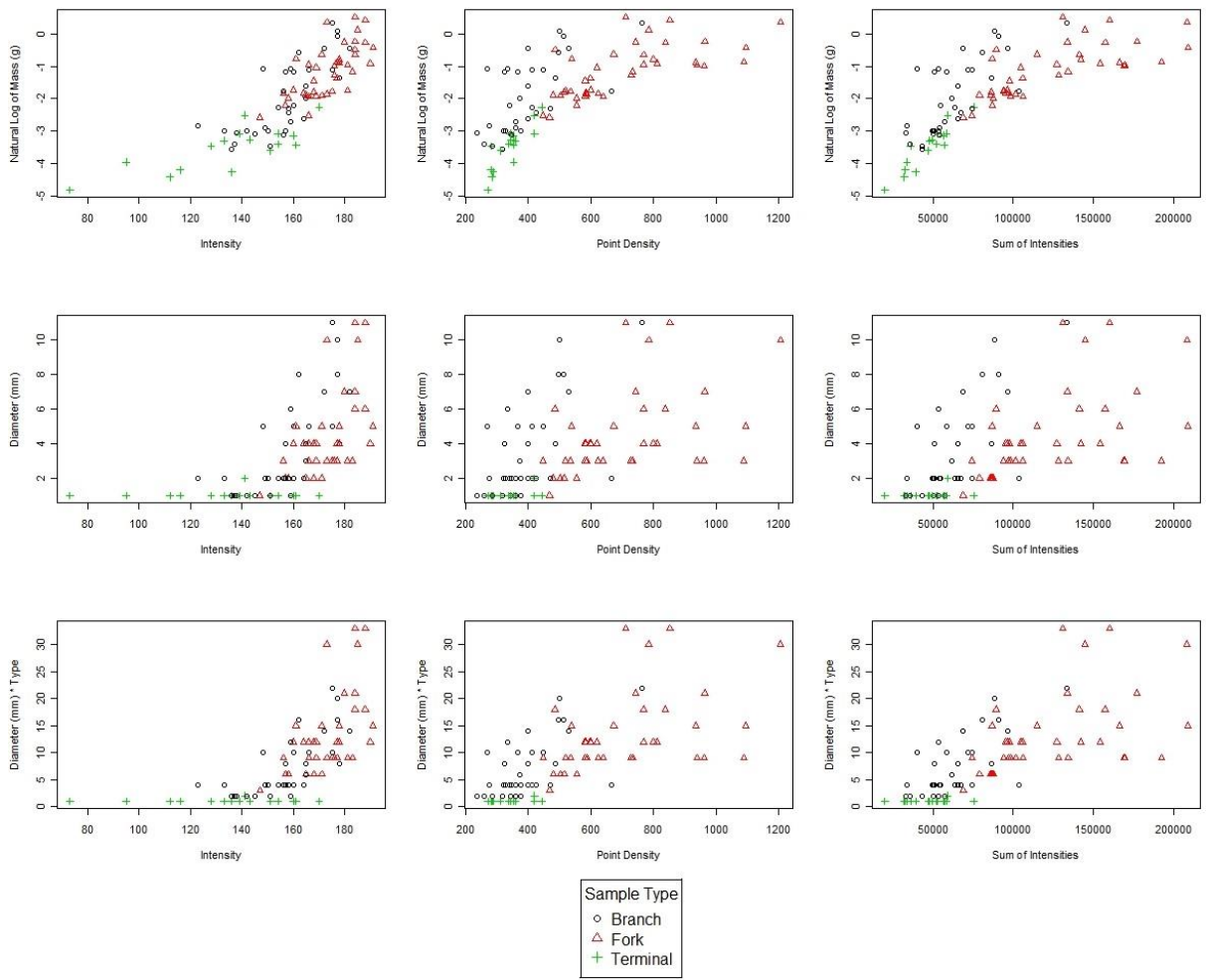


FIGURE I-I. LASER METRICS PLOTTED AGAINST BIOPHYSICAL TRAITS.

c) E3. Discussion

The intent of this research was to create a highly descriptive fuel bed model and that included attributing descriptive traits to the model based upon the laser data produced from scanning. By relating the laser point cloud metrics to biophysical attributes we show the potential to use TLS data as not only a geometric description, but also a physical description of the target. The relationships between TLS point cloud measurements and biophysical traits show that the instrument is capable of discerning fine-scale differences among samples of chamise. Understanding the relationships between the two could allow for the application of descriptive traits to fuel elements within a three-dimensional fuel bed model.

Diameter was significantly related to each laser point cloud metric, substantial variability was not accounted for with any one of the laser metrics (FIGURE I-1). Diameter was only one of the distinctive biophysical traits of the samples in this experiment that could have been interpreted by the laser data. Diameter of the sample was considered to be related to the laser metrics because with increasing diameter there would be increased occupation of the laser footprint. This singular measurement did not account for the variability of the sample regarding the branching structure and also the number and arrangement of needles on the sample. Only the width of the branch wood is accounted for and this leaves much of the variability undescribed in the laser metric regression models (TABLE I-1).

In an attempt to account for more of the variability of the samples, the diameter of each sample was multiplied by a factor according to the branch type. Diameter was multiplied by a factor of one, two, or three if the sample was a terminal ends, larger branches, or forks, accordingly. This was meant to increase the independent variable when the sample type was indicative of occupying more of the laser footprint. The laser would be more apt to detect greater energy from a forked branch, then a piece of branch wood, followed by a terminal end because of the general size of each sample. Using this factoring, the predictive capability of the laser metrics was improved to account for more of the variability in the samples (TABLE I-1). While there is still variability unaccounted for in the regression models, the predictive capability is vastly improved for laser metrics when diameter is factored by sample type.

Mass was a highly significant predictor of all three laser data metrics (FIGURE I-1). Unlike diameter, mass is a biophysical measurement that accounts for the entire sample, not

just the thickness and type. As biomass increases, whether it is a needle or branch wood, the visible size of the sample is typically increased. When the size of the sample increases, it occupies more of the laser footprint when scanned and more energy is returned to the instrument head. When more of the footprint is occupied, more pulses will return to the instrument which would cause the point count to increase as well as the amount of energy, increasing intensity values for the sample. Describing mass using the point cloud information is promising, but difficult to scale up to an entire fuel bed. The samples in this experiment were held stationary and isolated, meaning the halo point values also contributed to the average intensities. When scanning an entire fuel bed, halo values from a single 2 cm voxel will contribute to the averages of surrounding voxels, thereby increasing the average intensity for all voxels. While this problem is difficult to overcome, there is still potential to use laser intensity information to predict mass of a particular element within a fuel bed.

D. E4. (EXPERIMENT 4): TESTING THE EFFECTS OF ROTATIONAL GEOMETRY ON LASER INTENSITY AND DENSITY

In Experiment 3, as biomass increased, the average intensity of reflectance values increased for each sample. This relationship was statistically robust, but the reflectance values for a sample have potential to change with simple rotation, and thus, models relating intensity to biophysical variables may be sensitive to orientation of the shrub material. In Experiment 4, the effects of rotational geometry were tested by scanning samples from many angles and comparing their characteristics.

a) E4. Methods

The samples and design for this experiment were the same as for Experiment 3. Following scanning of the E3 samples, the suspended shrub specimens were rotated horizontally at random angles and scanned a second time (n=59). Angles between 0° and 180° were achieved throughout this process and no changes were made to the structure or composition of each sample. Statistical analysis performed on the data was to compare the sum of intensity for each sample to its corresponding twisted value using a linear regression. The sum of intensity was used to account for the entire value of the sample, rather than classifying by point count or intensity alone.

b) E4. Results

The linear regression for sum of intensity values showed strong correlation from one sample scan to the corresponding rotated sample scan. The relationship was highly significant (F-statistic: 737.6 on 1 and 57 DF, P-value: <0.001). Some variance is not explained due to randomness of the planar depiction of the sample from the laser perspective, but values of the sum of intensity described the majority of variability (Adj. R²: 0.927). The slope of the regression line was 1.027, very near to a 1:1 relationship. The intercept for the line was -0.002, very close to zero, however it was not statistically significant in the regression model (P-value: 0.485).

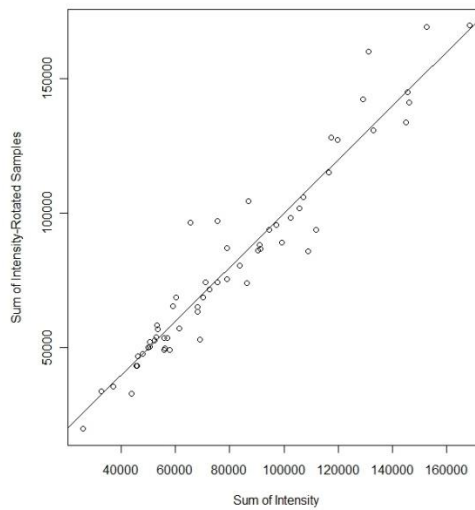


FIGURE I-J. VALUES FOR SUM OF INTENSITY FOR ROTATED AND NON-ROTATED SAMPLES. PLOTTED LINE IS NOT THE REGRESSION LINE, IT IS A 1:1 LINE.

c) E4. Discussion

As with most remote sensing analyses of natural materials, this experiment revealed unexplained variability associated with the rotational properties of diffuse structures as described by the laser. However, the rotational effect was small. The relationship between samples scanned at different orientations was unbiased, highly significant, and robust (FIGURE I-J), although natural variability in the size, shape, and orientation of diffuse structures produced some random variation. The amount and character of this variation provides a reasonable argument for not attempting a correction for orientation effects, and this research moves forward from this point without such a correction.

E. PHASE I DISCUSSION

The previous four laboratory experiments performed in Missoula, MT provide guidance for developing methods and interpreting data in whole-shrub scans obtained in a wind tunnel. The ghosting and halo effects were identified as primary concerns for sampling in confined areas, as was development of an intensity correction for range. Establishing predictive relationships between TLS metrics and physical properties of chamise samples was necessary for converting laser point clouds into biophysical data. And finally, orientation effects were tested and found to be small.

The ghosting phenomena produced a false representation of target geometry, making it a primary concern. It was shown that the proximity of a discrete surface behind a diffuse target caused an increase in ghost points. Ghosting could be minimized by scanning with backgrounds >2.5 meters from targets, or by placing properly angled, highly reflective backgrounds close to a target. The simplest and most effective method to prevent ghosting is to ensure there was no such background within 2.5 m of a diffuse target. The halo effect, caused by partial returns, is a necessary artifact of the data. While the measurements of targets at the halo are inaccurate, the points are located within one laser spot, approximately 10 mm, from the actual location of the target. The negative consequence of halo points is the filling in of canopy gaps smaller than the laser spot size (1 cm). It is possible that more sparsely occupied volumes could be considered empty, and this is examined in Phase II, below. Essentially, then, we deferred to accept the halo as inevitable, but attempted to minimize ghosting by scanning shrubs without backgrounds.

Intensity data from LiDAR are particularly interesting for their potential to aid in prediction of biophysical traits in addition to geometric location (Franceschi, et al., 2009). In order to accurately interpret intensity, we developed a normalization curve for the intensity data. The normalization curve was applied to each data set immediately following parsing so that all intensity data collected throughout this project could be interpreted on a normalized intensity scale.

Analyzing small, variable pieces of chamise branches proved useful for developing models relating TLS data to biophysical data. It found that the intensity of sample point clouds was related to mass of samples. This relationship lends credibility to the idea that mass, and more importantly mass loss following fire, could be inferred through the use of T-LiDAR.

As previously noted, shadowing caused by complex geometry while using a LiDAR instrument is problematic when sampling targets of any kind (Van der Zande, et al., 2006). The requirement to assess complex geometries from multiple angles raises the concern of whether or not the instrument characterizes shrub samples differently from different angles. During the rotational geometry experiment it was discovered that small samples were similarly described regardless of the angle at which they were scanned. This similarity and the randomness of shrub structure suggests that within a shrub, the orientation of a single branch, or portion of branch, will not greatly affect the integrity of the data collected while scanning a diffuse form shrub. Certainly, shadowing will occur within shrubs at whole-shrub scale, but an orientation correction is not necessary to adjust the characteristics of samples within the shrub.

II. PHASE II. MODELING SHRUBS USING T-LIDAR

The goal of phase II was to create a three-dimensional description of fuel elements in chamise and sagebrush fuel beds for use in leaf-scale fire behavior simulations. Phase I results were applied in order to assess the distribution of fuel elements in a number of plant structures and to produce a realistic description of the geometry and interrelation of fuel elements within shrubs. Essentially, the intent was to replace the current state of science (e.g., random distributions of fuel elements within hypothetical volumes) with descriptions of real fuel elements and their locations. Because fire propagation is dependent on the relative positions of combustible materials, we sought an accurate depiction of the location of plant material that burns during flame passage.

Phase II, Modeling Shrubs Using T-LiDAR, consisted of four objectives associated with the data produced from scanning shrub fuel beds. The first objective was to successfully build a shrub model from TLS data. We built the shrub models through collection and manipulation of TLS data obtained from scanning diffuse-form shrubs. The type of model created was a voxel volume array that was built in a Cartesian coordinate system.

It was then necessary to evaluate the created model for descriptive capabilities to determine whether or not the model presented any improvement from previously available fuel bed descriptions. The descriptive capabilities of the shrub models were assessed through an ocular comparison of voxel representations to RGB pictures taken of correspondent samples. We also analyzed the data for thorough representation within the model structure.

The potential for the produced fuel bed model to track changes was done in two separate analyses. The first attempt to track change in fuel beds was done through combustion of samples and comparing the pre- and post-combustion models. The second attempt involved a manual removal of plant material and the creation of model representations at each stage of sample alteration.

The final objective of phase II was an application of characteristic density descriptions to fuel elements within the shrub model to analyze the predictive potential prior to any manipulation of the fuel bed. We applied an empirical distribution of densities to the voxel models in an attempt to attribute each voxel with an individual value. Giving

each voxel a value represented the potential to attribute the array with more detailed information than a uniform description.

Throughout phase II it was difficult to determine the accuracy of the shrub models when compared to the physical shrubs studied in the experimentation. A review of the literature failed to yield any viable method for describing diffuse structures in three dimensional on the scale of the measurement that TLS data allows. The highly heterogeneous structure of diffuse shrubs makes the material not conducive to precise measurement with currently available technology. The labor required to accurately map a shrub using manual measurements would lead to questionable results simply due to the opportunity to incur error from mapping minute details with manual methods. Due to the lack of a feasible method to track volume change we employed mass loss as a viable representation of change to the samples. The assumption in this substitution is that measureable plant material has mass and that larger samples weigh more than smaller samples. In each portion of study we were able to track mass and have assessed the quality of shrub models by comparison of volume estimates to mass measurements. This relationship assumes that mass and volume are related to each other, in that more mass occupies more volume. Using mass allowed us to numerically track physical changes in the shrub samples that would otherwise be difficult to accurately verify.

A. BUILDING A SHRUB MODEL FROM TLS

1. DATA COLLECTION

Data were collected in three sets, once in Missoula, MT and twice in Riverside, CA. In each case, data collection included collection of shrub samples from the field, construction of shrub fuel beds, laser scanning, treatment (mechanical and fire) of shrubs, and measurements of treatments. In Missoula we mechanically removed biomass from shrubs, whereas in experiments in Riverside we combusted biomass in a wind tunnel. For the latter experiments, data were collected at the Pacific Southwest Research Station-Riverside's burn chamber during the dates December 16-20th, 2012 and again from July 29th-August 1st, 2013. Data collection during both sessions consisted of building diffuse form shrub fuel beds, scanning them with TLS, burning them in a controlled environment, and scanning them again after combustion. Data collection during combustion also included high speed video, thermal data, and mass/mass loss. During the December visit, thirteen constructed fuel beds of chamise were created, scanned, and burned. The July visit yielded sixteen

replications of scanning, burning, and re-scanning sagebrush. The Missoula data collection was for chamise only.

The collection site for chamise was located on the San Bernardino National Forest at 33.84° N by 116.88° W, elevation ranging from 3600-3900 feet ASL. Neighboring species at the collection site were typical of a chaparral fuel type, with manzanita (*Arctostaphylos manzanita*), scrub oak (*Quercus berberidifolia*) and Greenbark ceanothus (*Ceanothus spinosus*) making up the over story with California poppy (*Eschscholzia californica*) and annual grasses the primary components of the ground species. Samples were subject to a typical Mediterranean climate pattern of cool, wet winters with hot and dry summers (FIGURE II-A). Collection of sagebrush samples also occurred on the San Bernardino National Forest at 34.28° N by 116.78° W elevation ranging from 6900-7200 feet ASL. Neighboring species were typical of a high-desert ecotype with Pinyon pine (*Pinus edulis*) and California juniper (*Juniperus californica*). Ground species were sparse, but small patches of annual grasses were found growing the microclimate located under and around over story species. The climate on the site is typical of high elevation, Mojave Desert, receiving little rainfall with moderate winters and hot summers.



FIGURE II-A. CHAMISE IN EARLY JUNE (ANZA-BORREGO DESERT NATURAL HISTORY ASSOCIATION, 2013)

The vessel for combustion at the Pacific Southwest Research Station in Riverside, CA is a custom built wind tunnel framed with angle iron. Walls are constructed with high

temperature glass as well as sheet metal. The tunnel has a fan on the north end of the structure and is open on top and to the south. The eastern and western portions (sides) of the walls can be removed for access. In the sample placement area of the wind tunnel, the dimensions are approximately 1.2 m wide by 1.2 m tall. Fuel beds were placed on a scale for mass measurement before, during, and after combustion. Our fuel beds were limited to 2 m lengths to avoid shadowing caused by the structure of the tunnel. A mesh was created using Jackson fencing and chicken wire where stems of samples could be placed and held stationary during scanning and burning. Samples were assembled in the wind tunnel to create a variety of different burning conditions. The density of biomass in each replication was constructed to represent a range of fire behavior, rather than to re-create natural shrub structures explicitly. Observed fire behavior during experimentation ranged from active flame front passage that consumed most of the plant material (FIGURE II-B) to minimal fire behavior that consumed only small, isolated portions of plant material (FIGURE II-C).



FIGURE II-B. PICTURE OF CHAMISE BURNING IN THE RIVERSIDE BURN FACILITY. THIS PHOTO SHOWS THE WIND TUNNEL USED FOR COMBUSTION TRIALS. THIS VIEW IS FROM THE EAST, LOOKING WEST. THE NORTH END OF THE WIND TUNNEL THAT HOUSES THE FAN IS TO THE RIGHT.



FIGURE II-C. SAGEBRUSH SAMPLE 11 DURING COMBUSTION. EXIBITED LOW FIRE INTENSITY AND LIMITED CONSUMPTION OF BIOMASS.

The structure of the wind tunnel restricted the number of angles that samples could be scanned from. For each fuel bed a laser scan was taken from two opposite sides (east and west). During the first period of sampling, the chamise fuel beds were also scanned from the south side (downwind end) of the wind tunnel. Scans from the north end were not possible due to the location of the fan assembly. The southerly scans proved to be problematic, and were not included in the analysis. Ghosting, difficulty with alignment, and asymmetrical representation of the fuel beds in the absence of a north scan precluded their use. For side scans, the T-LiDAR instrument was placed at 4 meters range from the leading edge of the sample and was set at a height of 1.4 m above the ground, approximately equivalent height to the middle of each shrub sample. Scan locations were marked with tape on the floor of the wind tunnel facility and the scanner was fixed on the tripod for the duration of the experiments to ensure nearly identical geometry between scans.

Focus distance for the collected data was set at 4.0 m and the spot spacing was held at 1.0 mm. Raw data from each scan were saved to an external USB thumb drive as well as the hard drive of the laptop PC being used to control the TLS.

2. *DATA MANIPULATION AND SCRUBBING*

As noted previously, the raw data produced by the ILRIS™ 3⁶D-HD TLS are contained in binary digital files that must be parsed into different formats for analysis. The Optech Parser v. 5.0.2.7 was used to create the data files used in this research. Following data collection, files were parsed into two formats: .pif and .xyz. While parsing data, a range gate was applied to all files at 2 and 10 meters to exclude data outside these ranges.

The .pif files were used in Polyworks™ IM Align software for the purpose of creating a rotation matrix to align and merge the easterly and westerly scans. The Polyworks software allows users to specify point pairs with which to align two or more different point clouds. For each replication the region of interest scanned was larger than the shrub so common points within the wind tunnel were visible in the point clouds to allow for manual alignment. Following manual alignment, the IM Align software was used to apply an automatic alignment algorithm. When properly aligned an alignment matrix was output for each file.

Intensity data were corrected using an algorithm written in IDL. The intensity values reported in the .xyz files were altered from the native 16-bit, binned data format to the continuous 9-bit scale as described previously. After the data were re-scaled, intensity was then range-corrected based upon distance from the laser scanner. The range correction was written based upon the relationship developed in Experiment 2. The .xyz files were again altered following range correction by applying the alignment matrices created in IM Align. After alignment, the files from each fuel bed were then merged into one. The resulting files included the scan data from both the west and east side of the shrub with rescaled and range-corrected intensity.

The aligned and merged files for each scan were then passed through a series of visualizations and clippings to remove any points that were not a part of the shrub itself. The first visualization was completed in Polyworks™ IM Survey, where a range gate was defined for the x, y, and z coordinates to exclude the majority of reflections not from the shrub. The range gate was applied while importing the files into ArcMap 10 using a definition query that left only the target point cloud within the range gate. The data were projected in two dimensions, typically in the x, y plane, and a shapefile was created to manually clip any of additional points that were not to be included in the description of the

shrub (e.g., points from the wind-tunnel structure itself). This was done using the 'select by lasso' tool in ArcMap, which allowed the user to specify a custom boundary around the shrub in two dimensions. Remaining points were then exported as a text file and re-visualized again in IM Survey to check for any remaining erroneous points. If points remained, the file was re-projected on the x, z or the y, z plane and the process of manually selecting the shrub was repeated to remove the excess points from the file. After the excess points were adequately removed from the file, a final text file was exported and then saved. Text files at this point were typically 150-250 megabytes in size.

There was considerable deliberation on how to represent the point cloud accurately, but effectively. The aim was to represent the geometric complexity of fuel beds while maintaining a usable file structure that was not so large it was not beneficial. Additionally, we wanted to remove very fine details that were irrelevant to fire behavior and fuels representation at the scale of this study. The method decided upon to represent the fuel bed was the creation of a volume grid matrix based on the point cloud information. The volume elements (voxels) in the volume grid were created by establishing a volume grid around the shrub structure and filling each voxel with information from the point cloud, (e.g., average intensity and number of points). The voxel dimension was 8 cm³, or 2x2x2 cm voxels. The voxel dimensions corresponded with the size of the fuel elements used for combustion experimentation in the flat-flame burner facility of collaborators at BYU.

Voxel creation was completed by establishing a grid of centroids spaced at 2 cm in all directions. From each centroid, a search was performed for data points within a box with sides positioned 1 cm from the centroid in six directions. For each voxel, the number of points and average intensity were reported and recorded in a new file. The file output was a text file reporting locations in x, y, and z coordinates with average intensity and point count attached, or x,y,z,i,c. Voxels were classified as empty if there were less than five points found in the space, and retained in the grid structure. This was done in order to ensure that voxels were not being reported as full if a minimal number of points were found in the space.

3. DETERMINING OPTIMAL POINT PER VOXEL DENSITY

The initial voxel volume creation used a threshold of five points per voxel to define whether or not a voxel was occupied. This was done to ensure that a voxel was not represented as occupied based upon a single point return within the volume. After the initial threshold was employed to create the data set, a sensitivity analysis was necessary to

inform the most accurate threshold to occupy a voxel or not. The analysis completed here was done to test at what point per voxel count the data were optimally represented when relating volume loss estimations to mass loss measurements.

Based on spot spacing each voxel created had the potential to contain 8,000 points. However, due to shadowing the actual number of points that could be detected within the space of a 2 cm voxel was 400 from each scan or 800 total based on scan specifications. The creation process placed a threshold of 5 points per voxel but the potential of voxels being classified as filled even though the target contained little biomass remained an issue. Partial laser returns on very small targets had the potential to define a filled volume whether or not the target was substantial enough to matter to the overall shrub description. As shown in experiment 1, the halo effect associated with partial laser returns could be falsely representing the size and shape of a target.

The analysis completed was used to test at what point density the voxel representation best described the amount of mass lost during combustion. Proportion of mass change was predicted based upon the proportion of volume change in the model. The number of voxels was used to represent volume for each shrub and mass measurements were taken prior to and following combustion. The number of points within a voxel that would mean filling the space with data was changed in order to represent a range of possibilities. The threshold placed on the number of points was truncated at 5, 20, 40, 60, and 80 points per voxel. In each trial the number of voxels before and after combustion was used to derive volume loss and proportion of volume lost. After each threshold was applied, a linear regression predicting proportion of mass loss based on proportion of volume lost was created. Each model was then compared in an ANOVA test. For statistical comparison, the model with the lowest Residual Sum of Squares, Residual Standard Error, P-Value, and highest R-Squared value was accepted as the best level to threshold point density within a voxel. The point per voxel threshold that most accurately predicted proportion of mass lost was then used for data analysis and representation.

Using voxel volume estimates to predict mass loss is discussed in further detail later in Phase II. However, each model created from the different thresholds was statistically significant and showed that volume loss was a fairly good predictor of mass loss. The model with the highest significance and most predictive capability was created at a 20 point per voxel point density threshold (Adj. R²: 0.8554, P-Value: 4.586 e-13) (TABLE II-1). The lowest

Residual Sum of Squares reported during the ANOVA test also indicated the model created at 20 points per voxel was the model with the least amount of error (lowest RSS at 0.186). The result of this analysis led us to use a 20 point per volume threshold for data representation and analysis.

TABLE II-1. DESCRIPTIVE STATISTICS FOR LINEAR REGRESSION MODELS CREATED AT DIFFERING POINT DENSITY THRESHOLDS.

Points Per Voxel	Intercept	Slope	RSE	Adj. R ²	P-Value	RSS
5	-0.020 ± 0.040	0.768 ± 0.063	0.087	0.8414	1.614 e-12	0.204
20	-0.052 ± 0.040	0.804 ± 0.062	0.083	0.8554	4.586 e-13	0.186
40	0.081 ± 0.054	0.620 ± 0.088	0.132	0.6366	1.32 e-07	0.468
60	0.041 ± 0.042	0.781 ± 0.076	0.101	0.7871	8.824 e-11	0.274
80	0.153 ± 0.041	0.673 ± 0.854	0.122	0.6859	1.788 e-08	0.405

Through the process of scanning and data transformation we were able to create a three-dimensional model representation of a constructed, diffuse-form shrub. Data produced from the original laser scan was altered significantly to produce a final structure that represented some of the intricacies of a diffuse-form shrub. The data sets created showed a high level of spatial heterogeneity in all three dimensions that were visibly comparable to images of the target structure (FIGURE II-D, FIGURE II-E). The models produced were a manageable size to allow data processing on commonly available computing technology. While clipped and aligned point clouds produced data files up to 250 megabytes, the voxel representations ranged from 13 to 54 megabytes in size. While each voxel was generalized within the 8 cm³ space it represented, the overall voxel arrays represented a large amount of structural variability that included descriptive variables for each space. The final voxel array was a manageable data set from which descriptive statistics could also be extracted. Point distributions and intensity information within defined areas of the shrubs were easily extracted from the data sets and representative of rich data sets, even after the generalization of voxels.

B. EVALUATE CONSTRUCTED MODEL FOR DESCRIPTIVE CAPABILITIES

1. OCULAR EVALUATION OF SHRUB MODELS

The models of each shrub fuel bed were spatially heterogeneous, but the accuracy of the descriptions was unknown. The complexity of the data sets in three dimensions made it difficult to verify accuracy in any other way than ocular comparison. For this comparison,

models were visualized in three-dimensions and then compared to RGB images of the sampled shrubs (FIGURE II-D, FIGURE II-E). The profiles of the shrubs were examined, along with canopy gaps and areas of obvious post combustion change. The constructed models corresponded with biomass visible in the images, and the geometry of the exterior of the shrubs appeared to be described consistently in the models. This was especially apparent in post-fire samples where remaining foliage was more spread out and larger gaps easier to identify. Overall, the external shape and dimensions of the shrubs appear to be well-characterized by the laser and relatively modest changes in the shrub architecture due to burning are detected. Of the concerns identified with using T-LiDAR to characterize diffuse targets, none are known to influence the location of an initial return. The first object the laser intersects (absent a hard target background) is generally well-described in location.

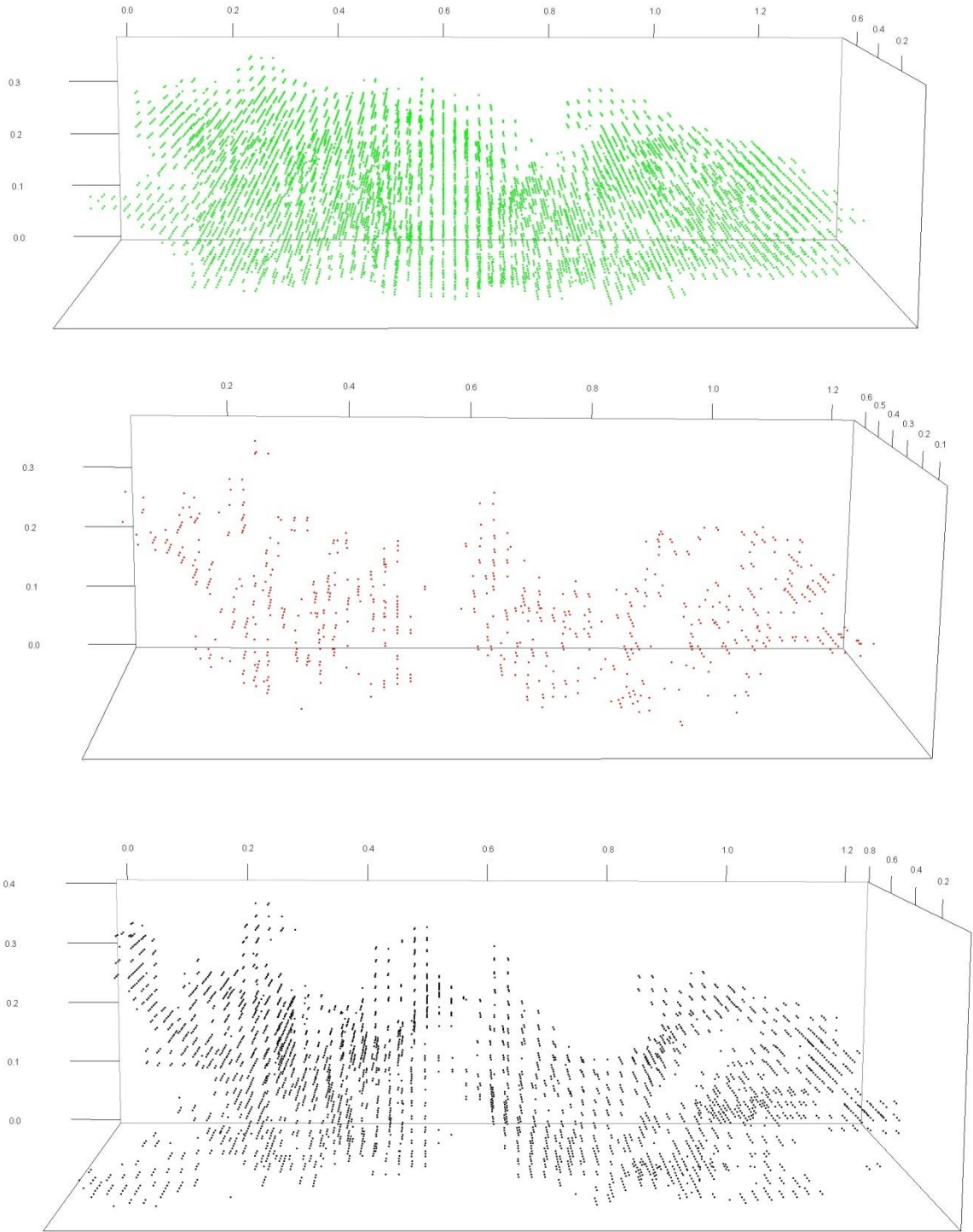


FIGURE II-D. VOXEL MODELS OF SAGEBRUSH SAMPLE 10. FROM TOP TO BOTTOM, PRE-COMBUSTION (GREEN), CHANGE FROM PRE- TO POST-COMBUSTION (RED), AND POST-COMBUSTION (BLACK).

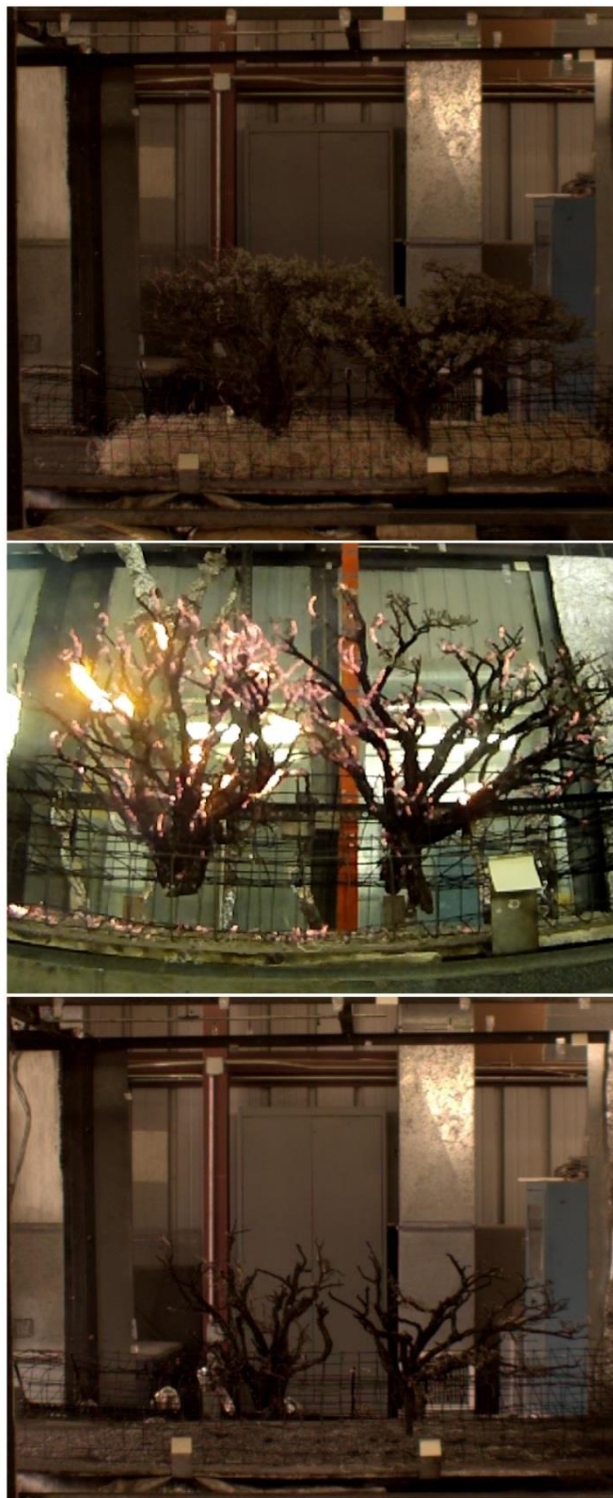


FIGURE II-E. PICTURES OF SAGEBRUSH SAMPLE 10. FROM TOP TO BOTTOM: PRE-COMBUSTION, DURING THE FINAL STAGES OF COMBUSTION, AND POST-COMBUSTION.

We could not verify the positional accuracy of individual points, but the qualitative evidence suggests that the voxel models fit the external dimensions of the shrubs.

2. *ASSESSMENT OF SHRUB INTERIORS*

Modeling the interior of the shrubs was likely inaccurate due to occlusion. Based on findings from the ghosting experiment (experiment 1), there is potential for points to occur toward the center of the shrubs as diffuse targets on the shrub hull align with hard targets in the background. 'Ghost' or 'air points' are the result of the two or more targets spatially close in the y-dimension that both return energy from the laser pulse and produce a single average return (Béland, et al., 2014). Separating these erroneous points from accurate returns would not be tractable.

Upon examination of shrub interiors, however, it became apparent that ghosting was not a significant issue. Rather, shrub interiors were largely void of any reflections (FIGURE II-F). When visualizing single planes in the center of the shrubs, substantial canopy gaps were evident where foliage material was expected to occur. Because the shrub fuel beds were constructed to distribute foliage material uniformly, there was a reasonable expectation that most of the shrub interiors were filled with material. The occlusion of data in the center of the shrubs was most likely due to the energy from the laser not penetrating the shrub hull. When laser energy is intercepted at the first piece of material, locational data are only collected for that material. Although some TLS instruments do allow for multiple returns from the same energy pulse after passing through semi-transparent material (Béland, et al., 2014), the ILRIS 3⁶D is not capable of detecting more than one reflection per pulse. In order to better understand occlusion within shrub interiors, we set out to identify the depth of penetration of the laser and the amount of volume not identified as being filled during the voxel model creation.

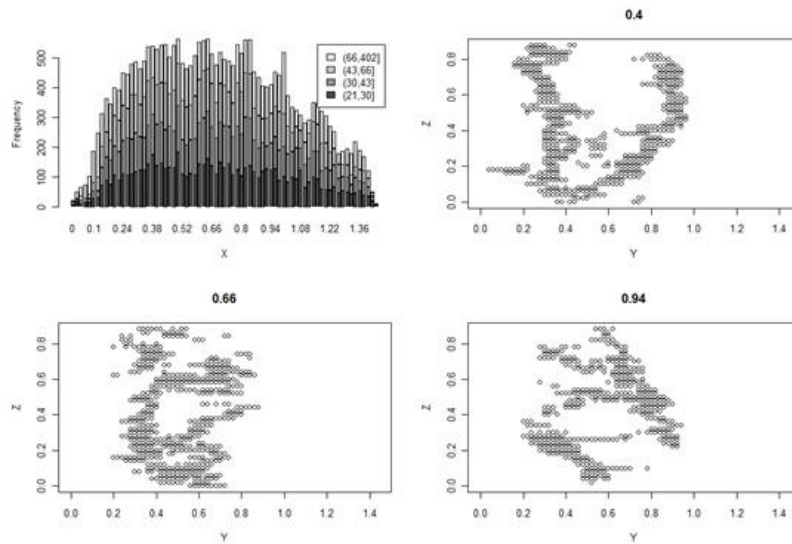


FIGURE II-F. TOP-CHAMISE SAMPLE 9 PICTURED ON THE Y-Z PLANE. BOTTOM (LEFT TO RIGHT, TOP TO BOTTOM) X-AXIS VOXEL FREQUENCY PLOT, Y-Z PLANE PLOTS OF VOXEL LOCATIONS, EACH A SLICE FROM 40 CM, 66 CM, AND 94 CM ALONG THE X-AXIS (25TH, 50TH, AND 75TH PERCENTILE).

a) **Methods**

Quantifying the amount of missing filled volume in the center of the voxel was done by counting the number of filled and unfilled voxels on single lines of data along the y axis (through the shrub). Lines of data were evaluated at nine different locations within six voxel models for each species for a total of 108 replications, from the twelve shrubs represented. The lines of data were located at the 25th, 50th, and 75th percentile values along the x-axis and at 0.2, 0.4, 0.6 m or 0.1, 0.3, 0.5 m height on the z-axis, respectively, for chamise and

sagebrush shrub models. Shrubs selected for this analysis were even-numbered chamise and odd numbered sagebrush trials. This method of assessment was selected because the only 'lost' volume in the center of the shrub was along the y axis due to occlusion along the direction of the scan. Because the proportion of voxels missing in one direction is directly related to the total volume, using a voxel count on only the lines of data assessed was an acceptable method of determining the total amount of missed volume. The proportion of missing voxels to total voxels was then plotted in a density histogram and fit with a statistical distribution.

b) Results

The depth of laser energy penetration and subsequent description in the models averaged 5.45 ± 2.27 voxels (10.9 ± 4.54 cm) (FIGURE II-G). Interior of this depth is mostly void except in cases where the total shrub width is less than ~ 24 cm. When expressed as a proportion of total width of shrub, the void space ranges from none to more than 75% of the total width (FIGURE II-H). In more than a quarter of the lines sampled, the length of the data was fully described and there were no voxels left unfilled in the model. In about half of the data lines, one third of the shrub was not described. At the least descriptive data line, the filled voxels represented 18% of the length sampled. The statistical distribution that best fit the proportion histogram was a logistic distribution. The resulting logistic model had a location of 0.305 with a scale of 0.156 with corresponding standard errors of 0.027 and 0.012. The Akaike information criterion (AIC) for the model fit was 25.9.

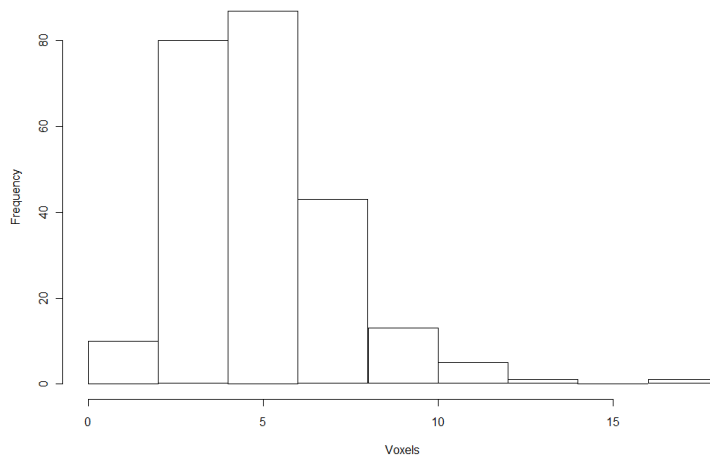


FIGURE II-G. HISTOGRAM OF THE NUMBER OF VOXELS COUNTED ALONG THE EDGE OF A SHRUB MODEL EACH VOXEL REPRESENTS 2 CM OF LASER PENETRATION INTO THE SHRUB ALONG THE Y-AXIS.

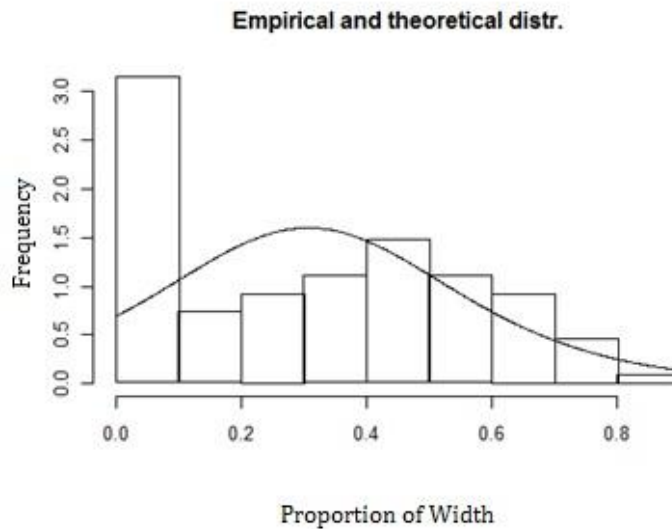


FIGURE II-H. HISTOGRAM OF PROPORTION OF TOTAL THAT WAS NOT REPRESENTED IN THE CENTER OF THE VOXEL MODEL. BARS ARE OBSERVED PROPORTION OF 'LOST' DATA AND THE LINE IS THE LOGISTIC MODEL FIT TO THE DATA.

c) Analysis

The empirical distribution of proportion empty space across the shrubs shows that the majority of the shrub volume located interior of the structure is represented, but a portion of the center is missing due to occlusion caused by the exterior of the shrub. For the purpose of this research, the logistic distribution was used to create a statistical adjustment that was applied to the volumes described in the data sets. The logistic distribution model was applied to the volume as a multiplying factor where a random number was selected for each voxel within a shrub. The numbers generated from the random number selection were then used to increase the total number of voxels. This was done to more accurately represent the volume described. It was a means to empirically adjust for the 'lost' data in the center of the shrub.

Representing shrubs with a hole of missing data is troublesome for the purpose of application to fire behavior modeling. Solving the problem of describing interior volume could be accomplished through several methods, all of which necessarily depend on the assumption the holes are fully occupied by material (e.g., no gaps). The most logical method to fill this empty space would be to search in each direction around each unfilled voxel, and if the search encountered a filled volume in every direction around that voxel, it would then be filled with a value (either a constant or derived from a statistical distribution). This logic would fill the volumes in the center of the shrub while maintaining the observed heterogeneity of the exterior shrub structure. This avenue for filling the unaccounted for volumes has not yet been pursued.

C. EVALUATING MODEL POTENTIAL FOR TRACKING FUEL BED CHANGE

Having achieved the goal of creating realistic three-dimensional models and addressing their shortcomings, the focus of this research shifted to testing the application of the models. The most direct application was comparing changes in volume associated with combustion and mechanical removal with changes in mass. The arrays of voxels lent themselves to a simple, yet direct, estimation of volume. Because each voxel represented 8 cm³ volume, the sum of all filled voxels (x8) represented the total volume of a fuel bed. This total volume was then compared with biomass pre- and post- treatment and with mass loss following treatment. This comparison assumes a direct relationship between volume and mass that is largely untested. However, the fuel bed volume estimate represents a large improvement over previous methods (cubes and spheres), and biomass is the only systematic 'field' measurement available. The mass measurements were taken during experimentation and put to use without adjustment. Both the volume estimates and mass measurements were taken from the two Riverside combustion experiments and a laboratory experiment performed in Missoula.

1. *COMBUSTION MASS LOSS*

The variety of burning conditions produced in each replication provided a range of consumption amounts and mass losses within the shrub structures. Mass loss during combustion ranged from 5.2 to 82.5 percent of total wet mass. Using volume estimates derived from the voxel arrays, volume loss was compared to mass loss for each replication, in sagebrush and chamise. Volume loss during combustion ranged from 21.1 to 92.7 percent of pre-combustion volume.

a) Methods

As noted previously, volume was represented by summing the number of voxels containing greater than 20 data points (filled voxels). In order to address missing (occluded) volume in the center of the shrubs, the logistic distribution created in the previous section was applied to the voxel counts. The logistic distribution model was applied to the volume as a multiplying factor where a random number was selected for each voxel within a shrub and then used to increase the total number of voxels. Adjusted post-combustion volumes were then subtracted from adjusted pre-combustion volumes to produce an estimate of total volume lost during combustion. Total mass following combustion was subtracted from total mass prior to combustion to provide mass loss for each trial. The method of statistical comparison was a multiple-linear regression analysis relating mass loss to volume loss and species burned.

b) Results

The multiple linear regression proved robust and highly significant (F-stat: 50.52 on 2 and 26 DF). The model (shown below) was produced using R statistical package where M_{loss} is mass loss in grams, Vox_{loss} is volume loss in voxels, and $Spec_{Sage}$ is the specification for species burned. The model accounted for 78% of the variability (Adj. R²: 0.7796) in mass loss and each predictive variable and the intercept were significant (P-values: Vox_{loss} 2.23 e-10, $Spec_{Sage}$ 9.72 e-06, Intercept 0.00415) (FIGURE II-1).

$$M_{loss} = Vox_{loss}(0.1398) + Spec_{Sage}(1277) - 982.9$$

$$Spec_{Sage} = \begin{cases} 1 & \text{for Sage} \\ 0 & \text{for Chamise} \end{cases}$$

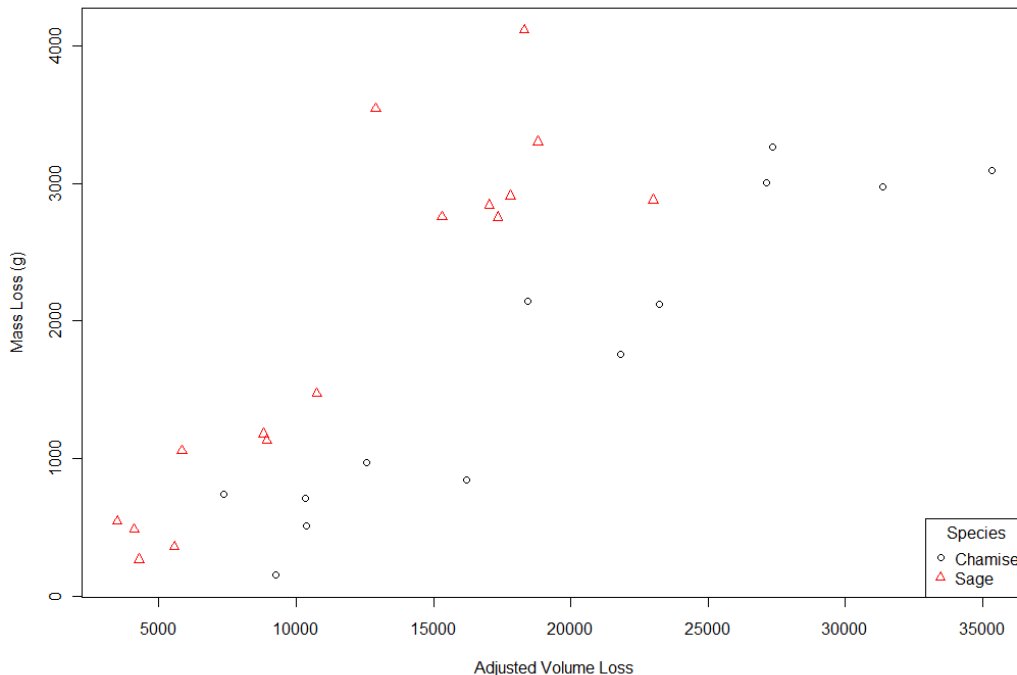


FIGURE II-I. MASS LOSS AND ADJUSTED VOLUME LOSS DURING COMBUSTION OF DIFFUSE FORM SHRUBS.

c) Analysis

The strong correlation between the loss of volume and the loss of mass showed that the T-LiDAR can be used to assess changes in biomass following combustion across a range of losses on a per shrub basis (FIGURE II-I). Near constant variance across the range of mass losses shows that the TLS can detect changes in the fuel bed effectively even when only parts of the fuel bed are consumed. Although the model does not numerically depict where the loss is occurring in the shrub fuel bed; ocular assessment of change shows that the TLS identifies the locations of mass loss (FIGURE II-D, FIGURE II-E). This is an important consideration for fire modelers wishing to track propagation of fire through the shrubs. The ability to accurately model mass loss using voxel volumes suggests that the application of TLS in diffuse-form shrub may be useful to fire modelers despite shortcomings identified previously. The regression also showed a significant difference between mass loss in chamise compared with sage (Intercept adjustment: 1277 g). The mass removed during combustion was different between the two species and this was represented in the voxel volumes. The linear regression fit the same slope to both species showing that the same mass loss to volume loss relationship was significant. However, the different intercepts

show that sagebrush volumes are represented as being denser and account for more mass loss with less volume than those of chamise.

d) Discussion

This comparison of volume loss to mass loss showed that T-LiDAR can detect the removal of biomass from a fuel bed across a full range of consumption. In instances of complete combustion, the laser correctly interprets an empty volume (less the large branch stubs remaining). The more interesting capability of the laser is the ability to detect partial mass loss that appears to be spatially explicit. When portions of a shrub were removed in the flaming front the laser detected changes from pre- to post-combustion and reported it as a change in volume (FIGURE II-I). Ocular comparison with photos and video show that the volume loss occurred in the correct locations (FIGURE II-J). While it is difficult to infer that the voxel arrays accurately portrayed mass loss in the center of the shrubs, the exterior geometries were altered in ways that were visible in the models. Further, there were no instances when the center of the shrubs burned and the hull did not, and this occurrence is not ever likely. Accurately locating the area in which mass was removed was not isolated to one or two instances in the samples but was the trend among all voxel models. The difficulty in directly comparing the two for a creation of a vegetation burned description came from the change in structure following combustion. One major shortcoming of this mass loss work was inability to produce a spatially explicit comparison of pre- and post- combustion scans when most of the biomass was removed by fire. In such cases, the structural integrity of the shrubs was lost during combustion and the remaining branch butts shifted and fell. The movement of branch stalks during combustion made it unfeasible to directly compare post-fire voxel arrays to pre-fire arrays in the context of creating constant geometry between scans.

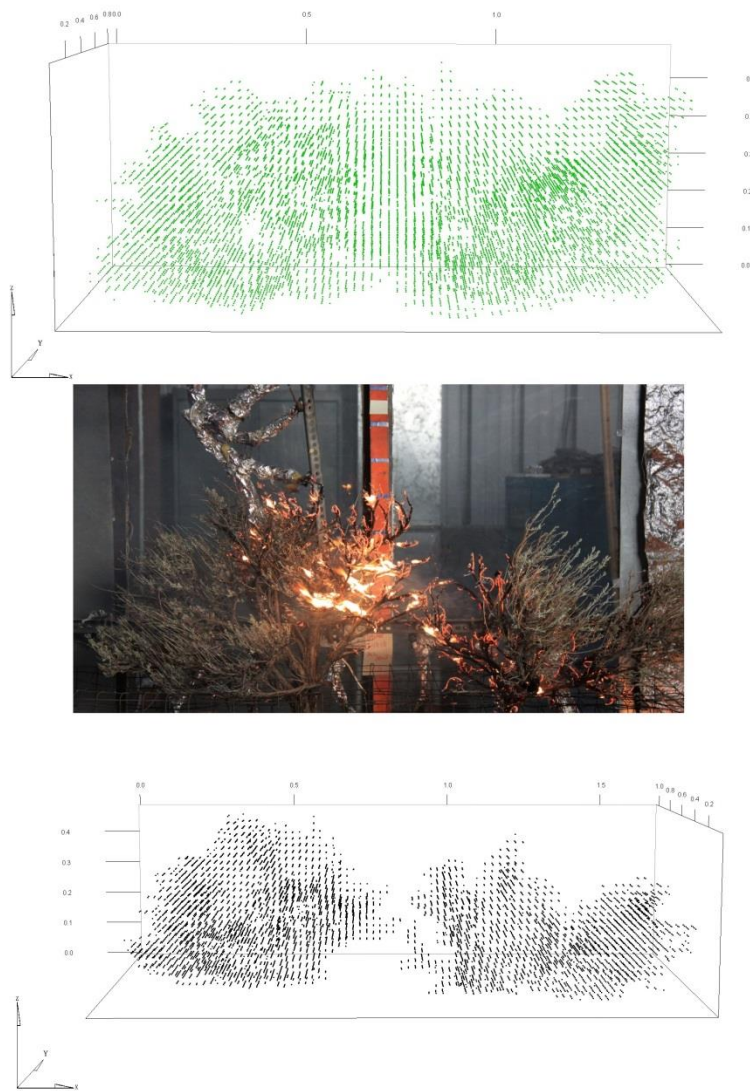


FIGURE II-J. SAGEBRUSH SAMPLE 1. PRE-FIRE VOXEL REPRESENTATION (TOP), PICTURE OF SAMPLE NEAR THE END OF COMBUSTION SHOWING WHERE MATERIAL WAS REMOVED (MIDDLE), AND POST-FIRE VOXEL REPRESENTATION.

2. *SIMULATED MASS LOSS*

Following combustion experiments, a third test was conducted to determine whether the T-LiDAR instrument could detect changes in mass associated with removal of different kinds of material (e.g., foliage-and-branches, branches-by-size-class, random). This experiment was conducted for chamise only. The purpose was two-fold: first to examine the sensitivity of volume loss to mass loss of different types of material; second to test whether random removals of material were detectable by laser-measured volume loss.

a) **Methods**

Samples of chamise were shipped from Riverside, CA to Missoula, MT for experimentation as outlined in the common methods of Phase I. Six branches were selected with similar masses, diameters, and dimensions (TABLE II-2). Each branch was sampled systematically by three methods with laser scans completed between each branch modification. The first method, termed foliage and diameter, was completed by removing all the needles, then removing branch wood sequentially by diameter thresholds. Branch wood was removed first at a diameter of one millimeter, then two, up to five millimeters. Each time a branch was altered, the removed material was collected, weighed, and kept separate from other samples. The second method, termed diameter, involved removing material from the branch in the same sequential fashion as above, but foliage was left on the branch. The third method, termed random, was done to mirror the amount of material lost in the second method, but with no consideration given to the size or location of the material removed. In short, material removed from the second replicate was weighed between each iteration and an equivalent weight was randomly removed from the third at each iteration. All removed material was collected separately, bagged, and dried at 75° C for a period of 24 hours to obtain dry weight.

TABLE II-2. BRANCH DESCRIPTIONS FOR SIMULATED MASS LOSS SAMPLES.

Branch	Height (cm)	Weight (g)	Base Diameter (mm)	Replicate
1	101	171	14	Foliage and Diameter
2	98	164.5	12	Diameter
3	108	176	12	Random
4	91	217.5	17	Foliage and Diameter
5	94	239.5	15	Diameter
6	99	214.5	14	Random

The ILRIS 3⁶D-HD TLS was used to collect a scan each time the branches were altered. The scanner range to target was 4.5 meters, corresponding focus distance. Spot spacing for each scan was 1.0 mm. Scans were processed in the same fashion as point clouds from the combustion experimentation described above and a voxel array was produced for each branch, replicate, and removal. The resulting data set produced 38 voxel arrays. Statistical analysis completed on the data set was creation of a multiple linear regression relating mass to voxel volume using variables of the type of removal.

b) Results

The multiple linear regression proved robust and significant (F-stat: 71.5 on 3 and 34 DF). The model (shown below) was produced using R statistical package where M is mass in grams, Vol is volume in voxels, and Rep is the specification for type of mass removal. The model accounted for 85% of the variability (Adj. R^2 : 0.8511) of mass using volume and mass removal method. The volume predictor was highly significant (P-value: <0.0001) but only the random mass removal method was discriminated from the others in the model (P-value: 0.003). The diameter based removal of mass was not significantly different from the foliage and diameter method (P-value: 0.6286).

$$M = Vol(0.0355) + Rep_{Rand}(-21.66) + Rep_{Seq}(-2.66) + 57.80$$

$$Rep_{Rand} = \begin{cases} 0 & \text{If Foliage and Diameter} \\ 0 & \text{If Diameter} \\ 1 & \text{If Random} \end{cases}$$

$$Rep_{Seq} = \begin{cases} 0 & \text{If Foliage and Diameter} \\ 1 & \text{If Diameter} \\ 0 & \text{If Random} \end{cases}$$

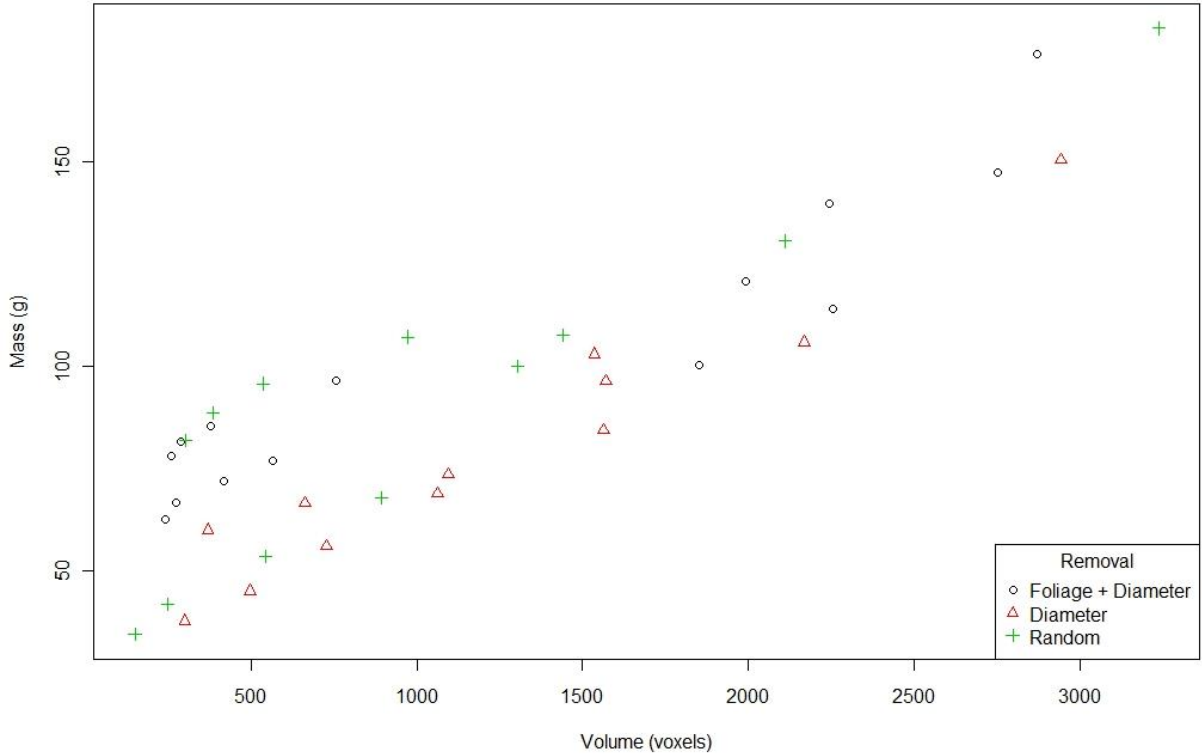


FIGURE II-K. MASS AND VOLUME DURING SIMULATED MASS REMOVAL FROM CHAMISE BRANCHES.

c) Analysis

The relationship between manual removal of mass and volume perceived by the voxel array remained robust when the method of removal was simulated, similar to combusted. The observed relationship showed that mass increased predictably with increasing volume. The volume representation did discriminate between random removal of mass and a diameter-based removal. However, the diameter-based, sequential removal of biomass was not significantly different between foliated and non-foliated branches. The voxel models showed change that occurred during each step of removal (FIGURE II-L, FIGURE II-M). The model also showed a significant difference between random removals and diameter based removals. It is likely that biomass removed in an occluded area was not represented during the change from one replication to another. It is more likely that the TLS produced models would show a diameter based biomass removal because that method inherently removes the top and sides from the branch, areas in which occlusion is not as prevalent.

The ability of the TLS to detect mass loss in a controlled experiment indicates that there is utility in detecting change to highly diffuse targets. More specifically, the ability to detect random mass removal indicates that the laser is spatially explicit in its ability to detect change. The voxel arrays were able to track mass loss with high significance, but the random removal of material indicates that the laser detects biomass removal even if it is not just removed from the exterior of the branch sample.

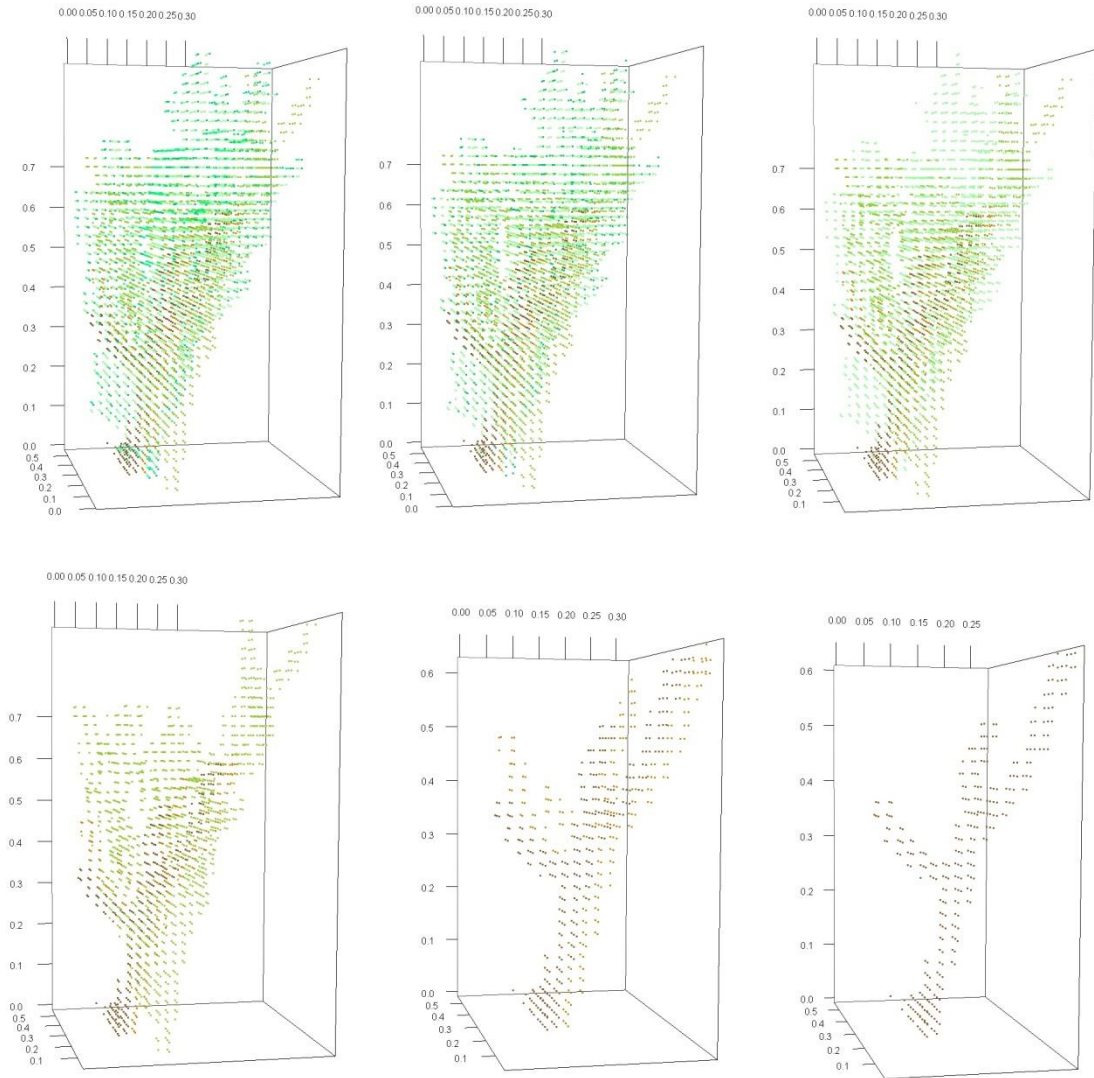


FIGURE II-L. VOXEL MODELS OF BRANCH THAT UNDERWENT A DIAMETER REMOVAL. LEFT TO RIGHT, TOP TO BOTTOM: UNALTERED BRANCH, <1MM REMOVED, <2 MM REMOVED, ETC. UNTL >5MM REMAINDER.



FIGURE II-M. PICTURES OF BRANCH THAT UNDERWENT A DIAMETER REMOVAL. LEFT TO RIGHT, TOP TO BOTTOM: UNALTERED BRANCH, <1MM REMOVED, <2 MM REMOVED, ETC. UNTL >5MM REMAINDER.

D. ATTRIBUTING FUEL ELEMENTS WITH BULK DENSITIES

The previous research has demonstrated that the voxel models produced from TLS are effective at characterizing mass loss when shrubs are altered through combustion and mechanical treatments. Ocular assessments show that biomass changes in the shrubs are

spatially consistent with observed changes in the voxel arrays. A primary shortcoming of the shrub models, however, remains the uncertainty in how much material resides in each voxel. Given the inevitable occurrence of shadowing (and perhaps ghosting), it is difficult to predict mass of individual voxels directly. An alternative approach is to develop a statistical distribution of mass per voxel (e.g., bulk density) that can be applied to whole shrubs. The numerous measurements of samples taken during this study provided many observations with which to create a statistical distribution of bulk densities for voxel values of chamise samples. By measuring mass and estimating volume, a method was derived to predict bulk densities for sampled shrubs. This method was applied to whole-shrub fuel beds by predicting mass based solely upon the TLS measured volume and a statistical estimation of density. The motivation for this line of inquiry was to demonstrate an application TLS data to predict the amount of biomass resident within a sample without measurements aside from the laser scan.

a) Methods

Estimates of bulk density were derived from each experiment where mass data were collected (Phase I: Experiment One and Phase II). For the 2 cm samples taken in Experiment One, each samples fit within a single voxel. In the combustion and simulated mass loss experiments, bulk densities were estimated by dividing total mass by the number of voxels in the array for a given sample. The voxel counts were adjusted in the combustion voxel arrays based on the empirical volume relationship created in a previous section (the holes within the shrub centers were filled and added to the voxel counts for each fuel bed). Weights were reported as a density in grams per voxel and done only for chamise samples. Because wet weight was the only reportable measurement for pre-combustion arrays, all values were based upon wet weight for each sample. The density histogram was fit with a gamma distribution to describe the variability in bulk density per voxel.

Mass estimations were performed only for pre-combustion arrays because predicting mass for post-combustion arrays would involve a separate density distribution that was not producible from the available data. Using the empirical volume adjustment and the density distribution, mass was predicted for the 13 pre-combustion chamise shrubs. Mass was predicted by first adjusting the volume according to the volume loss distribution. This was done by producing a random array of values based on the logistic distribution for volume adjustment. The resulting values produced a number of voxels to add to the partial volume to provide a logical voxel count that included an adjustment for the missing volume

on the interior of the shrub. With the adjusted volume a gamma distribution for density was then applied to each voxel. For each voxel within a shrub or branch a random density value was selected from the gamma distribution. The density values were used to derive masses that were then summed to produce a total mass for the shrub. The resulting total mass was the predicted weight based on the TLS produced volume. Total predicted mass was then plotted against the actual mass measurements for each sample and fit with a linear regression model.

b) Results

The distribution of voxel densities was best represented by a gamma distribution, as the majority of the values were small (FIGURE II-N). The voxel densities of chamise voxels ranged from .009 to 1.805 g/voxel. The 75th percentile of the density distribution was at 0.332 g/voxel showing that the majority of density values for chamise were low and very few densities were large by comparison. The gamma distribution fit to the data estimated a shape of 1.06 and a rate of 4.03 with an AIC of -88.7. The empirical data were also fit to a Weibull distribution which reported an AIC of -88.5.

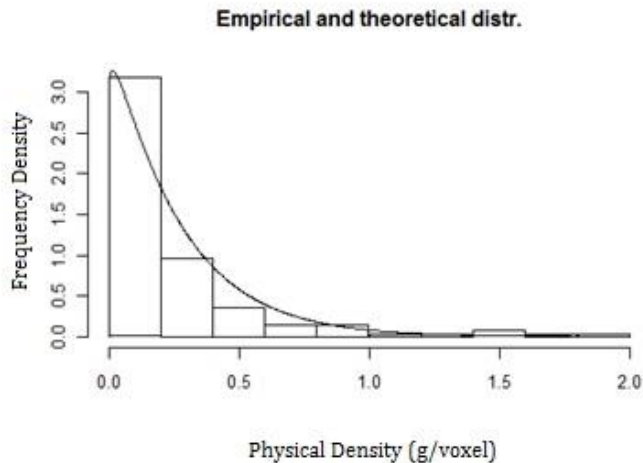


FIGURE II-N. HISTOGRAM OF VOXEL DENSITIES FOR CHAMISE SAMPLE WITH PREDICTED GAMMA DISTRIBUTION. BARS INDICATE OBSERVED FREQUENCIES AND THE LINE INDICATES THE GAMMA DISTRIBUTION FIT.

Predicted mass estimates consistently overestimated the observed mass measurements, but the predicted mass produced a linear regression model that accounted for ~59% of the variability within the measured mass values (Adj. R²: 0.598) (FIGURE II-O).

The linear model produced was robust (F-Statistic: 18.85 on 1 and 11 DF). The slope for the model was significant, but showed a prediction curve that was very close to a 1:1 relationship (Estimate: 1.022, P-Value: 0.00117). The intercept was not significant (Estimate: -3295, P-value: 0.1104) but helped to account for the majority of over-predicting mass. The resulting model is shown below, where M_{Emp} is the empirical, measured mass and M_{Pred} is the predicted mass value:

$$M_{Emp} = (1.0222)M_{Pred} - 3295$$

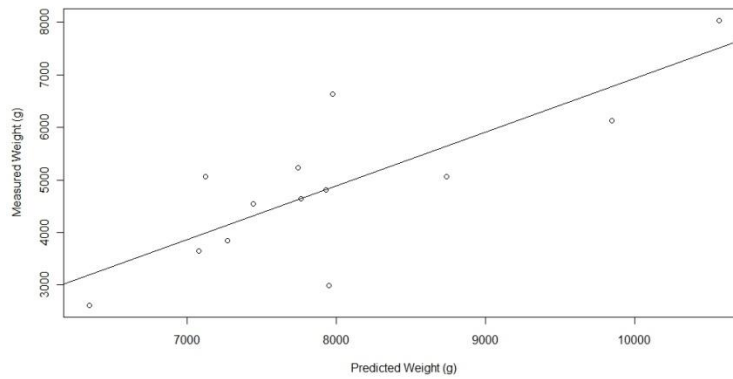


FIGURE II-O. TLS VOLUME PREDICTED MASS PLOTTED AGAINST MEASURED MASS VALUES.

c) Analysis

The linear regression model showed that using TLS-produced volumes to predict mass is a viable method of mass estimation without the need for destructive sampling. This portion of the research was meant to create a model that was to be validated against empirical observations and the one consistent measurement taken throughout this project was mass. By predicting mass from the voxel volume arrays, we were able to validate the descriptive capacity of the TLS derived data on a per-shrub basis. Applying a density distribution to each voxel within the volume allowed attribution of each piece of data with a randomized value representing of the range of densities observed within chamise shrubs. By attributing the data with an empirically defined range of densities, the linear regression model reveals that a high percentage of variability in measured mass was accounted for in estimated mass (FIGURE II-O).

Accounting for missing data in the center of the shrubs introduced significant limitations to the methodology of creating shrub models. The statistical adjustment

approach completed was not meant to be a temporary solution to allow for more accurate inferences by applying measured, empirical data. Additionally, accounting for the missing voxels in the center would allow for better attribution of physical characteristics, rather than reliance on an empirical relationship. The empirical approach did allow us to account for missing volume data where it would have otherwise not been assessed. The result was a model that, although statistically descriptive, was ultimately creating a spatially heterogeneous model with characteristically homogenous attributes.

E. SHRUB MODEL DISCUSSION

The creation of a three-dimensional model that was representative of diffuse-form shrubs, but still usable from a data processing perspective, proved to be an achievable task. The model produced in this research was a reasonable, three-dimensional depiction of the shrubs studied. Ocular inspection of the digital models showed that the models were spatially explicit and the continuity of data on the surrounding edges represented a fairly good description of the exterior of all scanned samples. The developed methodology minimized the trans-location of points away from the target of interest but it was not possible to accurately differentiate points from one another within the hull of the shrub. The hole in the center of the shrub models indicated that occlusion is an issue for describing the interior of samples. While not achieved in this study, a shrub model that accounted for the missing volume in the center and could apply specific physical attributes would greatly impact the state of fuel bed and fire behavior modeling.

The application of T-LiDAR made for a repeatable, efficient method for assessing the structure of a diffuse form that has historically been difficult to characterize. Using T-LiDAR to map structural properties across a landscape has proven to be effective (Akay, et al., 2009), but the application of the technique at fine scales has only been recently attempted in the literature (Omasa, et al., 2007). Our goals with developing a methodology for T-LiDAR use on the scale of a single shrub were to create a spatial model for use in fire behavior simulation and produce a base of knowledge that can be used for further research. We have shown that the technology is effective at interpreting the structure to a higher degree of detail than traditional fuel models (Scott & Burgan, 2005). If the majority of variation in mass loss can be predicted on a fine scale, it is likely that the application of T-LiDAR will prove useful on broader scales.

The voxel arrays were highly descriptive and showed utility, but issues remain with the integrity of the data sets that must ultimately be addressed. The primary concern associated with using the laser to assess diffuse structures is shadowing. Occlusion of the interior of the shrubs was shown to impact the accuracy of the voxel volume descriptions in the center of the volumes. An empirically derived distribution was used to adjust the volume to represent a hypothetically fully filled volume for the purposes of this study. While this is a short-term fix to the problem of omitting interior material, it allowed an improved representation of the volumes for mass and bulk density prediction. A more robust solution could involve filling interior empty voxels by searching surrounding voxels for filled space and identifying those that are entirely surrounded by biomass. This solution still assumes that all space within the interior of the shrub is filled, yet this assumption is reasonable based on how the fuel beds were constructed.

We found that ghosting when a diffuse target was in front of a discrete object (Phase I- Experiment One). The experiment in Phase I identified ghosting as a concern for scanning, specifically on the influence of discrete, bright backgrounds when scanning diffuse targets. This may have been from the instrument averaging points that had partial returns in multiple locations. So, if a laser point coincided with part of the target and part of the background, the laser reported that point in between the two actual locations. It is possible that ghosting also occurred within the structure of the diffuse-form target, without the influence of a background. With such a non-discrete target, points created in the interior of the model structure have the potential to be the result of partial-return point information that was averaged by the instrument (Béland, et al., 2014). There is no way to discern the accuracy of point location within the shrub structure with the information that was collected during experimentation and this is a subject that should be researched in the future. While this is a concern for scanning with a discrete object, the laser was shown to only be able to penetrate an average of 10-12 centimeters of the chamise or sagebrush shrubs. The data points within that penetration area would be averaged within that space in both location and intensity. This concern shows the need for further understanding of ghost points, but it is underscored by the inability of the laser to describe the whole depth of the shrub.

The use of intensity to better describe characteristics of the target, although interesting, proved difficult to apply when creating the volume array models. We found that increased intensity values within a small area were associated with an increase of biomass

(Phase I- Experiment 3). While the general premise of the relationship could be applied to the full-shrub data sets, the values associated with the linear regression were not unusable for this purpose. The reason for the linear regression not being applicable was the scale of samples being used. In the 2 cm sample relationships, the average intensity used to model against biomass was an average for only that 2 cm sample with no surrounding values. The 2 cm sample averages included partial return points around the edge (halo) that lowered the average intensity (FIGURE I-H). It was evident from whole shrub scans that the 2 cm voxels created from full shrubs did not have the same halo effect because the partial returns surrounding each point in the volume included point values from neighboring voxels. Rather than having low-intensity halo points, each 2 cm area in the shrub volumes had equivalent or higher intensity values contributing to the average intensity within the specified voxel. Applying the linear regression created in Phase I resulted in gross over-estimations of total mass for the shrubs created in Phase II. While the estimates of mass were not accurate, the general principle of associating intensity with mass was a reasonable assumption (Phase I- Experiment 3). The relationship between intensity and mass could still prove useful with additional research.

The product of this research was a volumetric description of a diffuse-form shrub that was surveyed prior to destructive sampling. The models produced describe three-dimensional geometry and show heterogeneity within the sampled volume. The models created demonstrate the applicability of T-LiDAR technology in describing fuels in great detail while still retaining the structure and heterogeneity for other sampling, in our case, destructive sampling done through combustion or manual mass removal. When sampling fuel beds, traditional descriptions rely upon representation and estimation. For example, in order to model fuels in fire behavior, researchers have been forced to destructively sample a neighboring plot to produce an estimate, while using a separate plot in burn experimentation. We have shown how T-LiDAR can create a descriptive representation of the same sample that is used in combustion, thereby potentially improving the association between fuel model description and fire behavior model inputs.

III. PROJECT DISCUSSION

The motivation for this research stemmed from the need to improve characterization of fuel beds for physics-based fire behavior simulations and to develop

shrub fire models that consider spatial heterogeneity of fuel elements. Airborne LiDAR has been applied to map fuels across the landscape and has been shown to increase the descriptive capability of fuels modeling on broad scale samples (Andersen, et al., 2005). Our results indicated that T-LiDAR is applicable on fine-scale fuel beds as well as useful in the creation of three-dimensional descriptions. The project was successful in establishing sampling protocols for laboratory settings produced realistic three-dimensional descriptions of diffuse-form shrubs. The base of knowledge provided by this study provides a starting point for improving the methodology and application of this tool in natural environments.

Diffuse-form shrubs were the target of interest for this research because of their atypical physiology and difficulty to describe in reliable, repeatable fashion. The species of interest were sagebrush and chamise, both of which are dominant species that make up primary components of two different wildland fire fuel models. Sagebrush has been modeled as a fuel using the crown dimensions of the plant with high predictability and has been tested against various stages of the life-cycle of the sampled plants (Rundel & Parsons, 1979; Frandsen, 1983; Cleary, et al., 2008). Chamise, on the other hand, has seen limited predictive evaluations of biomass and structure in the available literature (Countryman & Philpot, 1970). Obtaining crown dimensions was not addressed in this research because the data sets produced were more detailed and precise than field measurement and could allow for countless arbitrary selections of crown diameters. Additionally, the shrubs produced in the laboratory were artificial reconstructions of natural shrubs that were built to represent a variety of burning conditions, not necessarily natural shrub structures. Previous biomass assessments of diffuse form shrubs were completed using diameter and height measurements and were shown to be fairly descriptive of the shrub structures (Murray & Jacobson, 1982). The nature of TLS point clouds lend themselves to measuring diameter and height remotely without the need for manual measurements or altering the structure. While we did not pursue this approach during our study, the richness of TLS data sets easily allow for manipulation and the extraction of length, height, and width measurements.

Fuel bed modeling in the past has been used to provide a quantification of natural fuels present on the landscape for the purpose of providing numerical comparisons and inputs for fire behavior modeling (Brown, et al., 1982; Scott & Burgan, 2005). The method developed in this thesis, while not a traditional fuel model, shows great potential to derive descriptive values necessary to make up fuel model descriptions. With little adaptation,

these models have proven useful in estimating volume and biomass, allowing the user to derive a rough estimation of bulk density. The estimation of bulk density derived in this study was a statistical distribution of the chamise samples that were harvested for this project. The methodology used to create a distribution of bulk density values represents progress in understanding the form of chamise and the range and variability of bulk density. The distribution of bulk densities derived during this study was appropriate for this specific research. However, the methodology could be broadened to account for a wider range of samples that are more representative of a chamise plant, as a whole, from stalk to tip.

Our research shows its greatest potential outside of the laboratory and in the natural environment. The plants studied in this research are not only spatially heterogeneous within a single shrub, they are distributed heterogeneously across a landscape. The use of LiDAR, is increasing in the available literature as a viable means to determine forest characteristics on the landscape (Hopkinson, et al., 2004; Watt & Donoghue, 2005; Akay, et al., 2009) and also in ecosystems other than forests, such as the sagebrush-steppe ecosystem (Vierling, et al., 2012). The ability to locate shrubs on a landscape and describe in greater detail their volume and distribution presents users with the ability to rapidly collect a per-plant assessment of biomass, rather than a line-intercept estimation of fuels present. Different methods of TLS data processing have shown to be highly descriptive of biomass as well, suggesting that there are several ways to interpret LiDAR data and arrive at reasonable assessments of aboveground biomass (Olsoy, 2013). Our methods focused on one approach, but the general techniques and measurements derived through volume-based biomass estimation have even more potential. More fundamental work researching and improving this line of application is warranted.

The volumetric models presented here represent a substantial shift from traditional fuels models and simple fire behavior model inputs. Traditional fuels models assume homogeneity and continuity, which is a largely unrealistic description of landscape fuel beds (Anderson, 1982; Scott & Burgan, 2005). These assumptions are made in order to meet the requirements of simple fire behavior models that are used widely in operational fire management (Rothermel, 1972). Three-dimensional, detailed, computational fluid dynamics models have demonstrated sensitivity to heterogeneity in tree crowns (Parsons, et al., 2011), lending credibility to the argument that a diffuse-form shrub might better be described in detail, rather than in uniformity. This assumption has not yet been tested in new fire models, but needs to be before much additional TLS research is completed.

Understanding the heterogeneity of landscape fuel beds has been the subject of research using TLS in other, more continuous fuel types and is being lauded as a method to connect fire behavior models with empirical studies in an effort better predict fire dynamics and mixed fire effects (Hiers, et al., 2009). While rudimentary in their descriptive capability, the shrub models that were created in our study represent an initial step in the sampling diffuse-form shrubs for the purpose of characterizing the heterogeneity of a sparse and complex fuel bed in its natural environment. The benefit of using TLS in this setting allows for a preliminary description of the dynamism of the fuel structure and distribution. This description can then be used for fire behavior studies without having to generalize the landscape. By increasing the descriptive capability of fuels models we show great potential to increase the predictive ability of fire behavior models to better understand fire on the landscape and both its physical and ecological dynamism.

IV. CONCLUSIONS

The research conducted in this thesis has shown a novel application for T-LiDAR measurement of fuel beds. The difficulty in classifying sagebrush and chamise stems from their atypical forms and biomass distribution patterns. We have identified necessary steps for the using T-LiDAR in confined spaces that included correcting for range and reducing the number of falsely represented points. We developed a data processing method that produces a voxelized volume array that is heterogeneous and representative of the actual shrub and not a generalized statistical estimation. The investment involved in creating volumetric arrays from T-LiDAR data requires substantial data processing capabilities and time for sampling. However, the resulting product is an accurate description of where material exists in three dimensions, except the centers of wide fuel beds. Manual sampling and description of diffuse form shrubs would involve substantially more time investment, likely lead to the alteration of the subject of study, and produce a less geometrically correct subject. With limited ways to create models of shrubs, T-LiDAR is one of the few tools that allow for the creation of a model that maps more-or-less directly to the sampled shrub.

The volume arrays created in this research are useful in characterizing the amount and location of biomass lost during combustion. They have also shown the ability to determine biomass in advance of altering a sample. TLS allows users to collect observations for a different experimental purpose while still collecting highly precise data about the

sample being studied. By increasing the amount of vegetation descriptions created from T-LiDAR data, the field will expand in both the processing capacity and application of the data sets. T-LiDAR data sets are poised to become a very beneficial tool in multiple fields, one of particular interest being fire behavior modeling.

This research is novel and fundamental. It presents a base of knowledge that merits expanded research and wider application. This is a necessary first step and a feasible method to improve fuels descriptions and our understanding of the role physiological structure plays in the dynamism of fire behavior. Specific future work should include applying TLS generated fuel bed models in fluid dynamics fire behavior models to test for sensitivity to fuel bed heterogeneity. Additionally, this research should be applied in natural environments to test the utility on larger scales on the landscape. If the new generation of fire behavior models prove sensitive to TLS derived fuel bed models and methodologies are developed for landscape-scale TLS assessments, an ideal product would be a system that incorporates heterogeneous fuel beds and provides highly descriptive and accurate fire behavior predictions for use in research and in fire management.

REFERENCES

- Agee, J. K., 1993. *Fire Ecology of Pacific Northwest Forests*. Washington, D.C.: Island Press.
- Akay, A. E., Oguz, H., Karas, I. R. and Aruga, K., 2009. Using LiDAR technology in forestry activities. *Environ Monit Assess*, Volume 51, pp. 117-125.
- Albini, F. A., 1976. *Estimating wildfire behavior and effects*, Ogden, UT: U.S. Department of Agriculture, Forest Service.
- Albini, F. A., 1985. A Model for Fire Spread in Wildland Fuels by Radiation. *Combustion Science and Technology*, 42(5-6), pp. 229-258.
- Andersen, B. T. et al., In Progress. *Fundamental statistical multi-leaf model for fire spread through a manzanita shrub*. Provo: Brigham Young University.
- Andersen, H. E., McGaughey, R. J. and Reutebuch, S. E., 2005. Estimating forest canopy fuel parameters using LIDAR data. *Remote Sensing of Environment*, Volume 94, pp. 441-449.
- Anderson, H., 1982. *Aids to determining fuel models for estimating fire behavior*, Ogden: USDA Forest Service.
- Anza-Borrego Desert Natural History Association, 2013. *Chamise, Adenostoma fasciculatum*. [Online] Available at: http://www.abdnha.org/pages/03flora/family/rosaceae/adenostoma_fasciculatum.htm [Accessed 16 December 2013].
- Béland, M. et al., 2014. On seeing the wood from the leaves and the role of voxel size in determining leaf area distribution of forests with terrestrial LiDAR. *Agricultural and Forest Meteorology*, Issue 184, pp. 82-97.
- Boudon, F. et al., 2006. Estimating the fractal dimensions of plants using the two-surface method: An analysis based on 3D-digitized tree foliage. *Fractals*, 14(3), pp. 149-163.
- Brown, J. K., Oberheu, R. D. and Johnston, C. M., 1982. *Handbook for inventorying surface fuels and biomass in the Interior West*, Ogden, UT: U.S. Department of Agriculture, Forest Service, Intermountain Forest and Range Experimental Station.
- Cleary, M., Pendall, E. and Eewers, B., 2008. Testing sagebrush allometric relationships across three fire chronosequences in Wyoming, USA. *Journal of Arid Environments*, 72(4), pp. 285-301.
- Côté, J.-F., Widlowski, J.-L., Fournier, R. A. and Verstraete, M. M., 2009. The structural and radiative consistency of three-dimensional tree reconstructions from terrestrial lidar. *Remote Sensing of Environment*, Volume 113, pp. 1067-1081.

- Countryman, C. M. and Philpot, C. W., 1970. *Physical characteristics of chamise as a wildland fuel*, Berkeley, CA: U.S. Department of Agriculture, Forest Service.
- Dassot, M., Constant, T. and Fournier, M., 2011. The use of terrestrial LiDAR technology in forest science: application fields, benefits and challenges. *Annals of Forest Science*, Volume 68, pp. 959-974.
- Finney, M. A., 2004. *FARSITE: Fire Area Simulator-model development and evaluation*. RMRS-RP-4, Ogden, UT: U.S. Department of Agriculture, Forest Service.
- Fletcher, T. H. et al., 2007. Effects of moisture on ignition behavior of moist California chaparral and Utah leaves. *Combustion Science and Technology*, Issue 179, pp. 1183-1203.
- Franceschi, M. et al., 2009. Discrimination between marls and limestones using intensity data from terrestrial laser scanner. *ISPRS Journal of Photogrammetry and Remote Sensing*, Issue 64, pp. 522-528.
- Frandsen, W. H., 1983. Modeling big sagebrush as a fuel. *Journal of Range Management*, 36(5), pp. 596-600.
- Heinsch, F. A. and Andrews, P. L., 2010. *BehavePlus Fire modeling System, Version 5.0: Design and Features*. RMRS-GTR-249, Fort Collins, CO: U.S. Department of Agriculture, Forest Service, Rocky Mountain Research Station.
- Hiers, J. et al., 2009. The wildland fuel cell concept: an approach to characterizing fine-scale variation in fuels and fire in frequently burned longleaf pine forests. *International Journal of Wildland Fire*, Volume 18, pp. 315-325.
- Hoffman, C. et al., 2012. Numerical simulation of crown fire hazard immediately after bark beetle-caused mortality in lodgepole pine forests. *Forest Science*, 58(2), pp. 178-189.
- Hopkinson, C., Chasmer, L., Young-Pow, C. and Treitz, P., 2004. Assessing forest metrics with a ground-based scanning lidar. *Canadian Journal of Forest Research*, Volume 34, pp. 573-583.
- Johnson, E. A. and Miyanishi, K., 2001. *Forest Fires Behavior and Ecological Effects*. San Diego: Academic Press.
- Jow, W. M., Bullock, S. H. and Kummerow, J., 1980. Leaf turnover rates of *adenostoma fasciculatum* (Rosaceae). *American Journal of Botany*, 67(2), pp. 256-261.
- Loudermilk, E. L. et al., 2009. Ground-based LIDAR: a novel approach to quantify fine-scale fuelbed characteristics. *International Journal of Wildland Fire*, Volume 18, pp. 676-685.
- Martinuzzi, S. et al., 2009. Mapping snags and understory shrubs for a LiDAR-based assessment of wildlife habitat suitability. *Remote Sensing of Environment*, Volume 113, pp. 2533-2546.

- Means, J. E. et al., 1999. Use of Large-Footprint Scanning Airborne Lidar to Estimate Forest Stand Characteristics in the Western Cascades of Oregon. *Remote Sensing of Environment*, 67(3), pp. 298-308.
- Mell, W., 2013. *Simulating Fire Spread in Chamise Chaparral Fuel Beds*. Conference Presentation. Raleigh, NC: International Association of Wildland Fire's 4th Fire Behavior and Fuels Conference.
- Mell, W., Jenkins, M. A., Gould, J. and Cheney, P., 2007. A physics-based approach to modelling grassland fires. *International Journal of Wildland Fire*, Issue 16, pp. 1-22.
- Mell, W., Maranghides, A., McDermott, R. and Manzello, S. L., 2009. Numerical simulation and experiments of burning douglas fir trees. *Combustion and Flame*, Volume 156, pp. 2023-2041.
- Missoula Fire Sciences Laboratory, 2011. *Fire Behavior and Fire Danger Software*. [Online] Available at: <http://www.firemodels.org/> [Accessed 5 December 2011].
- Moorthy, I. et al., 2008. Retrieving crown leaf area index from an individual tree using ground-based lidar data. *Canadian Journal of Remote Sensing*, 34(3), pp. 320-332.
- Moorthy, I., Miller, J. R. and Jose Andtonia Jiminez Berni, P. Z.-T. B. H. J. C., 2011. Field characterization of olive (*Olea europaea* L.) tree crown architecture using terrestrial laser scanning data. *Agricultural and Forest Meteorology*, Volume 151, pp. 204-214.
- Murray, R. B. and Jacobson, M. Q., 1982. An evaluation of dimension analysis for predicting shrub biomass. *Journal of Range Management*, 35(4), pp. 451-454.
- NWCG, 2006. *S-390: Introduction to Wildfire Calculations*. s.l.:National Wildfire Coordination Group.
- Odion, D. C. and Davis, F. W., 2000. Fire, soil heating, and the formation of vegetation patterns in chaparral. *Ecological Monographs*, 70(1), pp. 149-169.
- Olsoy, P. J., 2013. *Determination of sagebrush aboveground biomass using terrestrial laser scanning (TLS)*, Pocatello, ID: MS of Science. Department of Geosciences. Idaho State University.
- Omasa, K., Hosoi, F. and Konishi, A., 2007. 3D lidar imaging for detecting and understanding plant responses and canopy structure. *Journal of Experimental Botany*, 58(4), pp. 881-898.
- Optech Inc. , 2009. *ILRIS Operation Manual*. Vaughan, Ontario: Optech Incorporated Industrial and 3D Imaging Division.
- Ottmar, R. D., Sandberg, D. V., Riccardi, C. L. and Prichard, S. J., 2007. An overview of the Fuels Characteristic Classification System - Quantifying, classifying, and creating fuelbeds for resource planning. *Canadian Journal of Forest Research*, Volume 37, pp. 2383-2393.

- Parsons, R. A., Mell, W. E. and McCauley, P., 2011. Linking 3D spatial models of fuels and fire: Effects of spatial heterogeneity on fire behavior. *Ecological Modeling*, Volume 222, pp. 679-691.
- Pickett, B. M. et al., 2009. Experimental measurements during combustion of moist individual foliage samples. *International Journal of Wildland Fire*, 19(2), pp. 153-162.
- Pickett, B. M. et al., 2010. Flame interactions and burning characteristics of two live leaf samples. *International Journal of Wildland Fire*, Volume 18, pp. 865-874.
- Rothermel, R. C., 1972. *A Mathematical Model for Predicting Fire Spread in Wildland Fuels*, Ogden: USDA-Forest Service.
- Rothermel, R. C., 1983. *How to predict the spread and intensity of forest and range fires*, 1983: U.S. Department of Agriculture, Forest Service.
- Rundel, P. W. and Parsons, D. J., 1979. Structural changes in chamise (*Adenostoma fasciculatum*) along a fire-induced age gradient. *Journal of Range Management*, 32(6), pp. 462-466.
- Scott, J. H. and Burgan, R. E., 2005. *Standard fire behavior fuel models: A comprehensive set for use with Rothermel's surface fire spread model*, Fort Collins: USDA Forest Service.
- Seielstad, C., Stonesifer, C., Rowell, E. and Queen, L., 2010. *Deriving conifer fuel mass for crown modeling using terrestrial laser scanning*. s.l., s.n.
- Streutker, D. R. and Glenn, N. F., 2006. LiDAR measurement of sagebrush steppe vegetation heights. *Remote Sensing of Environment*, Issue 102, pp. 135-145.
- Tullis, P., 2013. Into the Wildfire: What Science is Learning About Fire and how to Live With It. *The New York Times Magazine*, 22 September, p. 26.
- Van der Zande, D. et al., 2006. Influence of measurement set-up of ground-based LiDAR for derivation of tree structure. *Agricultural and Forest Meteorology*, Volume 141, pp. 147-160.
- van Leeuwen, M. and Niewenhuis, M., 2010. Retrieval of forest structural parameters using LiDAR remote sensing. *European Journal of Forest Research*, 129(4), pp. 749-770.
- van Noordwijk, M. and Mulia, R., 2002. Functional branch analysis as a tool for fractal scaling above- and belowground trees for their additive and non-additive properties. *Ecological Modeling*, 149(1-2), pp. 41-51.
- Vierling, L. A., Xu, Y., Eitel, J. U. and Oldow, J. S., 2012. Shrub characterization using terrestrial laser scanning and implications for airborne LiDAR assessment. *Canadian Journal of Remote Sensing*, 38(6), pp. 709-722.
- Vora, R. S., 1988. Predicting biomass of five shrub species in northeastern California. *Journal of Range Management*, 41(1), pp. 63-65.

Watt, P. J. and Donoghue, D. N. M., 2005. Measuring forest structure with terrestrial laser scanning. *International Journal of Remote Sensing*, 26(7), pp. 1437-1446.

Weber, R. O., 1991. Modelling fire spread through fuel beds. *Progress in Energy and Combustion Science*, 17(1), pp. 67-82.

APPENDICES

DATA PROCESSING WORKFLOW

Scan Collection

The process begins with the data collection. In the interest of consistency, we should be specifying a four meter range with 1.0mm spot spacing for every scan. Try to have the front of the sample (nearest to the scanner) ranged at 4 m, and have the sample built away from the scanner head. We can omit the 3rd scan, since there is no way to angle the scanner for an equal sampling in 3 directions. 2 scan directions, 180° from each other will be sufficient for data collection. The reasoning for this is best explained by imagining how the laser would scan a ball. A round object can be seen completely from 2 sides, but when you include a 3rd side without adding another scan from the 4th, the 3rd side becomes over-sampled and the point cloud will show a higher density of points on the side of the 3rd scan. The naming scheme for each sample should indicate the run number and scan direction. Document the interpretation of the name in the lab notebook. For the purposes of stitching, be sure there are some bright, hard surfaces with discrete corners or angles. Also, there should be sufficient external geometry so that auto-align will work (just the sample won't provide for good auto-align).



FIGURE IV-A. INSTRUMENT COLLECTING SCAN INFORMATION OF SAGEBRUSH SAMPLE IN RIVERSIDE BURN FACILITY.

Data Processing **Parsing**

When parsing the data, apply a range gate to each scan. For the shrubs in Riverside, an acceptable gate was 7 m. Parse into a .pif file as well as a .xyz file. The intensity output should be 16 bit-raw format. When parsing, make sure the box for 'keep saturated' is not checked. The reflective tape will saturate the laser and produce ghost points through the scene, it is best to just omit the saturated readings.

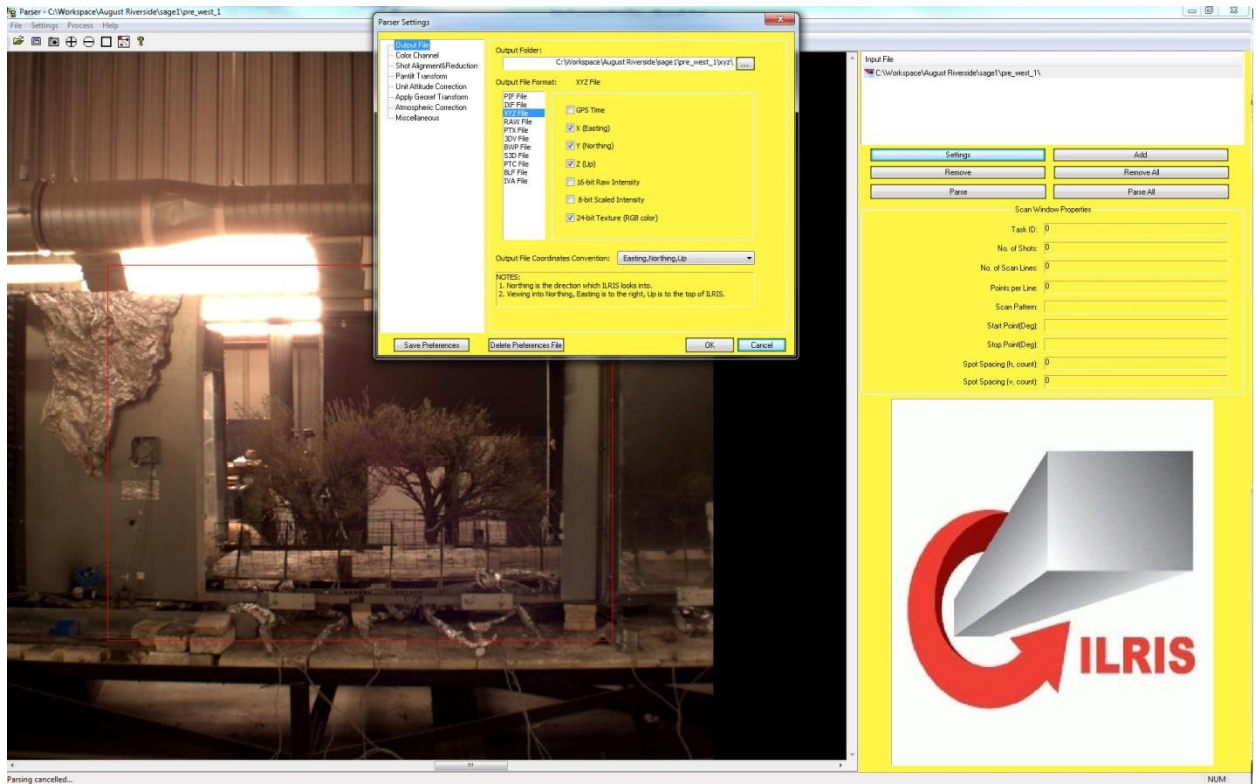


FIGURE IV-B. ILRIS PARSER 5.0.2.7 SOFTWARE WITH SETTINGS DIALOGUE BOX.

Aligning-.pif

Alignment can be done before the IDL code to correct for range and intensity because it is done using the .pif files in IM Align. Using the bright points placed in the scene start with an n-pair alignment using 4+ common points between the two scans. When you are aligning the scans, be consistent about which point cloud you upload first and which one you lock. For the chamise shrubs in December, I consistently locked the East scan and stitched to that. In retrospect, it might be beneficial to lock the West scan so that fire can move in a positive direction on the X axis as it propagates through the shrub. Either way should work, just be consistent. After the scans are sufficiently aligned, export the alignment matrices. I placed each alignment matrix in the main folder for the shrub that it corresponds to. The matrix should be easy to find.

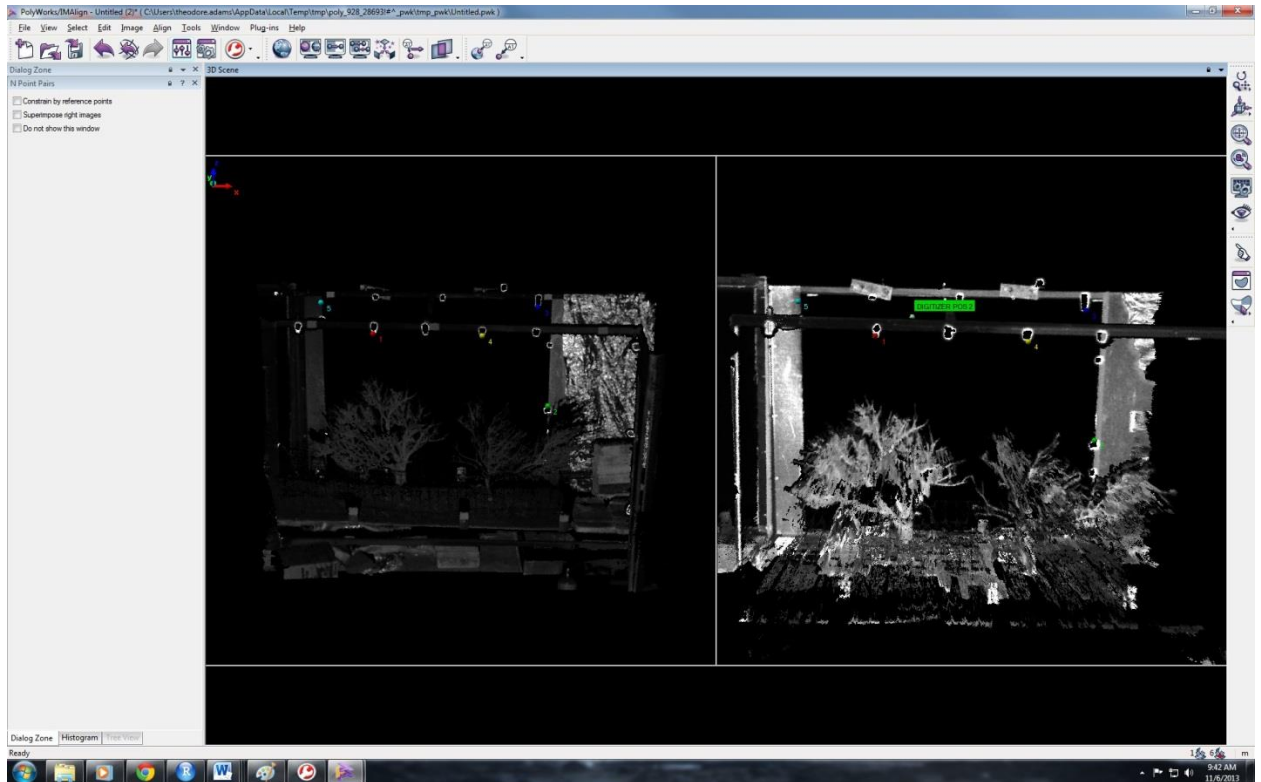


FIGURE IV-C. POLYWORKS IMALIGN SOFTWARE ALIGNING TWO POINT CLOUDS.

Correcting for range and 16 bit intensity

As we discovered early into the process, intensity averages change with a change in the range to the target, which were particularly notable in close-range scans. Each point cloud needs to be corrected for both the intensity range relationship, and the 16 bit raw intensity needs to be converted to the 9 bit raw value that it actually is. This is done using Eric's code 'normalizei.pro' in IDL. When you run this code it will create a second file in the same location, by the same name, with an extension of .xyz.xyz. Cut this file and paste it into a new folder titled 'Corrected.' It is important that this be done before aligning the .xyz files because the points need to be corrected relative to the scanner head, not to each other.

Aligning and Merging-.xyz

Taking the files that are in the 'Corrected' folder, you can then use Eric's other code 'TLSPprocessor.pro' in IDL to apply the alignment matrices to the corresponding .xyz file. When it asks what to save the file as, keep the same name, but place it in a folder labeled 'Aligned.' After each file has been aligned, use 'TLSPprocessor.pro' to merge the scans together. I have just been saving these files in the main folder corresponding to the sample. The file name can be shortened here to #pre or #post.

Clipping

The first step to clipping the merged file is to open it using IM Survey. Once the point cloud is opened, using View->Annotation->Coordinate Annotation-> Select from Picking, manually select the extent of the bounding box to be clipped. Manually record the extend for X [#,#], Y [#,#], and Z [#,#].

The format of the file coming from TLSprocessor.pro doesn't have a header and also has spaces in between the values. Using a text editor, I have been using Boxer, do a find and replace search where all spaces " " are replaced with no space "". Once it has completed, save the file with a .csv extension so that it can be imported into Arc.

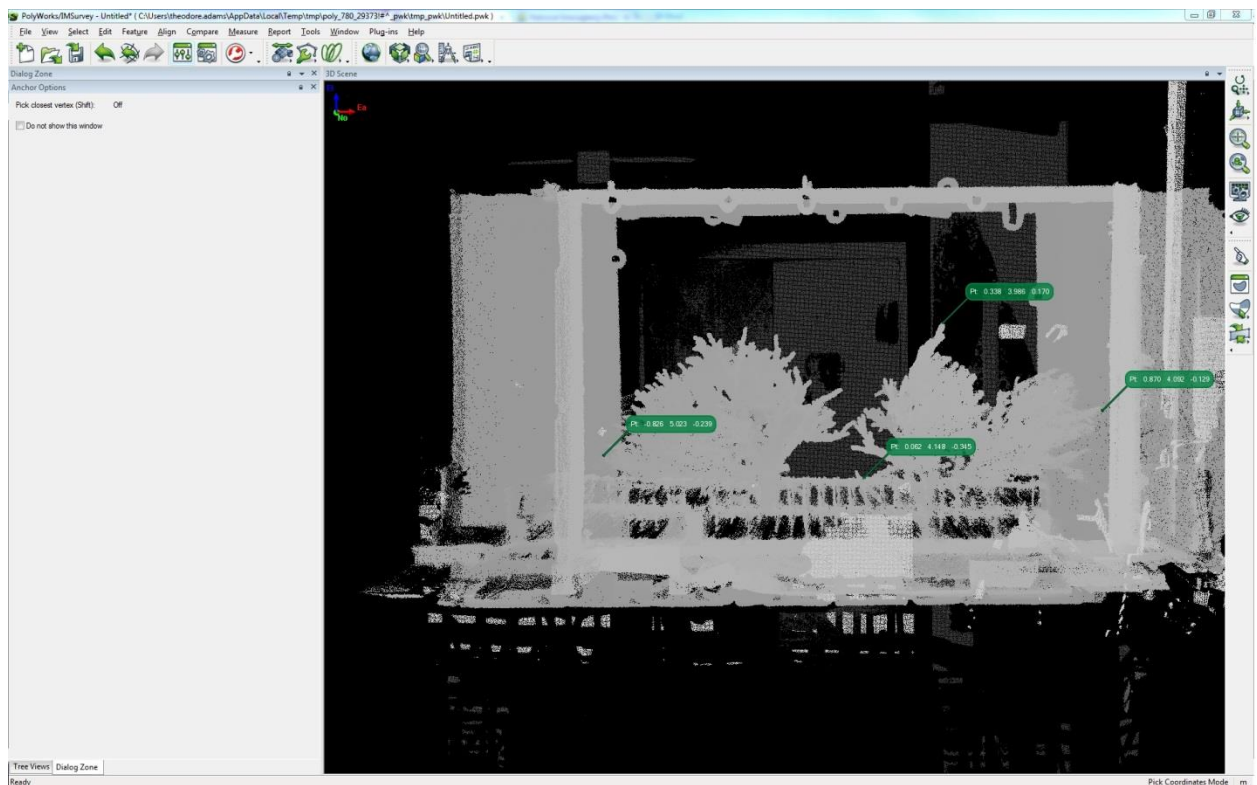


FIGURE IV-D. POLYWORKS IMSURVEY SOFTWARE SELECTING A BOUNDING BOX.

In Arc

This is where the bulk of the actual clipping happens and gets to be pretty involved. Using the .csv file for the point cloud, add XY data to the layer in ArcMap. This is where it is useful to pay attention to how the point cloud looked in IM Survey so you know which plane to project. If it has to start somewhere, start by projecting x as x and z as y. As the points are loading, right click on the layer and open the query builder. Apply the bounding box that was manually recorded from IM Survey by building the definition of $x > \#$ AND $x < \#$ (same for

Y and Z). After the bounding box has been applied, right click and export the file as a shapefile and add to the map as a layer. Remove the layer that isn't a shapefile because it can't be edited. Using the shapefile, select elements by lasso in order to remove the ghosting, or noise points, from around the actual structure of the shrub. When the elements are selected, right click and export the selected elements as a shapefile and save it as: #(pre/post)(XZ,XY,YZ)clip to show which plane has been clipped. After the shapefile has been exported, you will need to open the attribute table and export the table as a text file. When you do this, be sure to turn off any extra columns that arc created (FID, Shape, etc). Once the text file is exported you can load the file into arc the same way as before (add XY data) until it has been clipped on all 3 planes (if necessary). The order is unimportant, what does matter is that you clip as much as possible. If unsure about whether or not there are still ghost/noise points, any of the text files can be opened in IM Survey and visually assessed.

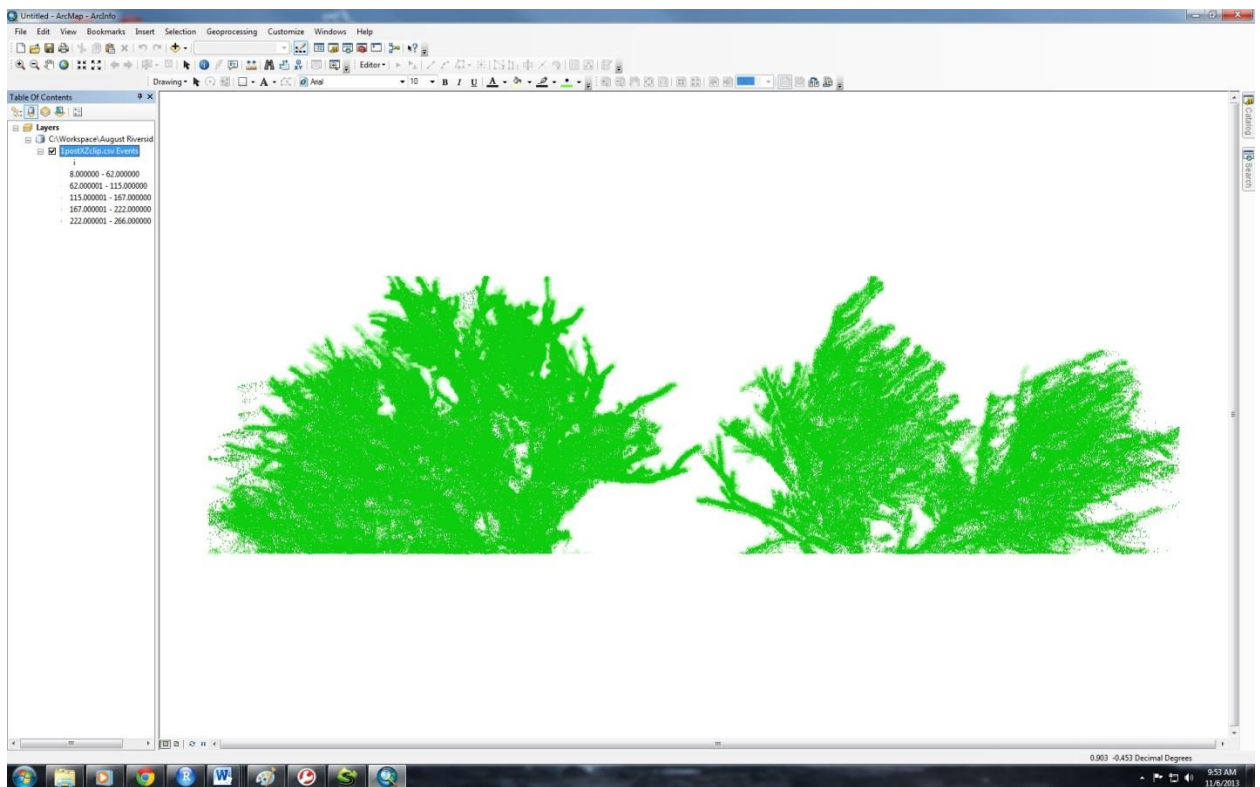


FIGURE IV-E. ARCMAP 10 PROJECTING POINT CLOUD ON THE X-Z PLANE FOR A SAGEBRUSH SAMPLE.

Voxel Array

The final clipped text file should have the format "FID","x","y","z","i" with a blank column under the FID. This is how the file will be read into IDL for the voxelizing code. Eric's code for the voxel array creation is 'voxel.pro' and can be run with a text file. The output will be a file called "voxellist" so be sure to keep track of which sample you are voxelizing so you can immediately save it with a meaningful name. The file name I used was: voxel#pre/post.

DESCRIPTIVE STATISTIC SPREADSHEETS

PHASE I-EXPERIMENT 1

Distance-the distance between the diffuse target and the discrete background in centimeters

Ghost-the number of points generated between the target and the background

Total-the total number of points making up the point cloud of the target and area ahead of the background

Logghost-Log base 10 values of the number of ghost points

TABLE IV-1. DESCRIPTIVE STATISTICS FOR THE NUMBER OF GHOST POINTS

distance	ghost	total	logghost
40	45498	106995	4.657992
50	49795	110433	4.697186
70	45739	93533	4.660287
80	16794	74047	4.225154
90	4560	71158	3.658965
100	1779	89597	3.250176
150	2701	164032	3.431525
200	21	164349	1.322219
250	7	164386	0.845098

PHASE I-EXPERIMENT 2

Sample-Number of 2 cm sample being scanned

Direction-Direction the TLS instrument was pointed during the scan, S being towards the South and N being towards the North

Range-Distance between the 2 cm sample targets and the TLS instrument, in meters

Mean-Mean intensity of laser return values for sample

Sum-Sum of intensity values for sample

TABLE IV-2. DESCRIPTIVE STATISTICS FOR RANGE-INTENSITY RELATIONSHIP WITHIN 3.5-6 M.

sample	direction	range	mean	sum
101	S	6	138	72032
101	S	5.5	157	77326
101	S	5	147	67880
101	S	4.5	142	65403

101	S	4	142	68442
101	S	3.5	129	43610
101	N	6	167	73974
101	N	5.5	168	70594
101	N	5	168	67885
101	N	4.5	165	65214
101	N	4	162	65072
101	N	3.5	151	50827
102	S	6	172	120697
102	S	5.5	167	108588
102	S	5	166	103770
102	S	4.5	171	108526
102	S	4	161	105617
102	S	3.5	161	74564
102	N	6	171	120919
102	N	5.5	171	107666
102	N	5	169	104166
102	N	4.5	167	102448
102	N	4	167	104945
102	N	3.5	163	83543
103	S	6	165	67272
103	S	5.5	146	70391
103	S	5	149	67556
103	S	4.5	145	66195
103	S	4	138	34535
103	S	3.5	131	43756
103	N	6	157	79063
103	N	5.5	148	70143
103	N	5	151	71360
103	N	4.5	149	70436
103	N	4	142	68238
103	N	3.5	131	51243
104	S	6	154	103670
104	S	5.5	164	99909
104	S	5	165	94488
104	S	4.5	162	90176
104	S	4	165	89688
104	S	3.5	161	62302
104	N	6	174	112038
104	N	5.5	176	105492
104	N	5	185	111610

104	N	4.5	179	108746
104	N	4	166	99648
104	N	3.5	161	78683
105	S	6	97	35298
105	S	5.5	107	34232
105	S	5	103	31581
105	S	4.5	99	29648
105	S	4	86	26286
105	S	3.5	91	19032
105	N	6	97	32071
105	N	5.5	104	33802
105	N	5	103	34433
105	N	4.5	103	32224
105	N	4	82	25763
105	N	3.5	81	19628
106	S	6	167	111202
106	S	5.5	169	106292
106	S	5	181	113475
106	S	4.5	175	105115
106	S	4	155	93730
106	S	3.5	152	63091
106	N	6	157	104744
106	N	5.5	161	102496
106	N	5	161	97007
106	N	4.5	165	100707
106	N	4	158	95700
106	N	3.5	153	76767
107	S	6	184	151605
107	S	5.5	185	141384
107	S	5	185	137381
107	S	4.5	183	137671
107	S	4	179	140015
107	S	3.5	172	96757
107	N	6	177	173406
107	N	5.5	176	164244
107	N	5	173	157473
107	N	4.5	179	165896
107	N	4	172	149837
107	N	3.5	163	119093
108	S	6	161	62797
108	S	5.5	159	58899

108	S	5	157	55752
108	S	4.5	157	55609
108	S	4	150	56816
108	S	3.5	145	38662
108	N	6	140	71854
108	N	5.5	145	68916
108	N	5	150	68462
108	N	4.5	144	64233
108	N	4	136	61797
108	N	3.5	124	42680
109	S	6	163	119832
109	S	5.5	167	113550
109	S	5	169	110347
109	S	4.5	164	107833
109	S	4	160	109918
109	S	3.5	152	74995
109	N	6	164	118404
109	N	5.5	168	112778
109	N	5	165	109151
109	N	4.5	164	108036
109	N	4	160	109304
109	N	3.5	154	86984
110	S	6	152	75792
110	S	5.5	146	65382
110	S	5	142	60969
110	S	4.5	141	59792
110	S	4	137	61838
110	S	3.5	131	42831
110	N	6	169	67118
110	N	5.5	167	62625
110	N	5	167	61554
110	N	4.5	166	60596
110	N	4	155	59329
110	N	3.5	150	46988

PHASE I-EXPERIMENT 3

Sample-Number of sample in scan

Type-Descriptive variable of the type of sample being scanned: Terminal being the end piece of a branch, Branch being a section of branch wood prior to the terminus, and Fork being a location where the branch forks

Dia-Diameter of sample in millimeters

Needles-Count of the number of needles on the sample
 Bunches-Count of the number of clusters where needles were bunched on the sample
 Forks-Number of times the sample forked
 Count-The number of TLS returns for the sample scan
 i-Mean intensity for the TLS scan
 Sum-Sum of intensity values for the TLS scan
 Wweight-weight of the sample prior to drying in grams
 Dweight-weight of the sample after oven drying in grams

TABLE IV-3. DESCRIPTIVE STATISTICS FOR 2 CM CHAMISE SAMPLES

sample	type	dia	needles	bunches	forks	count	i	sum	wweight	dweight
1	Terminal	1	29	7	0	353	95	33519	0.023	0.019
2	Terminal	1	24	8	0	284	112	31846	0.018	0.012
3	Branch	2	50	8	0	665	156	103799	0.197	0.173
4	Branch	2	40	5	0	425	158	67146	0.101	0.087
5	Fork	2	27	5	2	479	165	79038	0.179	0.15
6	Fork	2	10	4	2	555	158	87613	0.157	0.137
7	Branch	5	0	0	0	269	148	39772	0.357	0.337
8	Branch	5	0	0	0	365	160	58470	0.332	0.312
9	Fork	5	55	13	2	935	178	166470	0.449	0.415
10	Fork	5	86	20	5	1095	191	209174	0.718	0.652
11	Terminal	1	34	8	0	281	128	35912	0.038	0.031
12	Terminal	1	20	7	0	280	116	32482	0.021	0.015
13	Terminal	1	17	5	0	288	136	39169	0.018	0.014
14	Branch	3	25	5	0	373	165	61621	0.146	0.136
15	Branch	2	40	7	0	340	160	54454	0.125	0.111
16	Branch	4	35	7	0	485	178	86291	0.276	0.254
17	Fork	4	47	9	2	598	177	105815	0.274	0.253
18	Fork	4	115	23	4	812	190	154363	0.428	0.398
19	Fork	3	116	27	5	1088	177	192627	0.455	0.423
21	Branch	11	0	0	2	763	175	133487	1.518	1.424
22	Branch	8	0	0	0	513	177	90811	0.988	0.93
23	Fork	10	52	11	5	1205	173	208455	1.541	1.443
24	Fork	7	56	17	5	963	184	177226	0.839	0.786
25	Fork	6	71	12	3	837	188	157405	0.823	0.764
26	Fork	4	33	7	1	601	160	96229	0.195	0.178
27	Branch	4	10	3	0	325	157	50973	0.329	0.306
28	Fork	4	39	9	1	582	168	97854	0.254	0.233
29	Fork	3	55	14	5	734	183	134290	0.332	0.31
30	Terminal	2	66	4	0	419	141	59035	0.088	0.081
31	Terminal	1	20	6	0	359	133	47740	0.039	0.037
32	Fork	2	33	10	1	502	171	85883	0.16	0.148
33	Fork	3	70	18	5	962	176	169319	0.395	0.368

34	Fork	6	27	8	1	485	184	89234	0.659	0.614
35	Fork	10	12	3	2	784	185	145066	1.21	1.136
36	Fork	4	24	8	1	583	164	95552	0.171	0.161
37	Branch	1	24	4	0	237	138	32760	0.048	0.047
38	Branch	7	0	0	0	400	172	68802	0.675	0.638
39	Branch	1	27	7	0	318	136	43277	0.029	0.028
40	Fork	7	64	17	4	743	180	133788	0.831	0.777
41	Fork	11	12	3	2	711	184	130865	1.805	1.692
42	Fork	3	40	11	2	588	173	101773	0.164	0.156
43	Branch	1	25	5	0	343	145	49802	0.054	0.046
44	Terminal	1	31	6	0	352	160	56346	0.045	0.043
45	Fork	5	59	13	6	673	171	115095	0.566	0.532
46	Branch	8	0	0	0	496	162	80401	0.594	0.559
47	Branch	7	30	6	1	530	182	96519	0.684	0.643
48	Terminal	1	65	8	0	443	170	75391	0.111	0.104
49	Branch	2	41	6	0	411	154	63363	0.109	0.102
50	Branch	2	32	7	0	377	133	50133	0.054	0.05
61	Branch	10	0	0	0	498	177	88220	1.168	1.102
62	Fork	5	16	7	3	538	161	86695	0.488	0.46
63	Branch	2	0	0	0	275	123	33802	0.062	0.059
64	Fork	2	29	9	3	554	157	86908	0.119	0.111
65	Fork	1	59	9	1	468	147	68799	0.082	0.076
66	Fork	3	43	11	3	728	176	128212	0.295	0.277
67	Terminal	1	41	6	0	419	139	58305	0.051	0.046
68	Branch	1	27	4	0	359	159	57136	0.074	0.066
69	Fork	3	42	8	5	536	175	93841	0.188	0.169
70	Branch	6	5	2	0	333	159	52992	0.363	0.337
71	Fork	11	25	7	3	852	188	160144	1.644	1.541
72	Fork	3	27	6	1	582	169	98295	0.157	0.147
73	Fork	3	51	13	3	639	166	106075	0.153	0.143
74	Branch	5	8	2	0	447	166	74162	0.347	0.329
75	Branch	2	28	5	0	321	157	50473	0.053	0.05
76	Terminal	1	38	7	0	342	154	52646	0.047	0.046
77	Fork	4	37	9	2	619	169	104629	0.375	0.355
78	Branch	1	15	4	0	260	137	35632	0.035	0.033
79	Branch	2	27	5	0	328	150	49143	0.05	0.05
80	Terminal	1	45	7	0	338	154	52022	0.033	0.033
81	Fork	6	29	7	4	768	184	141310	0.56	0.526
82	Branch	1	32	4	0	376	142	53451	0.053	0.05
83	Terminal	1	68	8	0	311	151	46907	0.028	0.027
84	Fork	4	55	7	4	800	178	142390	0.479	0.451

85	Branch	2	73	6	0	469	158	74159	0.11	0.101
86	Branch	4	0	0	0	397	165	65451	0.218	0.203
87	Fork	3	35	7	1	622	156	97080	0.169	0.159
88	Terminal	1	0	0	0	271	73	19775	0.009	0.008
89	Branch	2	31	6	0	397	164	65135	0.078	0.074
90	Fork	2	56	10	3	514	168	86275	0.179	0.166
91	Terminal	1	78	7	0	353	161	56791	0.035	0.032
92	Fork	3	123	12	5	938	181	169733	0.425	0.385
93	Branch	5	2	1	0	410	175	71750	0.352	0.333
94	Branch	2	48	4	0	360	149	53593	0.06	0.055
95	Fork	3	139	18	3	448	166	74336	0.084	0.08
96	Fork	3	139	18	3	519	181	93982	0.185	0.175
97	Fork	4	57	7	3	768	166	127408	0.414	0.388
98	Branch	2	44	5	0	345	156	53786	0.044	0.044
99	Terminal	1	47	3	0	344	143	49197	0.038	0.038
100	Branch	1	35	4	0	286	151	43227	0.034	0.031

PHASE I-EXPERIMENT 4

Sample-Number for sample being scanned

i-mean intensity for original TLS scan of sample

sum-sum of intensity values for original TLS scan of sample

ti-mean intensity for the TLS scan of sample after it was rotated

tsum-sum of intensity values for the TLS scan of the sample after it was rotated

TABLE IV-4. DESCRIPTIVE STATISTICS FOR ROTATIONAL GEOMETRY EXPERIMENT

sample	i	sum	ti	tsum
31	133	47740	135	47765
32	171	85883	166	108973
33	176	169319	170	152674
34	184	89234	171	99184
35	185	145066	175	145486
36	164	95552	157	97058
37	138	32760	135	43637
38	172	68802	155	60171
39	136	43277	131	45447
40	180	133788	179	144918
41	184	130865	186	132956
42	173	101773	167	105665
43	145	49802	153	56093
45	171	115095	173	116578
46	162	80401	166	83791
47	182	96519	158	65512
48	170	75391	171	79025

49	154	63363	157	68223
50	133	50133	132	49960
61	177	88220	178	91152
62	161	86695	161	91278
63	123	33802	136	32560
64	157	86908	165	78852
65	147	68799	150	70060
66	176	128212	169	117482
67	139	58305	151	53033
68	159	57136	163	61360
69	175	93841	174	111738
70	159	52992	172	68991
71	188	160144	178	131109
72	169	98295	169	102488
73	166	106075	166	107161
74	166	74162	179	71074
75	157	50473	153	50471
76	154	52646	153	52325
77	169	104629	169	86955
78	137	35632	141	36993
79	150	49143	158	55912
80	154	52022	146	50534
81	184	141310	185	146319
82	142	53451	140	55840
83	151	46907	148	46149
84	178	142390	180	129068
85	158	74159	163	86293
86	165	65451	161	59005
87	156	97080	150	75457
88	73	19775	94	25899
89	164	65135	164	68256
90	168	86275	166	90389
91	161	56791	159	53382
92	181	169733	181	168456
93	175	71750	180	72613
94	149	53593	145	57000
95	166	74336	167	75476
96	181	93982	174	94523
97	166	127408	160	119707
98	156	53786	157	52801
99	143	49197	144	57765

100	151	43227	157	45780
-----	-----	-------	-----	-------

PHASE II-COMBUSTION MASS LOSS

Run-Number corresponding to the replication of sample that was scanned and burned
 Species-Type of plant species being combusted, sagebrush being sagebrush, Chamise being Chamise

Prewrite-measured mass of the sample prior to combustion

Massloss-Difference in mass between pre- and post-combustion

Postweight-measured mass of the sample following combustion

Voxpre-number of voxels in the modeled volume occupied with material, prior to combustion

Voxloss-difference in number of voxels in modeled volume between pre- and post-combustion

Voxpost-number of voxels in the modeled volume occupied with material, following combustion

TABLE IV-5. DESCRIPTIVE STATISTICS FOR COMBUSTION MASS AND VOLUME LOSS.

run	species	preweight	massloss	postweight	voxpre	voxloss	voxpost
1	Sage	2263	360	1903	12327	4265	8062
2	Sage	5272.2	2841	2431.2	17811	13052	4759
3	Sage	5051.4	2752	2299.4	16405	13250	3155
4	Sage	2176.1	267.5	1908.6	11338	3230	8108
5	Sage	5199.4	2910	2289.4	16531	13618	2913
6	Sage	5277.2	2878	2399.2	19067	17670	1397
7	Sage	1941.5	1133.3	808.2	8683	6846	1837
8	Sage	2161.7	1474	687.7	10024	8266	1758
9	Sage	4293.6	3542	751.6	10943	9881	1062
10	Sage	2950.3	1056	1894.3	7925	4488	3437
11	Sage	2304.1	487	1817.1	8712	3181	5531
12	Sage	5449.1	4113	1336.1	16540	13981	2559
13	Sage	2199.4	1180	1019.4	10440	6780	3660
14	Sage	2529.6	547	1982.6	12484	2692	9792
15	Sage	5299.5	2758	2541.5	18492	11667	6825
16	Sage	5308	3303	2005	17958	14365	3593
1	Chamise	2990	154	2836	29381	6986	22395
2	Chamise	6638	3090	3548	29803	27002	2801
3	Chamise	2613	847	1766	23690	12346	11344
4	Chamise	5065	3001	2064	26267	20762	5505
5	Chamise	4643	973	3670	29063	9581	19482
6	Chamise	6125	509	5616	36743	7962	28781
7	Chamise	5061	710	4351	32460	7849	24611
8	Chamise	3851	740	3111	27157	5719	21438
9	Chamise	5227	3264	1963	28979	20939	8040
10	Chamise	3647	1755	1892	26499	16826	9673
11	Chamise	8036	2119	5917	39070	17776	21294
12	Chamise	4816	2141	2675	29518	14151	15367

13	Chamise	4549	2977	1572	27630	23964	3666
----	---------	------	------	------	-------	-------	------

PHASE II-SIMULATED MASS LOSS

Branch-Number corresponding to the sample branch being scanned

Scan-number corresponding to the sequence of scans of the sample

Voxels-number of voxels in the modeled volume occupied with material

wweight-total wet mass of sample at the time of scan in grams

dweight-total dry mass of sample in grams

replicate-method of mass removal during experimentation: Foliage + Diameter being the sample

where foliage was removed initially then branch wood was removed by a sequentially increasing

diameter, Diameter being where material was removed by a sequentially increasing diameter,

Random being where an equivalent mass as the Diameter replication was removed with no

cause for location on the sample branch

TABLE IV-6. DESCRIPTIVE STATISTICS FOR SIMULATED MASS LOSS EXPERIMENT.

branch	scan	voxels	wweight	dweight	replicate
1	0	2244	165.7	139.8	Foliage + Diameter
1	1	2253	137.5	114	Foliage + Diameter
1	2	1853	122.1	100.4	Foliage + Diameter
1	3	565	95.9	76.9	Foliage + Diameter
1	4	418	90.2	71.9	Foliage + Diameter
1	5	273	84.2	66.7	Foliage + Diameter
1	6	242	79.4	62.5	Foliage + Diameter
2	0	1440	155.3	107.7	Diameter
2	2	1303	145	100	Diameter
2	3	892	102	67.9	Diameter
2	4	543	82	53.5	Diameter
2	5	248	64.9	41.9	Diameter
2	6	150	53.5	34.5	Diameter
3	0	1536	162.5	103	Random
3	2	1570	152.2	96.5	Random
3	3	1063	109.2	69	Random
3	4	727	89.2	56.1	Random
3	5	497	72.1	45.1	Random
3	6	301	60.7	37.8	Random
4	0	2871	210.9	176.4	Foliage + Diameter
4	1	2752	178.3	147.3	Foliage + Diameter
4	2	1993	148.6	120.9	Foliage + Diameter
4	3	756	120.8	96.4	Foliage + Diameter
4	4	378	108.4	85.3	Foliage + Diameter
4	5	287	104.3	81.6	Foliage + Diameter
4	6	258	100.5	78.2	Foliage + Diameter
5	0	3237	230.7	182.6	Diameter

5	2	2110	172.2	130.6	Diameter
5	3	974	144.9	107.2	Diameter
5	4	538	130.7	95.8	Diameter
5	5	385	121.6	88.7	Diameter
5	6	304	112.8	82	Diameter
6	0	2943	209.5	150.5	Random
6	2	2168	151	105.9	Random
6	3	1564	123.7	84.5	Random
6	4	1095	109.5	73.6	Random
6	5	663	100.4	66.7	Random
6	6	370	91.6	60.1	Random

PHASE II-INTERIOR VOLUME REPRESENTATION

Depth of Penetration

Sage-Count of number of voxels on one side of voxel model for sagebrush sample

Chamise-Count of number of voxels on one side of voxel model for chamise sample

TABLE IV-7. DESCRIPTIVE STATISTICS FOR HULL DEPTH

sage	chamise	sage	chamise	sage	chamise	sage	chamise
5	10	5	4	6	11	6	8
4	11	5	6	4	5	7	8
5	8	18	6	4	5	4	5
9	6	3	6	4	11	3	5
7	4	3	6	6	8	9	6
5	12	7	10	7	9	7	3
4	9	5	4	7	8	7	3
5	8	6	3	7	3	5	3
5	5	5	4	5	12	5	4
4	6	5	5	4	8	5	6
2	9	6	5	6	3	1	2
5	8	7	5	4	3	5	4
6	4	4	5	4	7	3	5
5	5	10	5	5	3	4	4
4	2	5	4	3	6	5	7
4	5	5	3	7	6	4	6
5	8	5	5	8	5	3	4
3	5	5	5	5	3	4	4
4	4	4	10	4	3	3	5
7	3	5	7	4	5	6	3
4	8	4	2	3	4	5	6
6	5	6	3	4	5	8	3
4	4	4	4	2	7	4	3

3	3	5	8	5	8	6	3
2	4	8	6	6	8	6	7
1	8	6	8	6	7	6	5
4	7	6	6	3	7	2	4
2	9	8	5	10	7	4	14
10	4	4	7	5	7	5	6
8	7	9	4	4	6	3	4

Missing Volume

Species-Type of plant represented in the voxel model

Number-Replication number during combustion experimentation

x-Location on the X-axis where the data line was sampled

z-Location on the Z-axis where the data line was sampled

Filled-Number of voxels along the data line with more than 20 points filling the volume

Empty-Number of voxels along the data line with less than 20 points filling the volume

Prop-Proportion of empty to filled voxels on the data line

Sum-Total number of voxel spaces along the data line from edge to edge of the shrub

Prop_total-Proportion of the number of empty voxels to the total number of voxels along the data line

TABLE IV-8. DESCRIPTIVE STATISTICS FOR MISSING VOLUME DISTRIBUTION.

species	number	x	z	filled	empty	prop	sum	prop_total
chamise	2	0.5	0.2	18	6	0.33	24	0.25
chamise	2	0.5	0.4	19	8	0.42	27	0.296296
chamise	2	0.5	0.6	15	4	0.27	19	0.210526
chamise	2	0.8	0.2	1	0	0	1	0
chamise	2	0.8	0.4	15	13	0.87	28	0.464286
chamise	2	0.8	0.6	13	8	0.62	21	0.380952
chamise	2	1.08	0.2	16	3	0.19	19	0.157895
chamise	2	1.08	0.4	6	21	3.5	27	0.777778
chamise	2	1.08	0.6	1	0	0	1	0
chamise	4	0.28	0.2	19	5	0.26	24	0.208333
chamise	4	0.28	0.4	9	12	1.33	21	0.571429
chamise	4	0.28	0.6	12	8	0.67	20	0.4
chamise	4	0.58	0.2	1	0	0	1	0
chamise	4	0.58	0.4	16	3	0.19	19	0.157895
chamise	4	0.58	0.6	1	0	0	1	0
chamise	4	0.96	0.2	17	21	1.24	38	0.552632
chamise	4	0.96	0.4	9	19	2.11	28	0.678571
chamise	4	0.96	0.6	1	0	0	1	0
chamise	6	0.32	0.2	18	4	0.22	22	0.181818
chamise	6	0.32	0.4	18	22	1.22	40	0.55
chamise	6	0.32	0.6	13	18	1.38	31	0.580645

chamise	6	0.64	0.2	1	0	0	1	0
chamise	6	0.64	0.4	10	10	1	20	0.5
chamise	6	0.64	0.6	16	23	1.44	39	0.589744
chamise	6	1.02	0.2	15	1	0.07	16	0.0625
chamise	6	1.02	0.4	15	4	0.27	19	0.210526
chamise	6	1.02	0.6	6	19	3.17	25	0.76
sage	5	0.38	0.1	1	0	0	1	0
sage	5	0.38	0.3	7	12	1.71	19	0.631579
sage	5	0.38	0.5	7	7	1	14	0.5
sage	5	0.68	0.1	10	5	0.5	15	0.333333
sage	5	0.68	0.3	12	16	1.33	28	0.571429
sage	5	0.68	0.5	1	0	0	1	0
sage	5	0.98	0.1	7	2	0.29	9	0.222222
sage	5	0.98	0.3	18	19	1.06	37	0.513514
sage	5	0.98	0.5	1	0	0	1	0
sage	3	0.38	0.1	9	29	3.22	38	0.763158
sage	3	0.38	0.3	9	17	1.89	26	0.653846
sage	3	0.38	0.5	10	19	1.9	29	0.655172
sage	3	0.64	0.1	9	32	3.56	41	0.780488
sage	3	0.64	0.3	9	36	4	45	0.8
sage	3	0.64	0.5	11	2	0.18	13	0.153846
sage	3	0.9	0.1	8	4	0.5	12	0.333333
sage	3	0.9	0.3	1	0	0	1	0
sage	3	0.9	0.5	7	4	0.57	11	0.363636
sage	1	0.44	0.1	11	2	0.18	13	0.153846
sage	1	0.44	0.3	7	11	1.57	18	0.611111
sage	1	0.44	0.5	1	0	0	1	0
sage	1	0.78	0.1	1	0	0	1	0
sage	1	0.78	0.3	11	4	0.36	15	0.266667
sage	1	0.78	0.5	1	0	0	1	0
sage	1	1.06	0.1	10	9	0.9	19	0.473684
sage	1	1.06	0.3	9	9	1	18	0.5
sage	1	1.06	0.5	1	0	0	1	0
sage	7	0.38	0.1	1	0	0	1	0
sage	7	0.38	0.3	11	6	0.55	17	0.352941
sage	7	0.38	0.5	1	0	0	1	0
sage	7	0.6	0.1	1	0	0	1	0
sage	7	0.6	0.3	11	13	1.18	24	0.541667
sage	7	0.6	0.5	1	0	0	1	0
sage	7	0.9	0.1	1	0	0	1	0
sage	7	0.9	0.3	10	1	0.1	11	0.090909

sage	7	0.9	0.5	1	0	0	1	0
sage	9	0.48	0.1	8	18	2.25	26	0.692308
sage	9	0.48	0.3	1	0	0	1	0
sage	9	0.48	0.5	1	0	0	1	0
sage	9	0.78	0.1	10	16	1.6	26	0.615385
sage	9	0.78	0.3	11	10	0.91	21	0.47619
sage	9	0.78	0.5	1	0	0	1	0
sage	9	1.02	0.1	11	11	1	22	0.5
sage	9	1.02	0.3	11	9	0.82	20	0.45
sage	9	1.02	0.5	1	0	0	1	0
chamise	8	0.42	0.2	16	3	0.19	19	0.157895
chamise	8	0.42	0.4	14	1	0.07	15	0.066667
chamise	8	0.42	0.6	12	9	0.75	21	0.428571
chamise	8	0.66	0.2	11	7	0.64	18	0.388889
chamise	8	0.66	0.4	11	6	0.55	17	0.352941
chamise	8	0.66	0.6	18	7	0.39	25	0.28
chamise	8	0.92	0.2	11	8	0.73	19	0.421053
chamise	8	0.92	0.4	16	8	0.5	24	0.333333
chamise	8	0.92	0.6	19	9	0.47	28	0.321429
chamise	10	0.48	0.2	16	4	0.25	20	0.2
chamise	10	0.48	0.4	1	0	0	1	0
chamise	10	0.48	0.6	15	12	0.8	27	0.444444
chamise	10	0.76	0.2	16	17	1.06	33	0.515152
chamise	10	0.76	0.4	1	0	0	1	0
chamise	10	0.76	0.6	9	18	2	27	0.666667
chamise	10	1.06	0.2	5	23	4.6	28	0.821429
chamise	10	1.06	0.4	10	7	0.7	17	0.411765
chamise	10	1.06	0.6	1	0	0	1	0
chamise	12	0.54	0.2	10	22	2.2	32	0.6875
chamise	12	0.54	0.4	12	3	0.25	15	0.2
chamise	12	0.54	0.6	14	10	0.71	24	0.416667
chamise	12	0.82	0.2	14	9	0.64	23	0.391304
chamise	12	0.82	0.4	12	4	0.33	16	0.25
chamise	12	0.82	0.6	10	13	1.3	23	0.565217
chamise	12	1.16	0.2	12	6	0.5	18	0.333333
chamise	12	1.16	0.4	10	10	1	20	0.5
chamise	12	1.16	0.6	1	0	0	1	0
sage	11	0.46	0.1	10	15	1.5	25	0.6
sage	11	0.46	0.2	1	0	0	1	0
sage	11	0.46	0.3	1	0	0	1	0
sage	11	0.8	0.1	8	9	1.13	17	0.529412

sage	11	0.8	0.2	10	9	0.9	19	0.473684
sage	11	0.8	0.3	1	0	0	1	0
sage	11	1.06	0.1	9	3	0.33	12	0.25
sage	11	1.06	0.2	9	7	0.78	16	0.4375
sage	11	1.06	0.3	9	14	1.56	23	0.608696

PHASE II-VOXEL BULK DENSITY

Experiment-Experiment from which data was pulled: Sim_mass_loss corresponds to the simulated mass loss experiment, comb_mass_loss corresponds to the combustion experimentation, and isb_2_cm corresponds to the chamise characteristics within a 2 cm segment experiment.

Run-Trial number in experiment

Replicate-Style of sample

Voxels-count of number of voxels in sample: Combustion samples have been adjusted for missing volume based on the volume distribution

Wweight-mass in grams of sample

Vox_density-Density of sample in grams per voxel

TABLE IV-9. DESCRIPTIVE STATISTICS FOR CHAMISE VOXEL DENSITY DISTRIBUTION.

experiment	run	replicate	voxels	wweight	vox_density
sim_mass_loss	0	Foliage_Diameter	2244	165.7	0.074
sim_mass_loss	1	Foliage_Diameter	2253	137.5	0.061
sim_mass_loss	2	Foliage_Diameter	1853	122.1	0.066
sim_mass_loss	3	Foliage_Diameter	565	95.9	0.170
sim_mass_loss	4	Foliage_Diameter	418	90.2	0.216
sim_mass_loss	5	Foliage_Diameter	273	84.2	0.308
sim_mass_loss	6	Foliage_Diameter	242	79.4	0.328
sim_mass_loss	0	Diameter	1440	155.3	0.108
sim_mass_loss	2	Diameter	1303	145	0.111
sim_mass_loss	3	Diameter	892	102	0.114
sim_mass_loss	4	Diameter	543	82	0.151
sim_mass_loss	5	Diameter	248	64.9	0.262
sim_mass_loss	6	Diameter	150	53.5	0.357
sim_mass_loss	0	Random	1536	162.5	0.106
sim_mass_loss	2	Random	1570	152.2	0.097
sim_mass_loss	3	Random	1063	109.2	0.103
sim_mass_loss	4	Random	727	89.2	0.123
sim_mass_loss	5	Random	497	72.1	0.145
sim_mass_loss	6	Random	301	60.7	0.202
sim_mass_loss	0	Foliage_Diameter	2871	210.9	0.073
sim_mass_loss	1	Foliage_Diameter	2752	178.3	0.065
sim_mass_loss	2	Foliage_Diameter	1993	148.6	0.075
sim_mass_loss	3	Foliage_Diameter	756	120.8	0.160

sim_mass_loss	4	Foliage_Diameter	378	108.4	0.287
sim_mass_loss	5	Foliage_Diameter	287	104.3	0.363
sim_mass_loss	6	Foliage_Diameter	258	100.5	0.390
sim_mass_loss	0	Diameter	3237	230.7	0.071
sim_mass_loss	2	Diameter	2110	172.2	0.082
sim_mass_loss	3	Diameter	974	144.9	0.149
sim_mass_loss	4	Diameter	538	130.7	0.243
sim_mass_loss	5	Diameter	385	121.6	0.316
sim_mass_loss	6	Diameter	304	112.8	0.371
sim_mass_loss	0	Random	2943	209.5	0.071
sim_mass_loss	2	Random	2168	151	0.070
sim_mass_loss	3	Random	1564	123.7	0.079
sim_mass_loss	4	Random	1095	109.5	0.100
sim_mass_loss	5	Random	663	100.4	0.151
sim_mass_loss	6	Random	370	91.6	0.248
comb_mass_loss	1	Chamise_pre	38379.55	2990	0.078
comb_mass_loss	2	Chamise_pre	39009.6	6638	0.170
comb_mass_loss	3	Chamise_pre	30919.61	2613	0.085
comb_mass_loss	4	Chamise_pre	34262.39	5065	0.148
comb_mass_loss	5	Chamise_pre	37938.27	4643	0.122
comb_mass_loss	6	Chamise_pre	48019.63	6125	0.128
comb_mass_loss	7	Chamise_pre	42492.92	5061	0.119
comb_mass_loss	8	Chamise_pre	35628.05	3851	0.108
comb_mass_loss	9	Chamise_pre	37857.56	5227	0.138
comb_mass_loss	10	Chamise_pre	34669.29	3647	0.105
comb_mass_loss	11	Chamise_pre	51004.03	8036	0.158
comb_mass_loss	12	Chamise_pre	38628.61	4816	0.125
comb_mass_loss	13	Chamise_pre	36045.71	4549	0.126
isb_2_cm	1	Terminal	1	0.023	0.023
isb_2_cm	2	Terminal	1	0.018	0.018
isb_2_cm	3	Branch	1	0.197	0.197
isb_2_cm	4	Branch	1	0.101	0.101
isb_2_cm	5	Fork	1	0.179	0.179
isb_2_cm	6	Fork	1	0.157	0.157
isb_2_cm	7	Branch	1	0.357	0.357
isb_2_cm	8	Branch	1	0.332	0.332
isb_2_cm	9	Fork	1	0.449	0.449
isb_2_cm	10	Fork	1	0.718	0.718
isb_2_cm	11	Terminal	1	0.038	0.038
isb_2_cm	12	Terminal	1	0.021	0.021
isb_2_cm	13	Terminal	1	0.018	0.018

isb_2_cm	14	Branch	1	0.146	0.146
isb_2_cm	15	Branch	1	0.125	0.125
isb_2_cm	16	Branch	1	0.276	0.276
isb_2_cm	17	Fork	1	0.274	0.274
isb_2_cm	18	Fork	1	0.428	0.428
isb_2_cm	19	Fork	1	0.455	0.455
isb_2_cm	21	Branch	1	1.518	1.518
isb_2_cm	22	Branch	1	0.988	0.988
isb_2_cm	23	Fork	1	1.541	1.541
isb_2_cm	24	Fork	1	0.839	0.839
isb_2_cm	25	Fork	1	0.823	0.823
isb_2_cm	26	Fork	1	0.195	0.195
isb_2_cm	27	Branch	1	0.329	0.329
isb_2_cm	28	Fork	1	0.254	0.254
isb_2_cm	29	Fork	1	0.332	0.332
isb_2_cm	30	Terminal	1	0.088	0.088
isb_2_cm	31	Terminal	1	0.039	0.039
isb_2_cm	32	Fork	1	0.16	0.160
isb_2_cm	33	Fork	1	0.395	0.395
isb_2_cm	34	Fork	1	0.659	0.659
isb_2_cm	35	Fork	1	1.21	1.210
isb_2_cm	36	Fork	1	0.171	0.171
isb_2_cm	37	Branch	1	0.048	0.048
isb_2_cm	38	Branch	1	0.675	0.675
isb_2_cm	39	Branch	1	0.029	0.029
isb_2_cm	40	Fork	1	0.831	0.831
isb_2_cm	41	Fork	1	1.805	1.805
isb_2_cm	42	Fork	1	0.164	0.164
isb_2_cm	43	Branch	1	0.054	0.054
isb_2_cm	44	Terminal	1	0.045	0.045
isb_2_cm	45	Fork	1	0.566	0.566
isb_2_cm	46	Branch	1	0.594	0.594
isb_2_cm	47	Branch	1	0.684	0.684
isb_2_cm	48	Terminal	1	0.111	0.111
isb_2_cm	49	Branch	1	0.109	0.109
isb_2_cm	50	Branch	1	0.054	0.054
isb_2_cm	61	Branch	1	1.168	1.168
isb_2_cm	62	Fork	1	0.488	0.488
isb_2_cm	63	Branch	1	0.062	0.062
isb_2_cm	64	Fork	1	0.119	0.119
isb_2_cm	65	Fork	1	0.082	0.082

isb_2_cm	66	Fork	1	0.295	0.295
isb_2_cm	67	Terminal	1	0.051	0.051
isb_2_cm	68	Branch	1	0.074	0.074
isb_2_cm	69	Fork	1	0.188	0.188
isb_2_cm	70	Branch	1	0.363	0.363
isb_2_cm	71	Fork	1	1.644	1.644
isb_2_cm	72	Fork	1	0.157	0.157
isb_2_cm	73	Fork	1	0.153	0.153
isb_2_cm	74	Branch	1	0.347	0.347
isb_2_cm	75	Branch	1	0.053	0.053
isb_2_cm	76	Terminal	1	0.047	0.047
isb_2_cm	77	Fork	1	0.375	0.375
isb_2_cm	78	Branch	1	0.035	0.035
isb_2_cm	79	Branch	1	0.05	0.050
isb_2_cm	80	Terminal	1	0.033	0.033
isb_2_cm	81	Fork	1	0.56	0.560
isb_2_cm	82	Branch	1	0.053	0.053
isb_2_cm	83	Terminal	1	0.028	0.028
isb_2_cm	84	Fork	1	0.479	0.479
isb_2_cm	85	Branch	1	0.11	0.110
isb_2_cm	86	Branch	1	0.218	0.218
isb_2_cm	87	Fork	1	0.169	0.169
isb_2_cm	88	Terminal	1	0.009	0.009
isb_2_cm	89	Branch	1	0.078	0.078
isb_2_cm	90	Fork	1	0.179	0.179
isb_2_cm	91	Terminal	1	0.035	0.035
isb_2_cm	92	Fork	1	0.425	0.425
isb_2_cm	93	Branch	1	0.352	0.352
isb_2_cm	94	Branch	1	0.06	0.060
isb_2_cm	95	Fork	1	0.084	0.084
isb_2_cm	96	Fork	1	0.185	0.185
isb_2_cm	97	Fork	1	0.414	0.414
isb_2_cm	98	Branch	1	0.044	0.044
isb_2_cm	99	Terminal	1	0.038	0.038
isb_2_cm	100	Branch	1	0.034	0.034

DATA PROCESSING CODE AND OUTPUT

PHASE I-EXPERIMENT 1

Code

```
library(lattice)
library(car)
ghost<-read.csv(file.choose())
summary(ghost)
plot(ghost$logghost~ghost$distance,
      ylab="Log 10 Number of Ghost Points",
      xlab="Distance from Target to Background (cm)")
fit<-lm(ghost$logghost~ghost$distance)
summary(fit)
coef<-summary(fit)$coeff
coef
int<-coef[1,1]
slope<-coef[2,1]
abline(int,slope)
```

Output

```
Call:
lm(formula = ghost$logghost ~ ghost$distance)
```

Residuals:

Min	1Q	Median	3Q	Max
-0.44683	-0.23222	0.02926	0.13978	0.70545

Coefficients:

	Estimate	Std. Error	t value	Pr(> t)
(Intercept)	5.63885	0.26681	21.135	1.34e-07 ***
ghost\$distance	-0.01942	0.00201	-9.659	2.69e-05 ***

Signif. codes: 0 '***' 0.001 '**' 0.01 '*' 0.05 '.' 0.1 ' ' 1

Residual standard error: 0.4052 on 7 degrees of freedom
Multiple R-squared: 0.9302, Adjusted R-squared: 0.9202
F-statistic: 93.29 on 1 and 7 DF, p-value: 2.689e-05

PHASE I-EXPERIMENT 2

Code

```
library(lattice)
library(car)
library(lme4)
range<-read.csv(file.choose())
summary(range)
sample.direction<-as.factor(paste(range$sample, range$direction,
sep="-"))
boxplot(range$mean~sample.direction)
type<-as.numeric(sample.direction)
plot(range$mean~range$range,
      col=type,
```

```

    pch=type,
    ylab="Mean Intensity",
    xlab="Range (m)",
    xlim=c(3,7)
  )
legend("bottomright",
  levels(sample.direction),
  pch=1:20,
  col=1:20,
  title="Sample and Direction"
)
mem<-lmer(range$mean~range$range + (1|sample.direction))
summary(mem)

```

Output

```

Call:
Linear mixed model fit by REML
Formula: range$mean ~ range$range + (1 | sample.direction)
   AIC   BIC logLik deviance REMLdev
 685.1 695.6 -338.6   683.2   677.1
Random effects:
 Groups          Name          Variance Std.Dev.
sample.direction (Intercept) 509.894  22.5808
Residual                21.215   4.6059
Number of obs: 100, groups: sample.direction, 20

Fixed effects:
              Estimate Std. Error t value
(Intercept) 117.7750     5.8562  20.11
range$range   7.7300     0.6514  11.87

Correlation of Fixed Effects:
          (Intr)
range$range -0.501

```

PHASE I-EXPERIMENT 3

Code

```

summary(r2cm)
is.factor(r2cm$type)
type<-as.numeric(r2cm$type)
summary(lm(r2cm$i~log(r2cm$dweight)))
anova(lm(r2cm$i~r2cm$dweight+r2cm$type))
plot(r2cm$i~log(r2cm$dweight),
  col=type,
  pch=type,
  ylab="Intensity",
  xlab="Log Value of Mass (g)",
)
legend("bottomright",

```

```

      levels(r2cm$type),
      pch=1:3,
      col=1:3,
      title="Sample Type")
tom<-lm(r2cm$i~log(r2cm$dweight))
dick<-lm(r2cm$i~log(r2cm$dweight)+r2cm$type)
summary(dick)
anova(tom,dick)

```

Output

Call:

```
lm(formula = r2cm$i ~ log(r2cm$dweight))
```

Residuals:

Min	1Q	Median	3Q	Max
-47.396	-6.433	1.835	8.018	21.785

Coefficients:

	Estimate	Std. Error	t value	Pr(> t)	
(Intercept)	185.940	2.277	81.66	<2e-16	***
log(r2cm\$dweight)	13.575	1.009	13.45	<2e-16	***

Signif. codes: 0 '***' 0.001 '**' 0.01 '*' 0.05 '.' 0.1 ' ' 1

Residual standard error: 11.89 on 87 degrees of freedom

Multiple R-squared: 0.6754, Adjusted R-squared: 0.6716

F-statistic: 181 on 1 and 87 DF, p-value: < 2.2e-16

Call:

```
lm(formula = r2cm$i ~ log(r2cm$dweight) + r2cm$type)
```

Residuals:

Min	1Q	Median	3Q	Max
-47.538	-5.953	0.517	7.578	24.778

Coefficients:

	Estimate	Std. Error	t value	Pr(> t)	
(Intercept)	179.310	3.271	54.817	< 2e-16	***
log(r2cm\$dweight)	11.314	1.333	8.486	5.93e-13	***
r2cm\$typeFork	7.132	2.911	2.449	0.0164	*
r2cm\$typeTerminal	-4.146	4.063	-1.021	0.3104	

Signif. codes: 0 '***' 0.001 '**' 0.01 '*' 0.05 '.' 0.1 ' ' 1

Residual standard error: 11.51 on 85 degrees of freedom

Multiple R-squared: 0.7029, Adjusted R-squared: 0.6924

F-statistic: 67.04 on 3 and 85 DF, p-value: < 2.2e-16

Analysis of Variance Table

```

Model 1: r2cm$i ~ log(r2cm$dweight)
Model 2: r2cm$i ~ log(r2cm$dweight) + r2cm$type
  Res.Df  RSS Df Sum of Sq      F Pr(>F)
1      87 12305
2      85 11261  2    1044.2 3.9411 0.02308 *
---
Signif. codes:  0 '***' 0.001 '**' 0.01 '*' 0.05 '.' 0.1 ' ' 1

```

PHASE I-EXPERIMENT 4

Code

```

summary(twist)
twistregress<-lm(twist$i~twist$ti)
summary(twistregress)
plot.new()
par(mfrow=c(1,2))
plot(twist$i~twist$ti,
      ylab="Intensity-Rotated Samples",
      xlab="Intensity")
abline(0,1)
twistsum<-lm(twist$sum~twist$tsum)
summary(twistsum)
plot(twist$sum~twist$tsum,
      ylab="Sum of Intensity-Rotated Samples",
      xlab="Sum of Intensity")
plot(twist$intensity~twist$tintensity)
abline(0,1)

```

Output

```

Call:
lm(formula = twist$sum ~ twist$tsum)

Residuals:
    Min       1Q   Median       3Q      Max
-23741  -4422  -1469    2565   31549

Coefficients:
            Estimate Std. Error t value Pr(>|t|)
(Intercept) -2.341e+03  3.332e+03  -0.702    0.485
twist$tsum   1.027e+00  3.783e-02  27.158 <2e-16 ***
---
Signif. codes:  0 '***' 0.001 '**' 0.01 '*' 0.05 '.' 0.1 ' ' 1

Residual standard error: 9750 on 57 degrees of freedom
Multiple R-squared:  0.9283, Adjusted R-squared:  0.927
F-statistic: 737.6 on 1 and 57 DF,  p-value: < 2.2e-16

```

PHASE II-COMBUSTION MASS LOSS

Code

```
summary(vol_mass_all)
```

```

plot(vol_mass_all$massloss~vol_mass_all$voxloss,
     col=type,
     pch=type)
type<-as.numeric(vol_mass_all$species)
plot.new()
summary(lm(vol_mass_all$massloss~vol_mass_all$voxloss+
           vol_mass_all$species))
plot(vol_mass_all$massloss~vol_mass_all$voxloss,
     col=type,
     pch=type,
     xlab="Volume Loss (voxels)",
     ylab="Mass Loss (g)")
legend("bottomright", c("Chamise","Sage"), pch = 1:2, col = 1:2,
title = "Species")

```

Output

```

Call:
lm(formula = vol_mass_all$massloss ~ vol_mass_all$voxloss +
vol_mass_all$species)

```

Residuals:

```

      Min       1Q   Median       3Q      Max
-860.6 -388.1  -57.9   258.5 1442.8

```

Coefficients:

	Estimate	Std. Error	t value	Pr(> t)
(Intercept)	-982.45563	312.11713	-3.148	0.0041
vol_mass_all\$voxloss	0.18269	0.01832	9.974	2.24e-10
vol_mass_all\$speciesSage	1276.43213	233.38615	5.469	9.79e-06

```

---
Signif. codes:  0 '***' 0.001 '**' 0.01 '*' 0.05 '.' 0.1 ' ' 1

```

Residual standard error: 562.5 on 26 degrees of freedom

Multiple R-squared: 0.7953, Adjusted R-squared: 0.7796

F-statistic: 50.51 on 2 and 26 DF, p-value: 1.107e-09

PHASE II-SIMULATED MASS LOSS

R-Code

```

summary(weightloss)
summary(lm(weightloss$dweight~weightloss$voxels+weightloss$replicate))
rep<-as.numeric(weightloss$replicate)
plot(weightloss$dweight~weightloss$voxels,
     col=rep,
     pch=rep,
     xlab="Volume (voxels)",
     ylab="Mass (g)")
legend("bottomright", c("Foliage + Diameter",

```

```

                                "Diameter",
                                "Random"),
    pch = 1:3,
    col = 1:3,
    title = "Removal")

```

Output

Call:

```
lm(formula = weightloss$dweight ~ weightloss$voxels +
weightloss$replicate)
```

Residuals:

```

      Min       1Q   Median       3Q      Max
-25.9623  -7.6053  -0.7728  11.6145  21.5505

```

Coefficients:

	Estimate	Std. Error	t value
Pr(> t)			
(Intercept)	57.795796	4.814784	12.004
8.92e-14 ***			
weightloss\$voxels	0.035534	0.002527	14.061
9.92e-16 ***			
weightloss\$replicateRandom	-21.657127	5.429761	-3.989
0.000335 ***			
weightloss\$replicateSequential	-2.663618	5.456511	-0.488
0.628574			

Signif. codes: 0 '***' 0.001 '**' 0.01 '*' 0.05 '.' 0.1 ' ' 1

Residual standard error: 13.8 on 34 degrees of freedom

Multiple R-squared: 0.8632, Adjusted R-squared: 0.8511

F-statistic: 71.5 on 3 and 34 DF, p-value: 9.16e-15

PHASE II-INTERIOR VOLUME REPRESENTATION

Depth of Penetration Code

```
hist(hull_voxel_depth_count$schamise)
```

```
hist(hull_voxel_depth_count$sage)
```

```
hull_depth<-
```

```
c(hull_voxel_depth_count$sage,hull_voxel_depth_count$schamise )
```

```
hist(hull_depth,
      xlab="Voxels",
      main="")
```

```
library(fitdistrplus)
```

```
norm<-fitdist(hull_depth, "norm")
```

```
summary(norm)
```

```
plot(norm)
```

```
summary(hull_depth)
```

Depth of Penetration Output

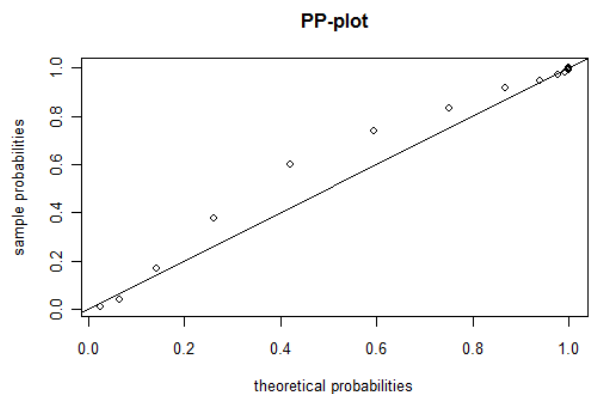
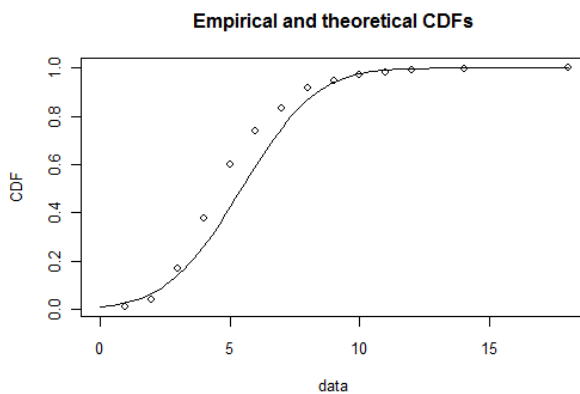
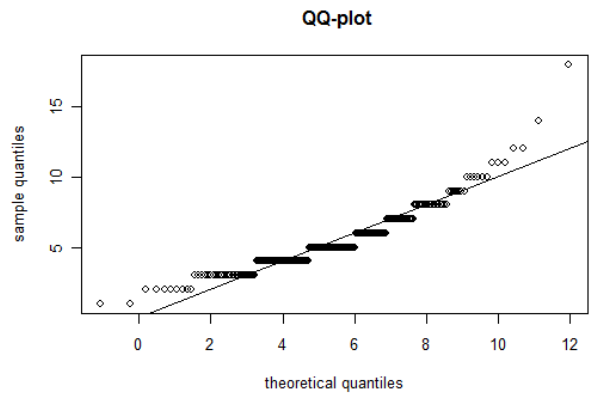
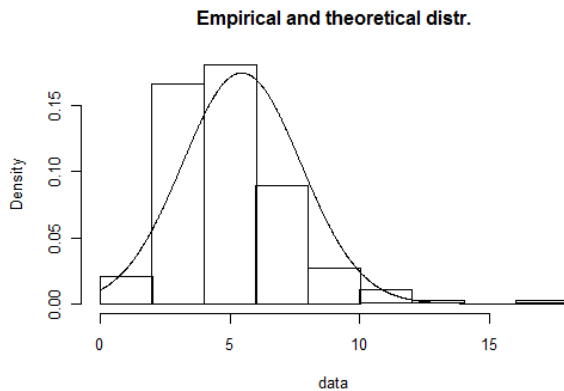
Fitting of the distribution ' norm ' by maximum likelihood

Parameters :

```
      estimate Std. Error
mean  5.454167  0.1471663
sd    2.279890  0.1040622
Loglikelihood: -538.3358  AIC: 1080.672  BIC: 1087.633
```

Correlation matrix:

```
      mean sd
mean   1  0
sd     0  1
```



Missing Volume Code

```
library(vcd)
```

```
library(fitdistrplus)
```

```
logis<-fitdist(hole_size_data$prop_total, "logis")
```

```
summary(logis)
```

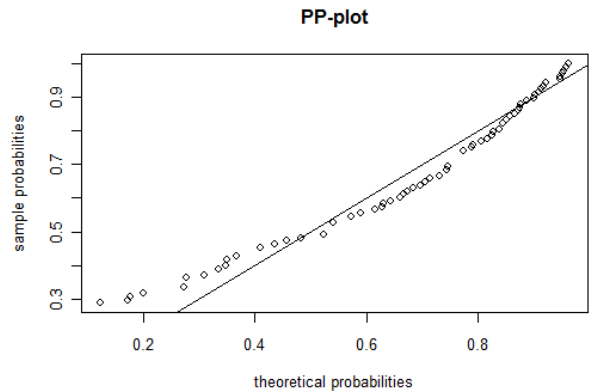
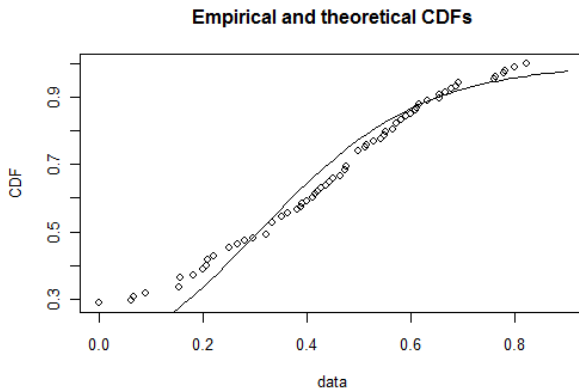
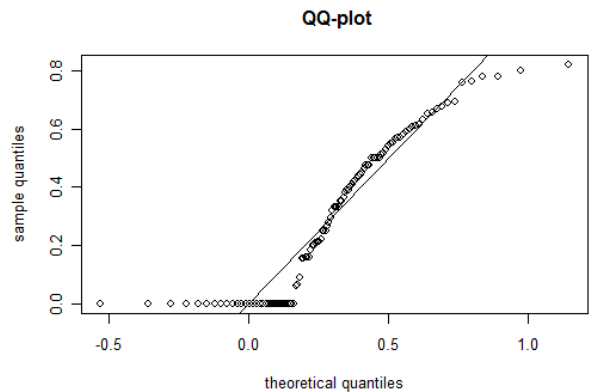
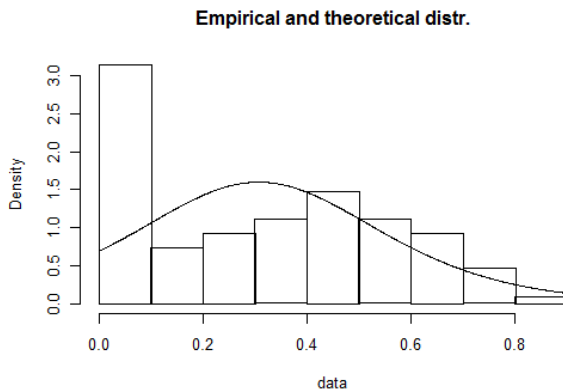
```
plot(logis)
```

Missing Volume Output

Fitting of the distribution ' logis ' by maximum likelihood

Parameters :

```
      estimate Std. Error
location 0.3071524 0.02700370
scale    0.1561923 0.01204362
Loglikelihood: -10.96602   AIC: 25.93203   BIC: 31.2963
Correlation matrix:
      location      scale
location 1.000000000 0.005907653
scale    0.005907653 1.000000000
```



PHASE II-VOXEL DENSITY DISTRIBUTION

Code

```
library(fitdistrplus)
library(vcd)

gamma<-fitdist(adj_chamise_density$vox_density, "gamma")
summary(gamma)
plot(gamma)
```

```
weibull<-fitdist(adj_chamise_density$vox_density, "weibull")
summary(weibull)
plot(weibull)
```

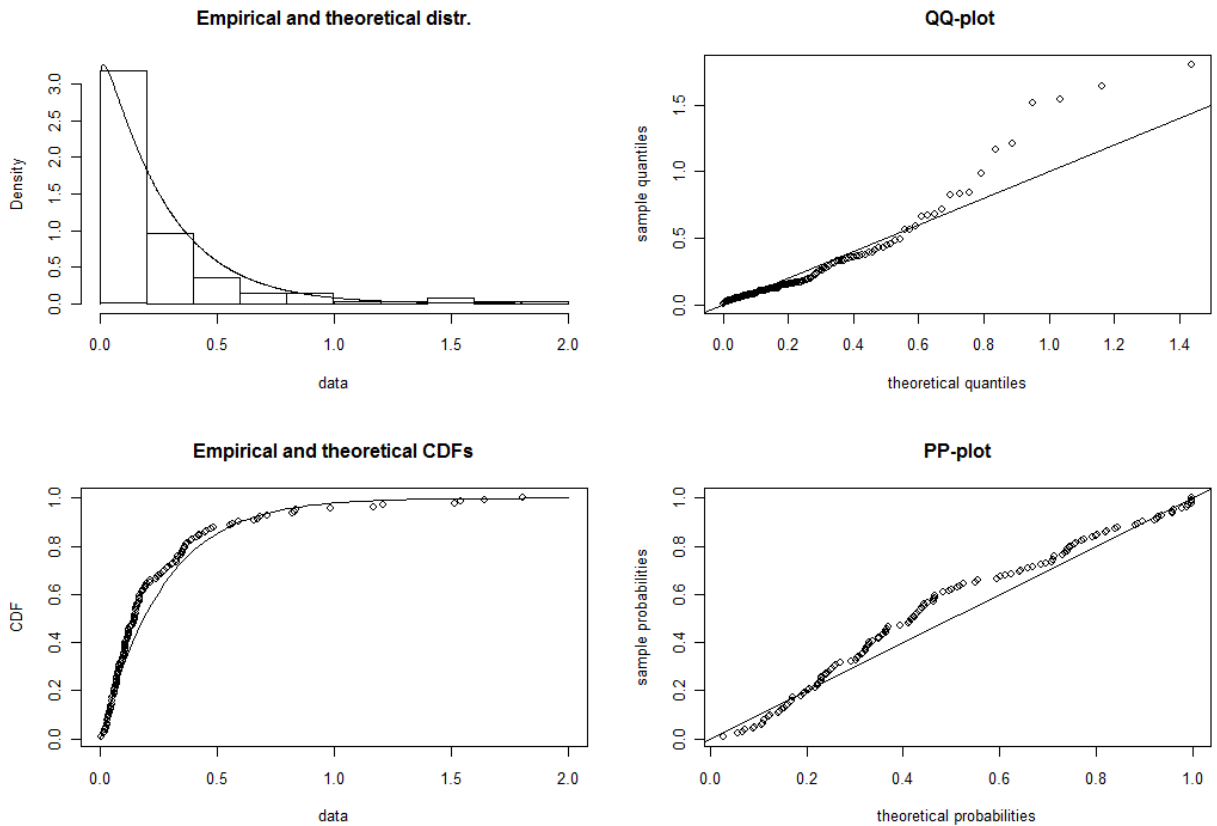
Output

Fitting of the distribution ' gamma ' by maximum likelihood

Parameters :

```
      estimate Std. Error
shape 1.064906  0.112690
rate  4.026085  0.538739
Loglikelihood: 46.35221  AIC:  -88.70441  BIC:  -82.82113
Correlation matrix:
```

```
      shape      rate
shape 1.0000000 0.7908214
rate  0.7908214 1.0000000
```



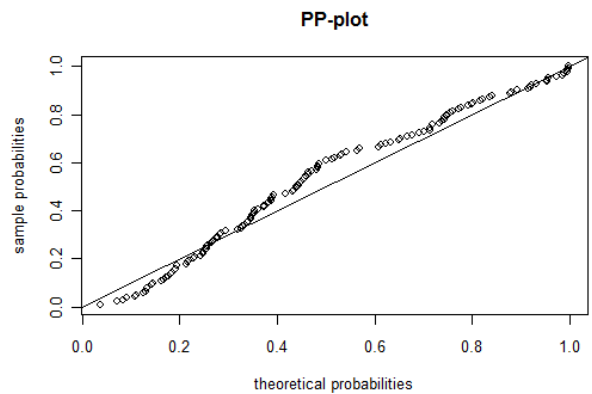
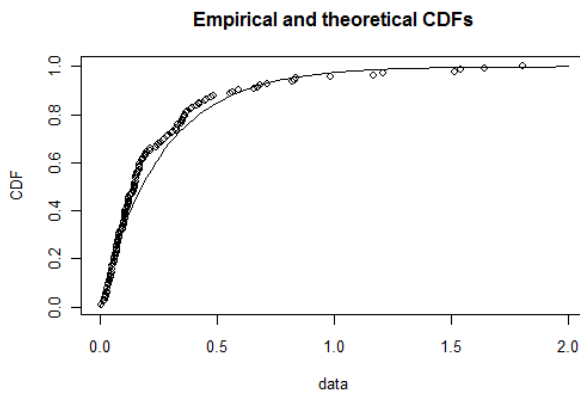
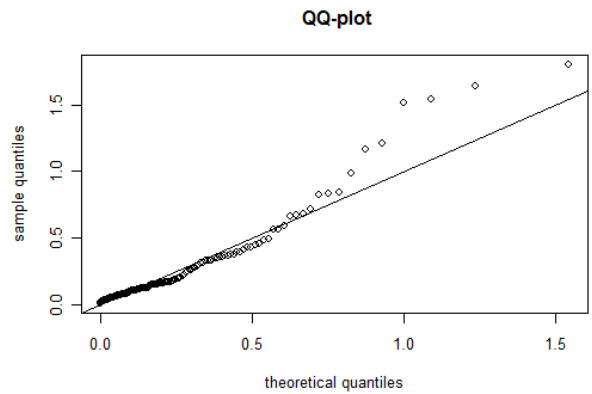
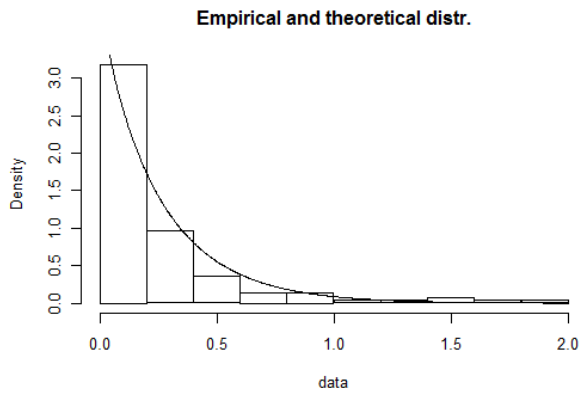
Fitting of the distribution ' weibull ' by maximum likelihood

Parameters :

```
      estimate Std. Error
shape 0.9715045 0.05943920
scale 0.2606213 0.02406447
Loglikelihood: 46.29217  AIC:  -88.58434  BIC:  -82.70106
Correlation matrix:
```

```
      shape      scale
shape 1.0000000 0.3353589
```

scale 0.3353589 1.0000000



MASS PREDICTION

Code

```
library(vcd)
library(fitdistrplus)

logis<-fitdist(hole_size_data$prop_total, "logis")
summary(logis)
plot(logis)

voxd<-combustion_density_chamise$voxels

gamweight<-numeric(1)
set.seed(1)
i=1
j=1
while(i<=13)
{

  j<-voxd[i]

  gam<-rgamma(j, shape=1.191366, rate=4.436428 )
```

```

gamweight[i]<-sum(gam)
i<-i+1
}

gammod<-lm(combustion_density_chamise$wweight~gamweight)

summary(gammod)

plot(gamweight,combustion_density_chamise$wweight,
      ylab="Measured Weight (g)",
      xlab="Predicted Weight (g)")

coef(gammod)

abline(coef(gammod))

```

Output

```

Call:
lm(formula = combustion_density_chamise$wweight ~ gamweight)

Residuals:
    Min       1Q   Median       3Q      Max
-1841.9  -575.5    -1.3    529.4  1779.6

Coefficients:
              Estimate Std. Error t value Pr(>|t|)
(Intercept) -3295.2136  1897.6568  -1.736  0.11037
gamweight     1.0222    0.2354   4.342  0.00117 **
---
Signif. codes:  0 '***' 0.001 '**' 0.01 '*' 0.05 '.' 0.1 ' ' 1

Residual standard error: 937.7 on 11 degrees of freedom
Multiple R-squared:  0.6315, Adjusted R-squared:  0.598
F-statistic: 18.85 on 1 and 11 DF,  p-value: 0.001171

```